

DOCTORAATSPROEFSCHRIFT

2009 | Faculteit Wetenschappen

Charge transfer complexes in polymer: fullerene bulk heterojunction solar cells

Proefschrift voorgelegd tot het behalen van de graad van
Doctor in de Wetenschappen, richting natuurkunde, te verdedigen door:

Koen VANDEWAL

Promotor: prof. dr. Jean V. Manca
Copromotor: dr. Abay Gadisa Dinku



Dankwoord

Ik wil graag enkele personen bedanken voor de tijd die ze in mij gestoken hebben, de steun die ze me boden en het vertrouwen dat ze in me hadden.

Financiële steun voor dit werk kreeg ik van het instituut voor de aanmoediging van innovatie door wetenschap en technologie in Vlaanderen (IWT).

Mijn promotor, Jean Manca, heeft me de kans gegeven om een doctoraat in zijn onderzoeksgroep te beginnen. Hij bood niet enkel een luisterend oor voor technische en wetenschappelijke problemen in het lab, maar bracht ook concrete oplossingen aan. Ik apprecieer ook enorm dat hij me verschillende keren de kans gaf om mijn werk zelf te gaan presenteren op buitenlandse conferenties.

The arrival of Abay Gadisa in our research group meant an injection of new ideas and concepts. I admire very much his enthusiasm and energy for work when trying new experiments. We had many stimulating discussions and I thank him for the critical reading of manuscripts and this thesis, especially at the end.

Dirk Vanderzande, Marlies Van Bael en Ken Haenen, bedank ik voor hun bijdragen en aanmoedigingen tijdens de phd meetings.

Dit doctoraat bouwt verder op het werk van Ludwig Goris. Hij was in de eerste jaren van mijn doctoraat altijd bereid tot geduldige uitleg, ook als het technische vragen waren in verband met PDS en FTPS meetopstellingen.

Verder gaat een zeer hartelijk bedankt gaat naar alle huidige en ex-collegas van de ONE groep: Wouter, Ann, Sabine, Ilse, Bert, Tine, Jean-Christophe, Gopala, Wanyun, Donato en Fortunato. Een hoogtepunt uit mijn vijfjarig verblijf om het IMO waren de skivakanties in Frankrijk die we gemaakt hebben, samen Michael, Ann en Ilse.

With Fortunato and Donato, I shared an office this last year. They thought me how to make real pizza. In return I tried to help them in their phd starting years. I hope the future work chapter of this thesis will be of use to them.

De volgende personen maken het leven en werken op IMO gemakkelijker: Erik zorgt voor het oplossen van computerproblemen, Johnny voor het ontwerpen, maken en repareren van samplehouders en voor het fixen van alle gloveboxproblemen, Christel en Hilde zorgen dat er steeds genoeg werkingsmateriaal is, elektronische problemen worden opgelost door Jan en Lieven. Administratie en het regelen van verblijfplaatsen en trips van en naar conferenties gebeurde altijd met de hulp van het secretariaat: Lea, Relinde en Marina.

Dankwoord

Het werk met polymeren bracht me in contact met mensen van andere vakgebieden. De samenwerking met de scheikundigen Wibren, sylvain en Joke was plezant. Ze hebben altijd veel geduld gehad om scheikundige termen begrijpelijk uit te leggen, ook voor een niet-scheikundige zoals ik. Wibren moet ik nog extra bedanken voor zijn expertise in verband met charge transfer complexen, die heel nuttig gebleken is.

Ik heb ook genoten van de halfjaarlijkse bijeenkomsten van het "Nanosolar" project en zijn vervolgproject "Polyspec", dat verschillende Vlaamse instellingen, zoals IMEC en de universiteiten van Antwerpen, Gent, Leuven en Hasselt samenbracht in gezamenlijk onderzoek naar organische zonnecellen.

Collaboration with the BIORGEL group under the guidance of Olle Inganäs of the University of Linköping in Sweden provided the electroluminescence experiments which were needed to complete this thesis. Kristofer gave me two months of his time, discussing and helping me with the measurements. All BIORGEL group members made it a pleasant winter for me in Sweden, inside as well as outside the lab.

Ten slotte wil ik mijn familie bedanken. Martijn, Guido en Godelieve. Zij hebben me altijd gesteund en aangemoedigd, in goede en moeilijke tijden en ik kan altijd op ze rekenen op de belangrijke momenten in mijn leven.

Koen Vandewal
Diepenbeek, Oktober 2009

Table of contents

DANKWOORD.....	I
TABLE OF CONTENTS.....	III
LIST OF PAPERS.....	V
TECHNICAL ACRONYMS	VII
LIST OF SYMBOLS.....	IX
PREFACE	1
1 DONOR/ACCEPTOR ORGANIC SOLAR CELLS	3
1.1 ORGANIC SOLAR CELLS.....	3
1.2 GENERAL WORKING PRINCIPLES	6
1.2.1 <i>Photons in, electrons out</i>	6
1.2.2 <i>Charge generation</i>	7
1.2.3 <i>Charge recombination</i>	8
1.3 EFFICIENCY OF A SOLAR CELL	9
1.3.1 <i>Power conversion efficiency</i>	9
1.3.2 <i>Photon-to-electron conversion efficiencies</i>	10
1.4 AIM OF THE THESIS	11
REFERENCES.....	13
2 BLACK AND GREY BODIES.....	17
2.1 THERMAL RADIATION	17
2.2 SOLAR POWER	18
2.2.1 <i>Solar temperature and total power</i>	18
2.2.2 <i>Standard solar spectra</i>	20
2.3 GENERALIZED RADIATION	21
2.3.1 <i>Chemical potential</i>	21
2.3.2 <i>Würfel's generalized radiation law</i>	22
2.3.3 <i>Reciprocity relation between absorption and emission</i>	24
2.4 APPLICATION TO PHOTOVOLTAICS	25
2.4.1 <i>Reciprocity between photovoltaic and electroluminescent actions</i>	25
2.4.2 <i>J-V curves from electro-optical measurements</i>	27
2.4.3 <i>The Shockley-Queisser maximum efficiency limit</i>	31
REFERENCES.....	34
3 FOURIER-TRANSFORM PHOTOCURRENT SPECTROSCOPY.....	35
3.1 INTRODUCTION	35
3.2 MONOCHROMATIC VERSUS DISPERSIVE TECHNIQUES	36
3.3 MEASUREMENT OF PHOTOCURRENT SPECTRA	39
3.3.1 <i>Setup with monochromator</i>	39
3.3.2 <i>Fourier-Transform Photocurrent Spectroscopy</i>	39

Table of contents

REFERENCES.....	44
4 GUIDE TO THE PAPERS	45
PAPER A.....	45
PAPER B.....	46
PAPER C.....	47
PAPER D	48
PAPER E	49
PAPER F	50
REFERENCES.....	51
5 CONCLUSION	53
6 FUTURE WORK.....	57
REFERENCES	61
NEDERLANSTALIGE SAMENVATTING	63
APPENDIX: PAPER A-F.....	67

List of papers

Papers are listed in chronological order. The publications which are included in this thesis are highlighted.

L. Goris, A. Poruba, A. Purkrt, K. Vandewal, A. Swinnen, I. Haeldermans, K. Haenen, J. V. Manca, M. Vanecek, "Optical absorption by defect states in organic solar cells", *J. non-cryst. Sol.* **352**, 1656 (2006)

O. Douheret, L. Lutsen, A. Swinnen, M. Bresselge, K. Vandewal, L. Goris, J. Manca, "Nanoscale electrical characterization of organic photovoltaic blends by conductive atomic force microscopy", *Appl. Phys. Lett.* **89**, 032107 (2006)

K. Vandewal, L. Goris, K. Haenen, Y. Geerts, J. V. Manca, "Highly sensitive spectroscopic characterization of inorganic and organic heterojunctions for solar cells", *Eur. Phys. J. Appl. Phys.* **36**, 281 (2006)

J. J. Benson-Smith, L. Goris, K. Vandewal, K. Haenen, J. V. Manca, D. Vanderzande, D. D. C. Bradley, J. Nelson, "Formation of a ground-state charge-transfer complex in polyfluorene/[6,6]-phenyl-C-61 butyric acid methyl ester (PCBM) blend films and its role in the function of polymer/PCBM solar cells", *Adv. Funct. Mater.* **17**, 451 (2007)

K. Vandewal, A. Gadisa, W. D. Oosterbaan, S. Bertho, F. Banishoeib, I. Van Severen, L. Lutsen, T. J. Cleij, D. Vanderzande, "The relation between open-circuit voltage and the onset of photocurrent generation by charge-transfer absorption in polymer: fullerene bulk heterojunction solar cells", *Adv. Funct. Mater.* **18**, 2064 (2008)

I. Haeldermans, I. Truijen, K. Vandewal, W. Moons, M. K. Van Bael, J. D'Haen, J. V. Manca, J. Mullens, "Water based preparation method for 'green' solid-state polythiophene solar cells", *Thin solid films* **516**, 7245 (2008)

K. Vandewal, L. Goris, I. Haeldermans, M. Nesladek, K. Haenen, P. Wagner, J. V. Manca, "Fourier-Transform Photocurrent Spectroscopy for a fast and highly sensitive spectral characterization of organic and hybrid solar cells", *Thin solid films* **516**, 7135 (2008)

I. Haeldermans, K. Vandewal, W. D. Oosterbaan, A. Gadisa, J. D'Haen, M. K. Van Bael, J. V. Manca, J. Mullens, "Ground-state charge-transfer complex formation in hybrid poly(3-hexyl thiophene):titanium dioxide solar cells", *Appl. Phys. Lett.* **93**, 223302 (2008)

K. Tvingstedt, K. Vandewal, A. Gadisa, F. Zhang, J. Manca, O. Inganäs, "Electroluminescence from Charge Transfer States in Polymer Solar Cells", *J. Am. Chem. Soc.* **131**, 11819 (2009)

A. Gadisa, W. D. Oosterbaan, K. Vandewal, J.-C. Bolsée, S. Bertho, J. D'Haen, L. Lutsen, D. Vanderzande, J. V. Manca, "Effect of alkyl side-chain length on photovoltaic properties of poly(3-alkylthiophene)/PCBM bulk heterojunctions", *Adv. Funct. Mater.* **19**, 3300 (2009)

K. Vandewal, K. Tvingstedt, A. Gadisa, O. Inganäs, J. V. Manca, "On the origin of the open-circuit voltage of polymer-fullerene solar cells", *Nature Mater.* **8**, 904 (2009)

K. Vandewal, W. D. Oosterbaan, S. Bertho, V. Vrindts, A. Gadisa, L. Lutsen, D. Vanderzande J. V. Manca, "Varying polymer crystallinity in nanofiber poly(3-alkylthiophene):PCBM solar cells: Influence on charge transfer state energy and open-circuit voltage", *Appl. Phys. Lett.* **95**, 123303 (2009)

A. Gadisa, K. Tvingstedt, F. Zhang, K. Vandewal, J. V. Manca, O. Inganäs, "Bipolar charge transport in fullerene molecules in a bi-layer and blend of polyfluorene co-polymer and fullerene", *Adv. Mater.*, accepted (2009)

S. Chambon, R. Mens, K. Vandewal, M. Scharber, L. Lutsen, D. Vanderzande, J. Manca, J. Gelan, P. Adriaensens, "Investigation of the influence of octanedithiol on the nanomorphology of PCPDTBT:PCBM blends by solid-state NMR", *Adv. Funct. Mater.*, submitted (2009)

K. Vandewal, A. Gadisa, J. V. Manca, K. Tvingstedt, O. Inganäs, "Relating the open-circuit voltage to interface molecular properties of donor:acceptor bulk heterojunction solar cells", *Phys. Rev. B*, submitted (2009)

K. Vandewal, A. Gadisa, J. V. Manca, K. Tvingstedt, O. Inganäs, "The ultimate efficiency of organic donor/acceptor single junction solar cells", unpublished (2009)

Technical acronyms

AC	Alternating current
AM0	Air mass 0
AM1	Air mass 1
AM1.5	Air mass 1.5
AM1.5g	Air mass 1.5 global
AM-FTPS	Amplitude modulated step scan Fourier-transform photocurrent spectroscopy
APFO3	Poly[2,7-(9-di-octyl-fluorene)-alt-5,5-(4',7'-di-2-thienyl-2',1',3'benzothiadiazole)]
BB	Black body
BCP	Bathocuproine
BHJ	Bulk heterojunction
C ₆₀	Buckminsterfullerene, containing 60 carbon atoms
C ₇₀	Fullerene containing 70 carbon atoms
CaF ₂	Calcium fluoride
CIGS	Copper indium gallium diselenide
CS-FTPS	Continuous scan Fourier-transform photocurrent spectroscopy
CT	Charge transfer
CTC	Charge transfer complex
DC	Direct current
FTIR	Fourier-transform infrared spectroscopy
FTPS	Fourier-transform photocurrent spectroscopy
GaAs	Gallium arsenide

Technical acronyms

HOMO	Highest occupied molecular orbital
ITO	Indium tin oxide
KBr	Potassium bromide
LED	Light emitting diode
LUMO	Lowest unoccupied molecular orbital
MDMO-PPV	Poly[2-methoxy-5-(3,7-dimethyloctyloxy)-1,4-phenylenevinylene]
P3HT	Poly[3-hexylthiophene]
PC ₇₁ BM	[6,6]-phenyl C71 butyric acid methyl ester
PCBM	[6,6]-phenyl C61 butyric acid methyl ester
PCDTBT	Poly[N-9''-hepta-decanyl-2,7-carbazole-alt-5,5-(4',7'-di-2-thienyl-2',1',3'-benzothiadiazole)]
PDS	Photothermal Deflection Spectroscopy
PEDOT:PSS	Poly(styrenesulfonate) doped poly(3,4-ethylenedioxythiophene)
Si	Silicon

List of symbols

Variables

α	Absorption coefficient
δ	Path length difference
η	Power conversion efficiency
λ	Wavelength
σ	Wavenumber
σ_a	Absorption cross section
μ	Chemical potential
τ	Excited state lifetime
ϕ	Photon flux
A	Absorptivity: fraction of absorbed photons
A_{21}	Einstein coefficient for emission
B_{12}	Einstein coefficient for absorption
B_{21}	Einstein coefficient for stimulated emission
d	Sample thickness
E	Photon energy
E_g	Optical gap of the main absorber
EQE_{EL}	Electroluminescence external quantum efficiency
EQE_{PV}	Photovoltaic external quantum efficiency
f	Modulation frequency
FF	Fill factor
I	Depending on context: Irradiance; Interferogram

List of symbols

$IPCE$	Incident photon-to-electron conversion efficiency
IQE_{PV}	Photovoltaic internal quantum efficiency
J	Current density
J_{ph}	Photo generated current
J_{sc}	Short-circuit current
P	Power density
T	Absolute temperature
t	Time
V	Voltage
v	Mirror velocity
V_{oc}	Open-circuit voltage

Constants

σ_{HeNe}	Wavenumber of the HeNe reference laser line	15798 cm^{-1}
σ_{SB}	Stefan-Boltzmann constant	$5.67 \times 10^{-8} \text{ W m}^{-2} \text{ K}^{-4}$
c	Speed of light	$299792458 \text{ m.s}^{-1}$
h	Planck's constant	$6.626068 \times 10^{-34} \text{ m}^2.\text{kg}.\text{s}^{-1}$
k	Boltzmann constant	$1.3806503 \times 10^{-23} \text{ m}^2.\text{k.g}.\text{s}^{-2}.\text{K}^{-1}$
q	Elementary charge	$1.60217646 \times 10^{-19} \text{ C}$
r_e	Radius of the earth	$6.371 \cdot 10^6 \text{ m}$
r_s	Radius of the sun	$6.955 \cdot 10^8 \text{ m}$
r_{se}	Mean distance between earth and sun	$1.496 \cdot 10^{11} \text{ m}$
T_s	Absolute temperature of the solar surface	5762 K

Preface

This thesis contains part of the written result of the work carried out in a period of 5 years, from October 2004 to October 2009. In general, the goal of the work is the understanding of the fundamental working mechanisms of organic solar cells, in order to find pathways to improve their power conversion efficiency.

Solar cells based on organic materials are widely investigated nowadays, because they have the potential to be processed at low cost and on a large scale. The best performing, fully organic solar cells currently have an efficiency of $\sim 6\%$. The key component of the organic solar cell is a material interface between two organic materials, called the electron donor and electron acceptor, respectively. Most successful organic solar cells use a conjugated polymer as donor and a fullerene derivative as electron accepting material.

Due to the versatility of organic materials in general and conjugated polymers in particular, the number of donor/acceptor material combinations is endless. One of the aims in research on organic solar cells, and of this work in particular, is the identification of specific material properties which affect the solar cell performance. This will provide design rules, and allows us to choose the most optimal donor/acceptor combination, increasing the efficiency of organic solar cells beyond the currently achieved $\sim 6\%$.

To reach this objective, in this work, solar cells and active layers of material blends containing conjugated polymers and fullerenes are prepared and characterized by the innovative, highly sensitive technique named Fourier-transform photocurrent spectroscopy. This is not a standard characterization technique used in research on organic photovoltaics. The main task of this work is therefore to interpret the obtained measurements and find implications for device performance. This resulted in a number of publications in peer reviewed scientific journals. A complete list of all publications can be found on page v. In the appendix, the 6 papers which are most relevant in the framework of this thesis are included. It will be shown that new, weak spectral features in the material blends originate from ground-state interaction and so called charge transfer complex formation between donor and acceptor materials. This has a crucial impact on the overall solar cell behavior and on the production of photovoltage by such blends in particular.

However, underlying thesis is not just a bundled band of 6 papers. Chapters are included in order to provide background in the field of organic photovoltaics (chapter 1), to provide a theoretical framework (chapter 2) and to introduce the used experimental technique Fourier-transform photocurrent spectroscopy (chapter 3). Chapter 4 shortly introduces the content of the papers, including

Preface

their mutual relation and the motivation for writing them. Chapter 5 contains an overall conclusion and chapter 6 gives an outlook for future experiments and ways to improve the efficiency of organic solar cells. Reprints of the papers can be found in the appendix.

1 Donor/acceptor organic solar cells

In this chapter, organic solar cells based on interfaces between electron donating and electron accepting materials are introduced. An overview of the known photovoltaic working principles of these material systems is given and important, measurable solar cell characterization parameters, such as the power conversion efficiency, are defined. To conclude, the aim of the thesis is summarized.

1.1 Organic solar cells

Organic photovoltaic solar cells potentially offer solutions to many problems currently encountered with traditional photovoltaic technologies. Most notably, the technology offers the possibility for fast processing of low cost, light weight and flexible photovoltaic panels.

As compared to inorganic materials used in solar cells nowadays, typical organic small molecules and conjugated polymers have high absorption coefficients. A 100 nm thick device of such a material is sufficient to absorb virtually all the light with energy higher than its optical gap. Therefore it is no surprise that already in the beginning days of photovoltaics, people have attempted to prepare devices from strongly absorbing organic materials.¹ The power conversion efficiency of single layer organic materials sandwiched between two electrodes however, is disappointing ($< 1\%$).² This originates from the low dielectric constant of organic materials, causing the optical excitations to consist of an electron and hole which are still mutually attracting, with a typical binding energy of 0.5 eV.³ This binding energy is much too large for the internal fields in the device to break the excitons within their ~ 1 ns lifetime. This causes organic solar cells consisting of a single organic material sandwiched between two electrodes to generate low photocurrents resulting in low overall performances.

A breakthrough came in 1985 when Tang⁴ presented a two layer organic photovoltaic device with a power conversion efficiency of $\sim 1\%$. In such bilayer devices, the interface between the two organic layers is crucial in determining its photovoltaic properties. Excitons created in either of the two material phases are dissociated at the interface. The material in which the electron ends up after dissociation is named the electron acceptor, accepting the electron from the donor material. Today, the bilayer cell concept is still used for devices using evaporated organic small molecules.⁵

One of the most successful and most studied electron accepting material is the C₆₀ buckminsterfullerene. The discovery of ultrafast (~ 100 fs) electron transfer between C₆₀ and conjugated polymers⁶ stimulated interest in these systems for

photovoltaic applications. In bilayer devices comprising conjugated polymers and C_{60} , however, only excitons created within their diffusion length from the interface, can contribute to the photovoltaic effect. For conjugated polymers, exciton diffusion lengths of $\sim 5\text{-}7$ nm are typical. Within this distance, only a small fraction of the incident light is absorbed, resulting in low photocurrents for a bilayer configuration.⁷

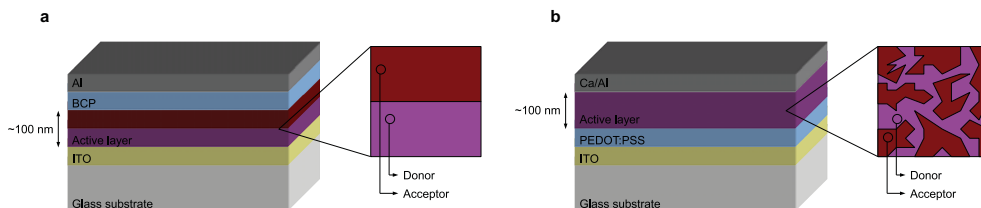


Figure 1-1: A representative contemporary architecture of (a) a bilayer device and (b) a bulk heterojunction device. The active layer is sandwiched between two electrodes. One of the electrodes indium tinoxide (ITO) is transparent. The use of interlayers of (transparent) organic conductors, such as poly(styrenesulfonate) doped poly(3,4-ethylenedioxythiophene) (PEDOT:PSS) and bathocuproine (BCP) have shown to improve device performance.

For polymer based systems, the bulk heterojunction (BHJ) concept provided a breakthrough.⁸ Active layers consisting of donor:acceptor material blends can be deposited by using a solution of soluble derivatives of fullerenes and conjugated polymers. By using a material blend, the interface is distributed over the bulk of the device. In this way, all excitons created in layers, sufficiently thick to absorb all the incident sunlight, can reach an interface within their natural lifetime. It is evident that with the introduction of the BHJ concept, the morphology of the active layer becomes a crucial issue. Today, the highest efficiencies reached using this approach are about 5-6 %.^{9,10,11} Figure 1-1 shows a comparison between the BHJ and bilayer concepts.

Figure 1-2 shows typical donor conjugated polymers and the most commonly used fullerene acceptor. MDMO-PPV (Figure 1-2 (a)) can be considered the work horse material in the early years of research on polymer:fullerene BHJ organic photovoltaics. Using this material the importance of the nanomorphology, and its control by selecting appropriate solvents became apparent.^{12,13} Later, P3HT (Figure 1-2 (b)) attracted lots of interest, due to its ability to form nanocrystalline phases in blends with fullerenes.^{14,15} An interesting donor material class consists of conjugated polymers with a backbone of alternating donor and acceptor units (Figure 1-2 (c) APFO3 and (d) PCDTBT). Using PCDTBT (Figure 1-2 (d)), an efficiency of 6% was achieved.¹¹

The most successful soluble acceptor materials up to date are the C_{60} derivative PCBM (Figure 1-2 (e)) and the C_{70} derivative PC₇₁BM. PCBM is a weak absorber,

while PC₇₁BM contributes to sunlight absorption when used in polymer:fullerene solar cells.¹⁶ Alternative electron accepting materials, such as n-type conjugated polymers¹⁷ and inorganic metal oxides¹⁸ are currently under investigation.

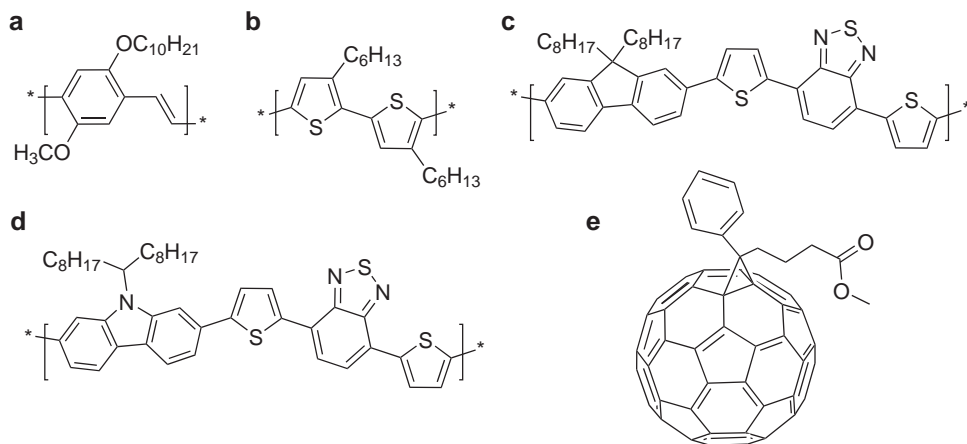


Figure 1-2: The chemical structure of (a) poly[2-methoxy-5-(3,7-dimethyloctyloxy)]-1,4-phenylenevinylene) (MDMO-PPV) (b) poly[3-hexylthiophene] (P3HT) (c) poly[2,7-(9-di-octyl-fluorene)- alt-5,5-(4',7'-di-2-thienyl-2',1',3'-benzothiadiazole)] (APFO3) (d) poly[N-9''-hepta-decanyl-2,7-carbazole-alt-5,5-(4',7'-di-2-thienyl-2',1',3'-benzothiadiazole)] (PCDTBT) (e) [6,6]-phenyl C₆₁ butyric acid methyl ester (PCBM).

Table 1-1 summarizes the confirmed power conversion efficiencies of several photovoltaic technologies.¹⁹ It reveals that, as compared to the other technologies, the organic solar cells still have a modest efficiency. One of the goals of research on organic photovoltaics therefore is to improve device efficiency together with device stability, while keeping the cost of the technology low.²⁰

Table 1-1: Confirmed submodule power conversion efficiencies (η) measured on a 1 cm² cell surface, under the standardized global AM1.5 spectrum (1000 W.m⁻²) at 25 °C for several photovoltaic technologies.¹⁹ The highest efficiency measured for organic solar cells is 5.2 %. However for cells smaller than 1 cm², efficiencies higher than 6 % have been reported.¹¹

Photovoltaic technology	η (%)
Silicon (Si)	
Mono-crystalline	25.0
Multi-crystalline	20.4
Amorphous	9.5
Gallium arsenide (GaAs)	26.1
Copper indium gallium diselenide (CIGS)	19.4
Dye sensitized	10.4
Organic	5.2

1.2 General working principles

1.2.1 Photons in, electrons out

In the past years, many reviews on organic solar cells have been written.²¹⁻²⁸ In most of them, the scheme in Figure 1-3 (a) is presented, depicting the simplified mechanism by which the incident photon flux is converted into an electrical current in organic donor/acceptor based devices. It has 4 fundamental steps.

While the efficiency of the exciton creation (step 1) and diffusion (step 2) depend strongly on sample thickness and bulk heterojunction morphology, the crucial charge generation mechanism (step 3), is believed to depend on the energetic interfacial structure and can be highly efficient in some well performing BHJ solar cells. However, up to now, this step is not fully understood and under vivid discussion. Once the electron on the acceptor material and the hole on the donor material have escaped each other's Coulomb binding energy, they are transported to the collecting electrodes (step 4).

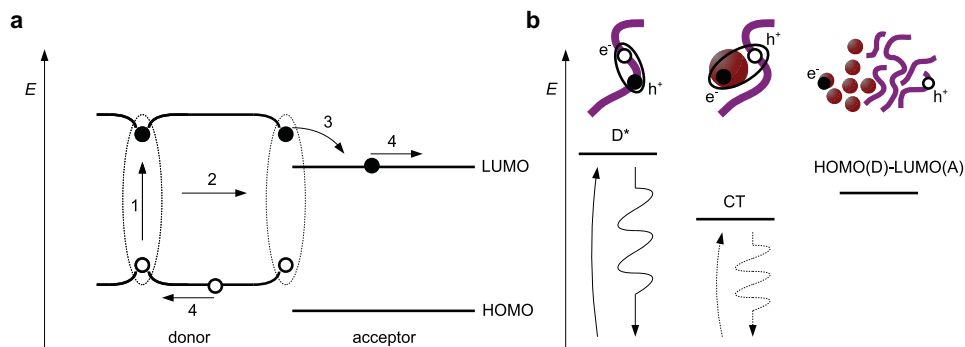


Figure 1-3: (a) General mechanism for photo-energy conversion in donor/acceptor organic solar cells. The four steps are: (1) Absorption of light, creating an exciton in the donor (acceptor) phase. (2) Diffusion of excitons to the donor/acceptor interface. (3) Dissociation of excitons yielding charge carriers. (4) Charge transport and collection at the electrodes. (b) A scheme of the energy of relevant pairs of electrons and holes: the donor excitonic state (D^*) and the charge transfer state (CT). The energy of a free electron on the acceptor phase and a free hole on the donor phase is equal to the difference between their respective molecular orbital energy levels.

1.2.2 Charge generation

The thought that the generation of free carriers occurs directly when the polymer exciton has reached the interface (step 3), has been abandoned by most authors in the field. In the free carrier generation process, an intermediate, charge transfer (CT) state exists, in which the hole on the donor phase is still bound to the electron on the acceptor phase. A scheme of the energy levels of the different bound electronic states is shown in Figure 1-3 (b). The energy of a completely dissociated pair yielding a free electron and hole is equal to the energetic difference between the highest occupied molecular orbital (HOMO) of the donor and the lowest unoccupied molecular orbital (LUMO) of the acceptor. The dissociation of the interfacial CT state into free carriers is a field and temperature dependent process. It competes with the decay of the CT state to the ground state. This type of decay is often referred to as *geminate recombination*. It was argued that incomplete dissociation of the CT state, due to geminate recombination, is the limiting step of the current generation process in MDMO-PPV:PCBM photovoltaic devices.²³

Due to weak ground state interaction between donor and acceptor material, a ground state charge transfer complex (CTC) is formed. Optical excitation of this newly formed CTC ground state yields the CT state. Direct evidence for the presence of such a state is obtained for many donor/acceptor interfaces: Both optical excitation to the CT state (CT absorption) and de-excitation of the CT

state (CT emission) have been observed in active layers of organic photovoltaic devices based on small molecule:C₆₀ co-evaporated layers,²⁹ polymer:fullerene blends³⁰⁻⁴⁰ and even polymer:metal oxide hybrid blends.⁴¹ Because of the weak transition probabilities associated with CTCs, highly sensitive techniques are needed to observe CT absorption and CT emission bands.

Furthermore, it has been observed that in donor/acceptor combinations, exhibiting a very low amount of charge generation, the CT related absorption and emission with energy lower than the optical gap of either donor or acceptor material, is absent.^{33,41} This implies that in this case, the CT state is no more the lowest energy excited state. Therefore, the detection of CT bands with energy lower than the optical gap of the blend constituents is a good method to investigate the photovoltaic potential of a particular material combination and will be one of the scopes of this thesis.

1.2.3 Charge recombination

Once free charge carriers are created within the two material phases, they have to find their way to the electrodes, preferably without recombining. This type of free carrier recombination or *non-geminate recombination* must be distinguished from geminate recombination, as described above. The exact sites and molecular mechanisms determining the non-geminate recombination are still unknown. It is argued that the non-geminate recombination mechanism in polymer:fullerene bulk heterojunction devices occurs at the polymer:fullerene interface and is a bimolecular mechanism, depending on both the concentration of free electrons and holes.^{42,43} As the interface states are CT states, radiative decay from these CT states to the ground state (or CT emission) can thus be the result of both geminate and but also non-geminate recombination.

In photoluminescence emission quenching by an electric field experiments, the photogenerated free charge carriers are all extracted by the field. In this way only the geminate recombination resulting in CT emission can be probed.³⁷ When one wants to probe the emission as a result of only non-geminate recombination however, one must inject free electrons and holes in the device, kept in the dark. This can be done by an electroluminescence measurement at forward bias.³⁹

1.3 Efficiency of a solar cell

1.3.1 Power conversion efficiency

The performance of a photovoltaic device is determined by recording the current density J versus voltage V , under solar illumination. The power P per surface unit of photovoltaic device equals the $J.V$ product. In the fourth quadrant of the coordinate system, this product is negative and power is generated.

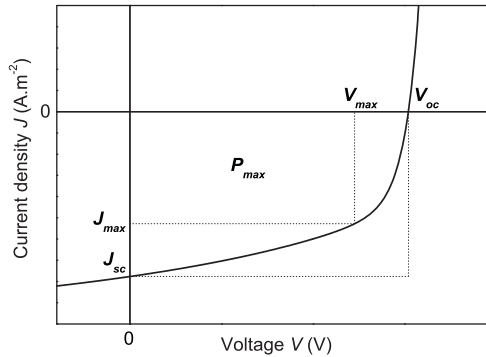


Figure 1-4: J - V curve of a solar cell. At one point (V_{max} , J_{max}) in the fourth quadrant, the generated power is maximal (P_{max}). Other relevant parameters such as the open-circuit voltage (V_{oc}) and the short-circuit current density (J_{sc}) are also indicated.

At two (V , J) points the generated power becomes zero: At open-circuit, at a voltage V_{oc} (open-circuit voltage), no net current is flowing into or from the device. At short-circuit, a current J_{sc} (short-circuit current) is flowing, but no potential difference is measured at the device contacts. The maximum output power density P_{max} is achieved at the voltage V_{max} and current J_{max} at which the $J.V$ product reaches a maximum. A quantity named fill factor (FF) is defined as

$$FF = \frac{P_{max}}{J_{sc} V_{oc}} = \frac{J_{max} V_{max}}{J_{sc} V_{oc}} \quad (1-1)$$

This quantity says something about the “squareness” of the J - V curve. It is equal to the ratio of the two squares indicated in Figure 1-4. The power conversion efficiency of the photovoltaic device is defined as the ratio between the maximum output electrical power P_{max} and the input optical power.

$$\eta = \frac{P_{max}}{P_{in}} = FF \frac{J_{sc} V_{oc}}{P_{in}} \quad (1-2)$$

In order to compare the performance of different photovoltaic devices under solar conditions, an internationally agreed, standardized input illumination spectrum, with a total power density P_{in} of 1000 W.m^{-2} is used (see also paragraph 2.2.2).

1.3.2 Photon-to-electron conversion efficiencies

Upon illumination of a solar cell, a power density P_{ph}^{in} consisting N_{ph}^{in} photons per second of photon energy E are incident onto the device, generating a photo-induced current J_{ph} , consisting of N_e^{out} electrons per second. The incident photon-to-electron conversion efficiency (*IPCE*) or photovoltaic external quantum efficiency EQE_{PV} is a spectral quantity and is defined as:

$$EQE_{PV} = IPCE = \frac{N_e^{out}}{N_{ph}^{in}} = \frac{EJ_{ph}}{qP_{ph}^{in}} \quad (1-3)$$

This is a spectral quantity, depending on the photon energy E or wavelength λ of the incident photons. Typically EQE_{PV} is measured under short-circuit ($V = 0$) conditions. However, in contrary to inorganic solar cells, for organic solar cells the number of photo-generated electrons can depend on the applied voltage.⁴⁴ This causes also EQE_{PV} to depend on voltage. Therefore, in this work, it will always be mentioned under which voltage conditions EQE_{PV} is measured.

Next to external quantum efficiency, also internal quantum efficiency IQE_{PV} , or absorbed photon-to-electron conversion efficiency, is defined. This is again a spectral quantity.

$$IQE_{PV} = \frac{N_e^{out}}{N_{ph}^{abs}} \quad (1-4)$$

Hereby is N_{ph}^{abs} the number of absorbed photons. This number can be related to N_{ph}^{in} by the absorptivity A :

$$A = \frac{N_{ph}^{abs}}{N_{ph}^{in}} \quad (1-5)$$

For inorganic and even organic solar cells, EQE_{PV} and IQE_{PV} values of respectively 70-80 % and 80-100% are not so exceptional. However, the overall power conversion efficiency η of a photovoltaic device, does not only depend on the flow of photo-generated electrons, but also on their electrical potential. Therefore, in our quest to improve the power conversion efficiency of organic solar cells, optimization and understanding of the photo-generated voltage is

equally important as optimization of the photon-to-electron conversion efficiencies.

Note that next to photon-to-electron conversion efficiencies, also electron-to-photon conversion efficiencies can be defined. When electrons and holes are recombining in an electroluminescent device, a fraction of these recombination events will result in the emission of photons N_{ph}^{out} . If N_e^{in} is the number of injected electrons, the electroluminescent external quantum efficiency (EQE_{EL}) is defined as

$$EQE_{EL} = \frac{N_{ph}^{out}}{N_e^{in}} \quad (1-6)$$

Note that a photovoltaic and electroluminescent effect is always present in the same device. While the emission of light is most visible under current injection conditions $J > 0$, the photovoltaic effect is the most visible when $J < 0$.

1.4 Aim of the thesis

Improvement of the efficiency and stability, while maintaining a low technology cost is the main motivation for research on organic photovoltaic solar cells. This thesis in particular will focus on the improvement of the power conversion efficiency. It aims to determine crucial factors governing the photovoltaic parameters. Especially the role of the donor/acceptor material interaction and the CT state in the generation of photocurrent but also on the photovoltage is not clear yet. In the studies performed in this thesis, the polymer:fullerene BHJ material system is used as a model system for donor/acceptor photovoltaics in general.

Under vivid discussion nowadays is the exact dissociation mechanism of the CT states, in particular the role of the energetic positions of the several excitonic states which are passed through before free carriers are generated.⁴⁵⁻⁴⁷ This relates to the important question of what would be the minimum difference between the energy of the CT state and donor or acceptor optical gap, which still allows efficient dissociation into free carriers. Determining these factors is crucial in the understanding and optimization of the photocurrent generation.

Another point of discussion and research concerns the factors that determine the generation of photovoltage. V_{oc} has been shown to depend on the donor/acceptor material combination⁴⁸⁻⁵⁰, the electrode material⁵¹, as well as light intensity and temperature.⁵² At fixed temperature and illumination conditions, and when using ohmic contacts, V_{oc} has been found to be linearly correlating with the difference of the HOMO of the donor and the LUMO of the acceptor. However, exceptions on this rule have also been reported.⁵³

Chapter 1

Based on such empirical relations between the donor HOMO - acceptor LUMO difference and V_{oc} and by assuming some maximum values for the FF and the EQE_{PV} , one can derive empirical maximum efficiency limits for organic donor/acceptor photovoltaic devices, in function of the energetic levels of the donor and the acceptor.^{27,50} However, a more fundamental maximum efficiency limit based on thermodynamic considerations should exist,⁵⁴ but it is not clear what this limit is for organic donor/acceptor photovoltaic devices.²⁷

Summarized, the questions addressed in this thesis are:

- (i) How does the CT state participate in photocurrent and photovoltage production?
- (ii) It is known that bulk heterojunction morphology plays a major role in polymer:fullerene solar cells. In particular, how do the morphological properties of the donor/acceptor blend affect the properties of the CT state?
- (iii) Which are ideal properties of the CTCs in order to maximize the power conversion efficiency? What is this maximum power conversion efficiency?

These questions are addressed with the aid of an innovative, highly sensitive technique to measure the photovoltaic EQE_{PV} spectrum, called Fourier-transform photocurrent spectroscopy (FTPS). The working principles of FTPS are described in chapter 3.

First, in chapter 2 we go deeper into the theory of black and grey bodies, in thermodynamic equilibrium and quasi-equilibrium. This theory makes abstraction of most of the internal processes inside the photovoltaic device and will allow us to relate CT bands present in the EQE_{PV} spectrum, to photovoltaic properties and to V_{oc} in particular.

Chapter 4 provides a guide to 6 of the papers, written in the framework of this Phd study. Reprints of the concerned papers can be found in the appendix. A summary of the thesis and an outlook for future research are given in respectively chapter 5 and chapter 6.

References

- 1 D. R. Kearns, M. Calvin, *J. Chem. Phys.* **29**, 950 (1958)
- 2 G. A. Chamberlain, *Sol. Cells* **8**, 47 (1983)
- 3 L. Sebastian, G. Weiser, *Phys. Rev. Lett.* **46**, 1156 (1981)
- 4 C. W. Tang, *Appl. Phys. Lett.* **48**, 183 (1986)
- 5 B. Rand, J. Genoe, P. Heremans, J. Poortmans, *Prog. Photovolt: Res. Appl.* **15**, 659 (2007)
- 6 N. S. Sariciftci, L. Smilowitz, A. J. Heeger, F. Wudl, *Science* **258**, 1474 (1992)
- 7 J.J.M. Halls, K. Pichler, R. H. Friend, S. C. Moratti, A. B. Holmes, *Appl. Phys. Lett.* **68**, 3120 (1996)
- 8 H. Hoppe, N. S. Sariciftci, *J. Mater. Res.* **19**, 1924 (2004)
- 9 W. Ma, C. Yang, X. Gong, K. Lee, A. J. Heeger, *Adv. Funct. Mater.* **15**, 1617 (2005)
- 10 J. Peet, J. Y. Kim, N. E. Coates, W. L. Ma, D. Moses, A. J. Heeger, G. C. Bazan, *Nature Mater.* **6**, 497 (2007)
- 11 S. H. Park, A. Roy, S. Beaupré, S. Cho, N. Coates, J. S. Moon, D. Moses, M. Leclerc, K. Lee, A. J. Heeger, *Nature Phot.* **3**, 297 (2009)
- 12 S. E. Shaheen, C. J. Brabec, N. S. Sariciftci, F. Padinger, T. Fromherz, J. C. Hummelen, *Appl. Phys. Lett.* **78**, 841 (2001)
- 13 T. Martens, J. D'Haen, T. Munters, Z. Beelen, L. Goris, J. Manca, M. D'Olieslaeger, D. Vanderzande, L. De Schepper, R. Andriessen, *Synt. Met.* **138**, 243 (2003)
- 14 F. Padinger, R. S. Rittberger, N. S. Sariciftci, *Adv. Funct. Mater.* **13**, 85 (2003)
- 15 M. Campoy-Quiles, T. Ferenczi, T. Agostinelli, P. G. Etchegoin, Y. Kim, T. D. Anthopoulos, P. N. Stavrinou, D. D. C. Bradley, J. Nelson, *Nature Mater.* **7**, 158 (2008)
- 16 M. M. Wienk, J. M. Kroon, W. J. Verhees, J. Knol, J. C. Hummelen, P. A. van Hal, R. A. J. Janssen, *Angew. Chem. Int. Ed.* **42**, 371 (2003)
- 17 S. C. Veenstra, J. Loos, J. M. Kroon, *Prog. Photovolt: Res. Appl.* **15**, 727 (2007)
- 18 J. Bouclé, P. Ravirajan, J. Nelson, *J. Mater. Chem.* **17**, 3141 (2007)
- 19 M. A. Green, K. Emery, Y. Hishikawa, W. Warta, *Prog. Photovolt: Res. Appl.* **17**, 320 (2009)

Chapter 1

- 20 C. J. Brabec, *Sol. En. Mater. Sol. Cells* **83**, 273 (2004)
- 21 C. J. Brabec, N. S. Sariciftci, J. C. Hummelen, *Adv. Funct. Mater.* **11**, 15 (2001)
- 22 H. Spangaard, F. Krebs, *Sol. Energy Mater. Sol. Cells* **83**, 125 (2004)
- 23 P. W. M. Blom, V. D. Mihailetchi, L. J. A. Koster, D. E. Markov, *Adv. Mater.* **19**, 1551 (2007)
- 24 S. Günes, H. Neugebauer, N. S. Sariciftci, *Chem. Rev.* **107**, 1324 (2007)
- 25 A. C. Mayer, S. R. Scully, B. E. Hardin, M. W. Rowell, M. D. McGehee, *Mater. Today* **10**, 28 (2007)
- 26 B. C. Thompson, J. M. J. Fréchet, *Angew. Chem. Int. Ed.* **47**, 58 (2008)
- 27 G. Dennler, M. Scharber, C. J. Brabec, *Adv. Mater.* **21**, 1323 (2009)
- 28 B. Kippelen, J.-L. Brédas, *Energy Environ. Sci.* **2**, 251 (2009)
- 29 G. Ruani, C. Fontanini, M. Murgia, C. Taliani, *J. Chem. Phys.* **116**, 1713 (2002)
- 30 Y. Wang, A. Suna, *J. Phys. Chem. B* **101**, 5627 (1997)
- 31 L. Goris, K. Haenen, M. Nesladek, P. Wagner, D. Vanderzande, L. de Schepper, J. d'Haen, L. Lutsen, J. V. Manca, *J. Mater. Sci.* **40**, 1413 (2005)
- 32 L. Goris, A. Poruba, L. Hod'akova, M. Vanecek, K. Haenen, M. Nesladek, P. Wagner, D. Vanderzande, L. de Schepper, J. V. Manca, *Appl. Phys. Lett.* **88**, 052113 (2006)
- 33 J. J. Benson-Smith, L. Goris, K. Vandewal, K. Haenen, J. V. Manca, D. Vanderzande, D. D. C. Bradley, J. Nelson, *Adv. Funct. Mater.* **17**, 451 (2007)
- 34 M. A. Loi, S. Toffanin, M. Muccini, M. Forster, U. Scherf, M. Scharber, *Adv. Funct. Mater.* **17**, 2111 (2007)
- 35 D. Veldman, O. Ipek, S. C. J. Meskers, J. Sweelssen, M. M. Koetse, S. C. Veenstra, J. M. Kroon, S. S. van Bavel, J. Loos, R. A. J. Janssen, *J. Am. Chem. Soc.* **130**, 7721 (2008)
- 36 K. Vandewal, A. Gadisa, W. D Oosterbaan, S. Bertho, F. Banishoeib, I. Van Severen, L. Lutsen, T. J. Cleij, D. Vanderzande, J. V. Manca, *Adv. Funct. Mater.* **18**, 2064 (2008)
- 37 M. Hallermann, S. Haneder, E. Da Como, *Appl. Phys. Lett.* **93**, 053307 (2008)
- 38 T. Drori, C. X. Sheng, A. Ndobe, S. Singh, J. Holt, Z. V. Vardeny, *Phys. Rev. Lett.* **101**, 037401 (2008)
- 39 K. Tvingstedt, K. Vandewal, A. Gadisa, F. L. Zhang, J. Manca, O. Inganäs, *J. Am. Chem. Soc.* **131**, 11819 (2009)

- 40 Y. Zhou, K. Tvingstedt, F. Zhang, C. Du, W.-X. Ni, M. R. Andersson, O. Inganäs, *Adv. Funct. Mater.* **19**, 3293 (2009)
- 41 I. Haelderms, K. Vandewal, W. D. Oosterbaan, A. Gadisa, J. D'Haen, M. K. Van Bael, J. V. Manca, J. Mullens, *Appl. Phys. Lett.* **93**, 223302 (2008)
- 42 C. G. Shuttle, A. Maurano, R. Hamilton, B. O'Regan, J. C. deMello, J. R. Durrant, *Appl. Phys. Lett.* **93**, 183501 (2008)
- 43 C. G. Shuttle, B. O'Regan, A. M. Ballantyne, J. Nelson, D. D. C. Bradley, J. R. Durrant, *Phys. Rev. B* **78**, 113201 (2008)
- 44 V. D. Mihailetchi, L. J. A. Koster, J. C. Hummelen, P. W. M. Blom, *Phys. Rev. Lett.* **93**, 216601 (2004)
- 45 D. Veldman, S. C. J. Meskers, R. A. J. Janssen, *Adv. Funct. Mater.* **19**, 1939 (2009)
- 46 H. Ohkita, S. Cook, Y. Astuti, W. Duffy, S. Tierney, W. Zhang, M. Heeney, I. McCulloch, J. Nelson, D. D. C. Bradley, J. R. Durrant, *J. Am. Chem. Soc.* **130**, 3030 (2008)
- 47 J.-L. Brédas, J. E. Norton, J. Cornil, V. Coropceanu, *Acc. Chem. Res.* ASAP (2009)
- 48 C. J. Brabec, A. Cravino, D. Meissner, N. S. Sariciftci, M. T. Rispens, L. Sanchez, J. C. Hummelen, T. Fromherz, *Thin Solid Films* **403**, 368 (2002)
- 49 Gadisa, M. Svensson, M. R. Andersson, and O. Inganas, *Appl. Phys. Lett.* **84**, 1609 (2004)
- 50 M. C. Scharber, D. Muhlbacher, M. Koppe, P. Denk, C. Waldauf, A. J. Heeger, and C. J. Brabec, *Adv. Mater.* **18**, 789 (2006)
- 51 V. D. Mihailetchi, P. W. M. Blom, J. C. Hummelen, and M. T. Rispens, *J. Appl. Phys.* **94**, 6849 (2003)
- 52 B. P. Rand, D. P. Burk, and S. R. Forrest, *Phys. Rev. B* **75**, 115327 (2007)
- 53 M. D. Perez, C. Borek, S. R. Forrest, M. E. Thompson, *J. Am. Chem. Soc.* **131**, 9281 (2009)
- 54 W. Shockley and H. J. Queisser, *J. Appl. Phys.* **32**, 510 (1961)

2 Black and grey bodies

This chapter reviews the theory used to describe the emission by black and non-black, "grey" bodies, in equilibrium and quasi-equilibrium. The concept of reciprocity between absorption and emission is introduced and applied to photovoltaic devices. With a generalized Planck law, we can describe the sun as a black body at 5762 K, but also the photovoltaic device as a grey body, at room temperature, at a certain potential. Maximum efficiency limits in this framework, for a material with a single optical gap, are derived.

2.1 Thermal radiation

In 1901 the era of quantum mechanics started by the derivation of a formula for thermal radiation of a black body (BB), by Max Planck. A BB is an idealized object that absorbs all incident electromagnetic radiation. It was derived that the energy density per photon energy interval dE , inside the BB is

$$e(E)dE = \frac{8\pi}{c^3 h^3} \frac{E^3}{\exp\left(\frac{E}{kT}\right) - 1} dE \quad (2-1)$$

The BB irradiance $I_{BB}(E)dE$ or energy per unit surface area, per unit time emitted into a hemisphere in a photon energy interval between E and $E+dE$, is given by

$$I_{BB}(E)dE = \frac{2\pi}{c^2 h^3} \frac{E^3}{\exp\left(\frac{E}{kT}\right) - 1} dE \quad (2-2)$$

BB radiation is also called thermal radiation, because both its intensity and spectrum are a function of the black body temperature T only. The total emitted radiation power per unit surface area is obtained by integrating expression (2-2) over all possible photon energies.

$$I_{BB}^{tot} = \sigma_{SB} T^4 \quad (2-3)$$

Hereby is σ_{SB} the Stefan-Boltzmann constant, equal to $5.67 \times 10^{-8} \text{ W m}^{-2} \text{ K}^{-4}$.

The above formulas may be extended to non-black, or grey bodies, having an absorptivity $A(E) < 1$. For such grey bodies, the irradiance per photon energy interval dE is equal to the product of $A(E)$ with the BB spectrum (2-2)

$$I(E)dE = \frac{2\pi}{c^2 h^3} \frac{A(E)E^3}{\exp\left(\frac{E}{kT}\right) - 1} dE \quad (2-4)$$

This law is known as Kirchoff's law of thermal radiation. The photon flux $\phi(E) = I(E) \cdot E^{-1}$ is given by

$$\phi(E)dE = \frac{2\pi}{c^2 h^3} \frac{A(E)E^2}{\exp\left(\frac{E}{kT}\right) - 1} dE \quad (2-5)$$

The above expressions give spectral irradiance power per photon energy interval dE . Sometimes it is useful to have an expression for the irradiance power per wavelength interval $d\lambda$. It should be taken into account that $E = hc\lambda^{-1}$, and $dE = hc \cdot \lambda^{-2} d\lambda$.

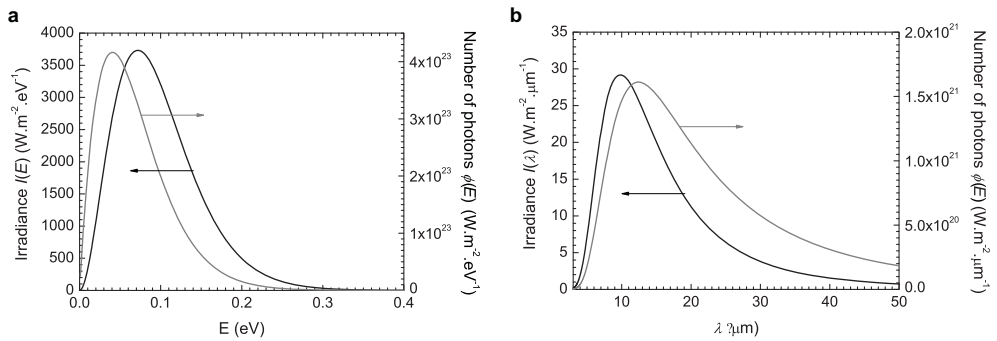


Figure 2-1: Black body spectra for a temperature of 300 K. Spectra are depicted for the photon energy scale (a) and for the wavelength scale (b). Graphs are shown for irradiance (right axis) as well as photon flux (left axis).

For a BB at 300 K, the irradiance $I_{BB}(E)$ and photon flux $\phi_{BB}(E)$ per photon energy interval, and $I_{BB}(\lambda)$ and $\phi_{BB}(\lambda)$ per wavelength interval are shown in Figure 2-1 (a) and (b) respectively. Note that $I_{BB}(E)$ peaks at a higher energy than $\phi_{BB}(E)$. At high photon energies, the emission spectra decrease exponentially.

2.2 Solar power

2.2.1 Solar temperature and total power

The sun can be considered as a black body at a temperature T_s and the power emitted by 1 m² of solar surface is equal to

$$I_s = \sigma_{SB} T_s^4 \quad (2-6)$$

The total power emitted by the sun is obtained by multiplying I_s with the total surface of the sun, a sphere with radius r_s . When this power reaches the surface of the earth, it is distributed over a larger sphere, with radius r_{s-e} . The incoming solar spectral irradiance in the vicinity of the earth I_e is thus diluted with respect to I_s

$$I_e = \frac{4\pi r_s^2}{4\pi r_{s-e}^2} I_s = \frac{r_s^2}{r_{s-e}^2} I_s \quad (2-7)$$

Using values for $r_s = 6.96 \times 10^8$ m and $r_{s-e} = 1.50 \times 10^{11}$, we obtain a dilution factor of 2.16×10^{-5} .

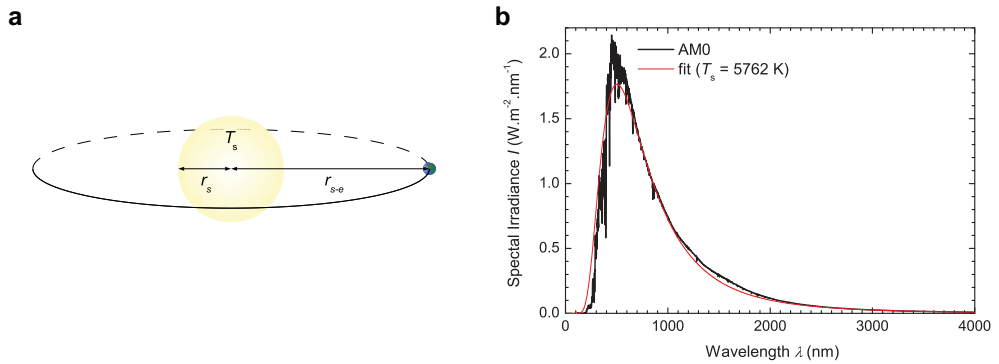


Figure 2-2: (a) The sun and the earth, with an indication of the relevant dimensions. (b) The spectral irradiance measured outside the earth's atmosphere (AM0), fitted with the expected spectral irradiance assuming the sun is a black body, taking into account the dilution factor. From the fit, a solar temperature of 5762 K can be obtained.

In Figure 2-2, the spectral irradiance from the sun, measured outside the earth's atmosphere is depicted. It is called the Air Mass 0 (AM0) spectrum. If the dilution factor of 2.16×10^{-5} is taken into account, this spectrum can be fitted with a black body spectrum, at a temperature

$$T_s = 5762 \text{ K} \quad (2-8)$$

This is the temperature of the surface of the sun. The temperature in the core of the sun is much higher, about 16×10^6 K.¹ The amount of solar power received by the earth can be calculated by equation (2-6), or by integrating the AM0 spectrum over all possible wavelengths. This value is standardized and is called the solar constant.²

$$I_e = 1366.1 \text{ W.m}^{-2} \quad (2-9)$$

This is the average amount of radiation power generated by the sun and received by the earth, under the assumption that the orbit of the earth around the sun is a circle. The term solar constant is somewhat misleading in the sense that in reality, the orbit of the earth around the sun is elliptical and I_e varies from a maximum value of 1412 W.m^{-2} in January to a minimum value of 1321 W.m^{-2} in July.³

The photon flux I_e is a source of costless energy. The difficulty lies in converting this radiation into directly usable or storable, electrical power. This power conversion process is expected to have losses. We will look into this specifically in paragraph 0.

2.2.2 Standard solar spectra

About 1366.1 W.m^{-2} of power is available just outside the earth's atmosphere. When passing through the atmosphere, it will be reduced and the solar irradiance spectrum will change as a cause of the selective absorption by atmospheric gasses in certain wavelength regions. For the equator region this results in the Air Mass 1 (AM1) spectrum. For northern-Europe and United States, a 1.5 times longer distance must be traveled by the sunlight (Figure 2-3 (a)). For these regions two standards are available, termed "Air Mass 1.5 direct" (AM1.5) and "Air Mass 1.5 global" (AM1.5g).⁴

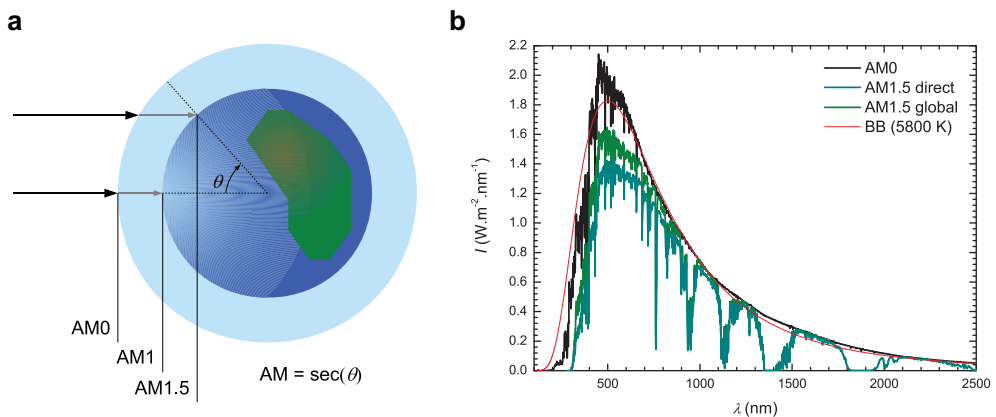


Figure 2-3: (a) Illustration of the air masses AM0, AM1 and AM1.5. For AM1, 1 atmospheric distance is traveled by the light. For AM1.5, 1.5 times the atmospheric distance is traveled. This corresponds to $\theta = 48.2^\circ$. (b) AM0, AM1.5 and AM1.5g standard spectra. The total power is respectively 1366 W.m^{-2} , 902 W.m^{-2} and 1000 W.m^{-2} . The AM1.5g spectrum also takes into account diffusively scattered light by the earth's atmosphere.

The total power contained in the AM1.5 spectrum is $902 \text{ W}\cdot\text{m}^{-2}$, originating only from direct solar illumination. In the AM1.5g spectrum, the diffusively scattered light by the earth's atmosphere is also taken into account. The total power contained in AM1.5g spectra is $1000 \text{ W}\cdot\text{m}^{-2}$. The AM1.5g standard is used as the standard in all photovoltaic measurements discussed in this thesis. In the IMO-UHasselt lab, a class A solar simulator, mimicking this standard is available.⁵

2.3 Generalized radiation

2.3.1 Chemical potential

In paragraph 2.1, laws for thermal emission were given. They can be successfully used to describe the radiation emitted by the surface of the sun (see paragraph 2.2). However, the "grey" body laws can be used for any given, arbitrary material, including materials used in solar cells. These materials have a temperature around 300 K, and with known absorptivity $A(E)$, their equilibrium thermal emission can be calculated via equation (2-4) or (2-5).

Under illumination, or when an electric current is injected however, the solar cell is not in equilibrium anymore. Under modestly low illumination intensities or injection conditions, a quasi-equilibrium approach can be used. Therefore, for systems in quasi-equilibrium, the concept of a chemical potential difference can be used.

Consider an absorbing molecule or molecular complex. Upon absorption of light, the ground states of the molecules M are converted to excited states M^*



The chemical potentials μ^M and μ^{M^*} respectively of M and M^* are

$$\mu^M = \mu_0^M + kT \ln[M] \quad (2-11)$$

$$\mu^{M^*} = \mu_0^{M^*} + kT \ln[M^*] \quad (2-12)$$

The bracketed quantities are molecular fractions, proportional to the concentration of each species. In such expressions, the second term involving the natural logarithm of the molecular fraction is purely entropic ("entropy of mixing", related to the probability to encounter M or M^*). The first term (standard potential with subscript '0') reflects molecular properties of M or M^* (their intrinsic molecular free energy).

At equilibrium, the concentrations of M and M^* adjust so that the chemical potentials are equal:

$$\frac{[M^*]}{[M]} = \exp\left(-\frac{\mu_0^{M^*} - \mu_0^M}{kT}\right) = \exp\left(-\frac{E_g}{kT}\right) \quad (2-13)$$

Hereby is $E_g = \mu_0^{M^*} - \mu_0^M$ the energy of the electronic transition from M to M^* .

If M and M^* are not at equilibrium the free energy which can be retrieved when converting M into M^* equals

$$\mu = \mu^{M^*} - \mu^M = E_g + kT \ln \frac{[M^*]}{[M]} \quad (2-14)$$

Rewriting gives us

$$\frac{[M^*]}{[M]} = \exp\left(-\frac{E_g - \mu}{kT}\right) \quad (2-15)$$

The chemical potential difference μ can be seen as the potential difference driving the reaction $M \rightarrow M^*$. In general, $\mu \neq E_g$ but it depends via equation (2-15) logarithmically on the steady-state fraction of M^* that can be sustained.

2.3.2 Würfel's generalized radiation law

Würfel derived a generalized Planck law, for materials at a chemical potential $\mu > 0$.⁶ Consider a material with an energetic difference E between the ground state M and excited state M^* . Possible electronic transitions are depicted schematically in Figure 2-4.

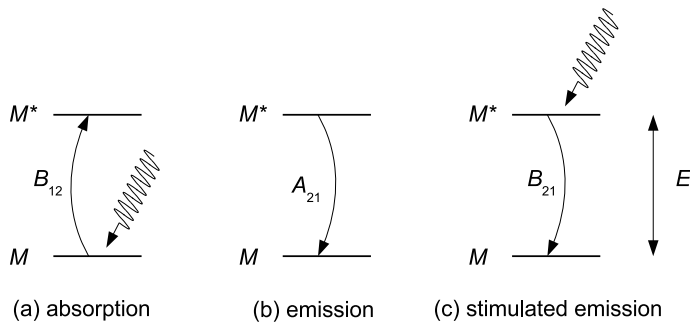


Figure 2-4: Possible electronic transition between ground state M and excited state M^* , with energetic difference E . (a) Absorption, proportional to the radiation energy at E and the number of ground states $[M]$. (b) Emission, proportional to the number of excited states $[M^*]$. (c) Stimulated emission, proportional to the radiation energy at E and the number of excited states $[M^*]$.

The number of absorbed photons is proportional to the total radiation energy $e(E)$ at photon energy E and the number of ground states $[M]$. The number of spontaneously emitted photons is proportional to the number of excited states $[M^*]$ only. The number of emitted photons by stimulated emission is proportional to both $[M^*]$ and $e(E)$. The proportionality constants A_{12} , B_{12} and B_{21} are called the Einstein A and B constants. Emission and stimulated emission will result in an increase in ground states, while absorption will result in a decrease of ground state molecules:

$$\frac{d[M]}{dt} = A_{21}[M^*] - B_{12}e(E)[M] + B_{21}e(E)[M^*] \quad (2-16)$$

Since in equilibrium, the relative populations of each level remain constant, absorption and emission events balance, and the rate equation (2-16) is equal to zero. We can then solve expression for the spectral density at the given frequency.

$$e(E) = \frac{A_{21} \frac{[M]}{[M^*]} - B_{21}}{B_{12} \frac{[M]}{[M^*]} - B_{21}} = \frac{A_{21}}{B_{12} \exp\left(\frac{E - \mu}{kT}\right) - B_{21}} \quad (2-17)$$

Hereby it was taken into account that the ratio $[M^*]/[M]$ of the populations in the two levels is given by equation (2-15).

In complete thermal equilibrium ($\mu=0$) the spectral density must match the Planck energetic density formula (2-1).

$$8\pi \frac{E^3}{h^3 c^3} \frac{1}{\exp\left(\frac{E}{kT}\right) - 1} = \frac{A_{21}}{B_{12} \exp\left(\frac{E}{kT}\right) - B_{21}} \quad (2-18)$$

And we can find the following relation between the A and B coefficients, called the Einstein relations:

$$B_{12} = B_{21} \quad (2-19)$$

$$A_{21} = 8\pi \frac{E^3}{h^3 c^3} B_{12} \quad (2-20)$$

Under quasi-equilibrium conditions, equation (2-17) is valid. Quasi-equilibrium further assumes that the Einstein relations (2-19), (2-20) and kirchoff's law of thermal radiation remain valid under application of a chemical potential μ . A generalized Planck law for materials at a temperature T , with an absorptivity $A(E)$ and at chemical potential μ can then be obtained by combining these laws:

$$I_{BB}(E, \mu) = \frac{2\pi}{c^2 h^3} \frac{E^3}{\exp\left(\frac{E - \mu}{kT}\right) - 1} \quad (2-21)$$

Taking into account Kirchoff's law of thermal radiation we get:

$$I(E, \mu) = \frac{2\pi}{c^2 h^3} \frac{A(E)E^3}{\exp\left(\frac{E - \mu}{kT}\right) - 1} \quad (2-22)$$

If $E - \mu \gg kT$, expression (2-22) can be approximated by

$$I(E, \mu) = \frac{2\pi}{c^2 h^3} A(E)E^3 \exp\left(-\frac{E}{kT}\right) \exp\left(\frac{\mu}{kT}\right) \quad (2-23)$$

2.3.3 Reciprocity relation between absorption and emission

The Einstein relations (2-19) and (2-20) imply a reciprocity between absorption and emission events for material in (quasi-) equilibrium. The A_{21} coefficient is after all, also the emission rate constant, and $1/A_{21}$ is the natural lifetime of the excited states M^* . This means, that in the absence of other non-radiative recombination processes, the decay of excess excited states, induced by, for example a light pulse, is described by (see Figure 2-4 (b))

$$\frac{d[M^*]}{dt} = -A_{21}[M^*] \quad (2-24)$$

This is a differential equation with as solution

$$[M^*] = A \exp(-A_{21}t) + [M^*]_0 \quad (2-25)$$

Hereby is $[M^*]_0$ the dark equilibrium concentration of excited states. If other, non-radiative recombination processes are present in the device, the real lifetime τ is always smaller than τ_{rad} .

$$\tau^{-1} = \tau_{rad}^{-1} + \tau_{non-rad}^{-1} \quad (2-26)$$

One can also show that the B_{12} coefficient is related to the absorption cross-section σ_a .⁷

$$\sigma_a = \frac{EB_{12}}{c} \quad (2-27)$$

Hereby is σ_a related to the absorption coefficient α ⁷

$$\alpha = \sigma_a [M] \quad (2-28)$$

σ_a is thus also related to the emission rate A_{21}

$$A_{21} = 8\pi \frac{E^2}{h^3 c^2} \sigma_a \quad (2-29)$$

This important reciprocity relation implies that an absorbing molecule will always emit light at a rate proportional to its absorption cross-section σ_a . This means that strongly absorbing molecules, with *high* σ_a , will unavoidably be also *fast* emitters, causing a *fast* decay of excited states. This has major implications for solar cells: in order to have sufficient light absorption in a thin film, a *high* σ_a is needed. However, for the excited molecule to be dissociated into free carriers which are then transported effectively to the electrodes, *low* decay or emission rates and thus *low* σ_a are requested. These contradicting requirements make the fabrication of thin film, organic photovoltaic devices, very challenging. The rather large exciton binding energy causes the dissociation rate to be much lower than the decay rate, in these strongly absorbing materials.

2.4 Application to photovoltaics

2.4.1 Reciprocity between photovoltaic and electroluminescent actions

In the previous paragraph 2.3.3, it is shown that a reciprocity relation between absorption and emission events can be derived. This means that absorption and emission are closely related processes, and that a light absorbing material, must also emit light (Figure 2-5). Applied to photovoltaic devices, a reciprocity relation relating the photovoltaic actions of a solar cell with its electroluminescent actions, could be derived by Rau.⁸ In this paragraph an intuitive derivation of this relation will be presented.

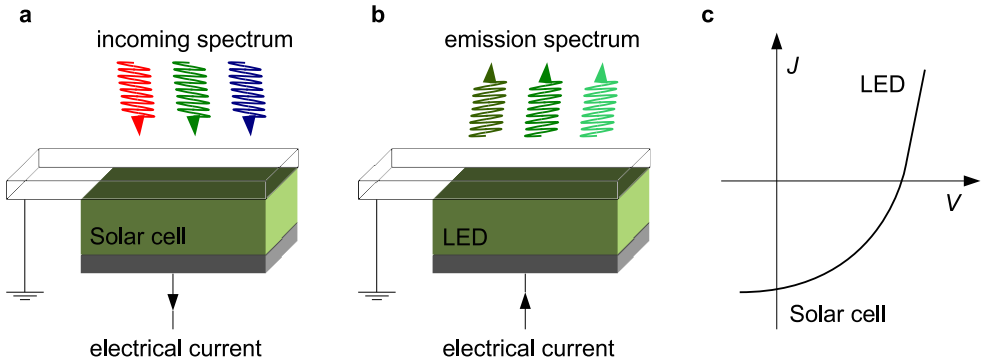


Figure 2-5: A material sandwiched between electrodes can be regarded as (a) a solar cell or (b) an LED, depending on the applied voltage. (c) Under injection conditions the device operates as a LED. At low and negative voltages, current is extracted and the device works as a solar cell. The photovoltaic and electroluminescent actions are connected via the reciprocity relation (2-34).

Consider a photovoltaic device with an external quantum efficiency $EQE_{PV}(E)$. This means that per incident photon of photon energy E , $EQE_{PV}(E)$ free electrons are created and collected at the electrodes. The free charge carrier generating state cannot distinguish between photons which are coming from the sun, a black body at 5762 K, or the environment, a black body at temperature T , about 300 K. So even in the dark, at an equilibrium temperature of 300 K, free electrons are created at a rate

$$EQE_{PV}(E)\phi_{BB}(E) \quad (2-30)$$

Following the principle of detailed balance, in equilibrium, no net free electron build up can occur, and no net energy from the environment can be absorbed, for every photon energy E . Thus the creation of free electrons must be counter balanced by the inverse process, the decay of charge carrier pairs by a radiation flux $\phi(E, \mu = 0)$.

$$\phi(E, 0) = EQE_{PV}(E)\phi_{BB}(E) \quad (2-31)$$

Let $[M^*]_0$ denote the number of excited states that is sustained in the dark equilibrium, and $[M^*]$ the number of excited states in quasi-equilibrium under application of a chemical potential. $[M^*]$ and $[M^*]_0$ are related by (paragraph 2.3)

$$[M^*] = [M^*]_0 \exp\left(\frac{\mu}{kT}\right) \quad (2-32)$$

The chemical potential μ of a free charge carrier generating state equals qV , with q the elementary charge. In quasi-equilibrium, thus, $[M^*]$ states instead of $[M^*]_0$ states recombine. This affects the number of emitted photons, which is proportional to the number of excited states:

$$\phi(E, V) = \phi(E, 0) \exp\left(\frac{qV}{kT}\right) \quad (2-33)$$

The net emitted photon flux is equal to the difference between the emitted photon flux (equation (2-33)) and the absorbed photon flux (equation (2-31))

$$\phi(E, V) = EQE_{PV}(E) \phi_{BB}(E) \left(\exp\left(\frac{qV}{kT}\right) - 1 \right) \quad (2-34)$$

If qV and $E \gg kT$ this can be approximated by

$$\phi(E, V) = \frac{2\pi}{c^2 h^3} EQE_{PV}(E) E^2 \exp\left(-\frac{E}{kT}\right) \exp\left(\frac{qV}{kT}\right) \quad (2-35)$$

For the irradiance $I(E, V) = E \cdot \phi(E, V)$ we get

$$I(E, V) = \frac{2\pi}{c^2 h^3} EQE_{PV}(E) E^3 \exp\left(-\frac{E}{kT}\right) \exp\left(\frac{qV}{kT}\right) \quad (2-36)$$

Note the resemblance between this equation and Würfel's generalized Planck law, equation (2-23). One can use Würfel's law to derive the **emission** spectrum under **chemical** potential μ from $A(E)$. With the knowledge of $EQE_{PV}(E)$, however, one can use the law (2-35) or (2-36) to derive the **electroluminescence** emission spectrum under application of an **electrical** potential V .

A more rigorous proof of the above equation (2-34) can be found in ref 8. Possible breakdown of this relation for p-i-n junction solar cells is discussed in ref 9. This breakdown originates from non-linearity in the transport of free carriers in such devices. However, deviations from equation (2-34) for practical devices were found to be within one order of magnitude.

2.4.2 J-V curves from electro-optical measurements

a Dark J-V curves

It is now possible to relate the J-V curves of a general photovoltaic device in the dark and under illumination to the electro-optical measurable quantities EQE_{PV} and EQE_{EL} . Starting with the dark J-V curve, light emission via

electroluminescence will, as a consequence of reciprocity, occur in every photovoltaic material. The total emitted photon flux $\phi(V)$ as a function of the applied voltage V can be calculated by integrating equation (2-34):

$$\phi(V) = \int EQE_{PV}(E)\phi_{BB}(E)dE \left(\exp\left(\frac{qV}{kT}\right) - 1 \right) \quad (2-37)$$

This photon flux is caused by the non-geminate recombination of free charge carriers. However, not every recombination event results in the emission of a photon. By definition, only a fraction EQE_{EL} of the injected free carriers will recombine radiatively. The current $J_{inj}(V)$ which thus must be injected to sustain the emitted photon flux given by equation (2-37) is

$$J_{inj}(V) = qEQE_{EL}^{-1} \int EQE_{PV}(E)\phi_{BB}(E)dE \left(\exp\left(\frac{qV}{kT}\right) - 1 \right) \quad (2-38)$$

Schematically, the above described process is shown on the right hand side of Figure 2-6. Equation (2-38) can also be written as

$$J_{inj}(V) = J_0 \left(\exp\left(\frac{qV}{kT}\right) - 1 \right) \quad (2-39)$$

with J_0

$$J_0 = \frac{q}{EQE_{EL}} \int_0^{+\infty} EQE_{PV}(E)\phi_{BB}(E)dE \quad (2-40)$$

Using the expression for the black body spectrum, we get

$$J_0 = \frac{q}{EQE_{EL}} \int_0^{+\infty} \frac{2\pi}{c^2 h^3} EQE_{PV}(E) E^2 \exp\left(-\frac{E}{kT}\right) dE \quad (2-41)$$

Note that equation (2-39) represents a diode equation, derived without using any formula assuming that a classical p-n junction is present in the device. Note that EQE_{EL} can in principle depend on the charge density and thus on the applied voltage. This causes the introduction of the so called ideality factor n (see also paper D). Usually dark J - V curves of organic solar cells can be fitted in with a diode equation in the low voltage region. At higher voltages, space charge and resistive effects can play a role.

Note that for the calculation of J_0 via equation (2-41), the low energy region of the $EQE_{PV}(E)$ spectrum is crucial. Therefore the use of sensitive techniques to explore this spectral region is motivated. In this work, with the aid of the FTPS

technique described in chapter 3, the validity of the above reciprocity relation for polymer:fullerene solar cells will be shown in paper C.

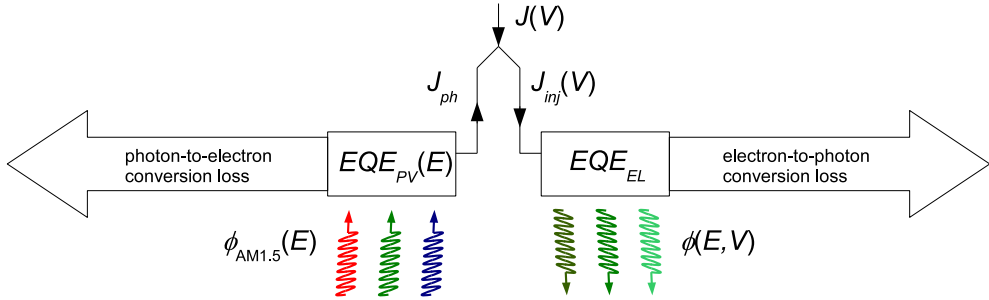


Figure 2-6: Schematic representation of the relation between photovoltaic J-V curves and the electro-optical measurable quantities EQE_{PV} and EQE_{EL} . The total current $J(V)$ under application of a voltage V of a photovoltaic device can be seen as the sum of an injected current J_{inj} causing radiative recombination at an efficiency EQE_{EL} and a photo-generated current J_{ph} originating from the conversion of photons to electrons at an efficiency EQE_{PV} .

b J-V curves under illumination

Upon illumination, the total current versus voltage curve of the photovoltaic device is the sum of the photogenerated current and the injected current, taking into account the right direction of the two currents (Figure 2-6).

$$J(V) = J_{inj}(V) - J_{ph} = J_0 \left(\exp\left(\frac{qV}{kT}\right) - 1 \right) - J_{ph} \quad (2-42)$$

Next to J_0 (previous section), J_{ph} can be calculated under solar conditions with the knowledge of the $EQE_{PV}(E)$ spectrum:

$$J_{ph} = q \int_0^{+\infty} EQE_{PV}(E) \phi_{AM1.5}(E) dE \quad (2-43)$$

In general, EQE_{PV} takes into account optical losses, transport losses and losses due to geminate recombination.

For polymer:fullerene solar cells, the field dependent dissociation of geminate CT states causes EQE_{PV} and J_{ph} to depend on voltage (Figure 2-7).^{10,11} If we denote $EQE_{PV}^0(E)$ the $EQE_{PV}(E)$ spectrum measured at short circuit, and assume that the spectral shape of the $EQE_{PV}(E)$ spectrum does not change with applied voltage, we can write

$$EQE_{PV}(E) = \gamma(V) EQE_{PV}^0(E) \quad (2-44)$$

Hereby does $\gamma(V)$ depend on V only, with $\gamma(0) = 1$. In paper G it is shown that the spectral shape of $EQE_{PV}(E)$, even in the low energy CT region, indeed does not change with changing V . It follows:

$$J_{ph} = \gamma(V)J_{sc} \quad (2-45)$$

In reference 10 and 11, the voltage dependence of $\gamma(V)$ for MDMO-PPV:PCBM devices is described using the Onsager-Braun theory of field dependent geminate ionic pair dissociation.¹²

Figure 2-7 schematically represents a J-V curve in the dark and under illumination conditions. It is indicated in the figure in which region the curve is dominated by geminate recombination and in which region it is dominated by non-geminate recombination.

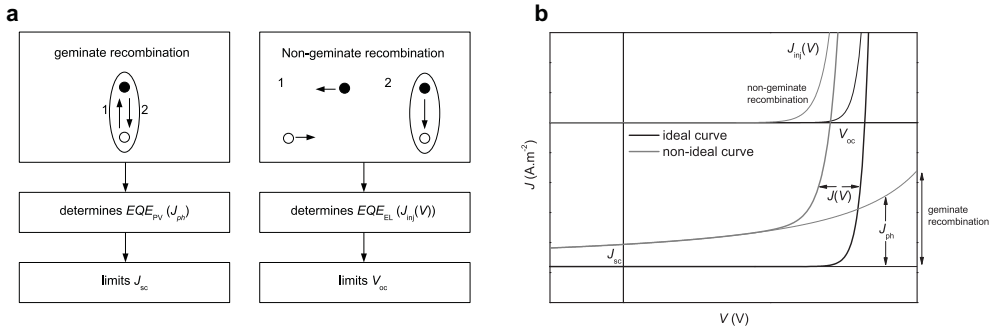


Figure 2-7: (a) Schematic clarification of the difference between geminate and non-geminate recombination. Geminate recombination affects J_{sc} , while V_{oc} is affected by non-geminate recombination. (b) The J - V curve under dark conditions and under illumination. The black curve represents the absence of geminate recombination and a low non-geminate recombination rate. For the grey curves a field dependent, geminate pair dissociation and a higher non-geminate recombination rate is assumed. The dark curve is given by equation (2-39), the photocurrent by equation (2-43). The full J - V curve under illumination is given by equation (2-42).

c Short-circuit current and open-circuit voltage

At short-circuit, $J_{sc} = J_{ph}(V=0)$ and

$$J_{sc} = \gamma(0)q \int_0^{+\infty} EQE_{PV}(E) \phi_{AM1.5}(E) dE \quad (2-46)$$

At open circuit, $J(V_{oc}) = J_{inj}(V_{oc}) - J_{ph}(V = V_{oc}) = 0$. It follows from equation (2-42)

$$V_{oc} = \frac{kT}{q} \ln \left(\frac{J_{ph}(V = V_{oc})}{J_0(V = V_{oc})} + 1 \right) \quad (2-47)$$

As both J_{ph} and J_0 are proportional to EQE_{PV} (equation (2-43) and (2-40)), they are also both proportional to $\chi(V)$. As $\chi(V)$ is the only term containing V , the ratio $J_{ph}(V)/J_0(V)$ is thus the same, independent on which voltage V it is evaluated, therefore

$$V_{oc} = \frac{kT}{q} \ln \left(\frac{J_{sc}}{J_0} + 1 \right) \quad (2-48)$$

With J_{sc} and J_0 given by equations (2-43) and (2-40) with herein $EQE_{PV}(E)$ measured under short-circuit conditions.

2.4.3 The Shockley-Queisser maximum efficiency limit

In 1961 W. Shockley and H. Queisser calculated a maximum efficiency limit for single absorber, single junction photovoltaic devices, in a seminal paper.¹³ They used an approach similar to the one described above and made the following assumptions about the ideal photovoltaic material:

- (i) There is perfect absorption of photons with an energy higher than the bandgap E_g , with each photon creating exactly one electron/hole pair.
- (ii) Collection of charge carriers is perfect
- (iii) Radiative recombination is the only allowed recombination mechanism. Non-geminate recombination is absent.

The only properties used to describe this idealized photovoltaic material are its bandgap E_g and its temperature T . Assumptions (i)-(iii) imply that EQE_{PV} is 0 below E_g and 1 above E_g . Assumption (iii) implies $EQE_{EL} = 1$.

From these assumptions we can calculate the maximum J_{sc} , minimum J_0 and maximum V_{oc} under solar illumination conditions via equations (2-43), (2-41) and (2-48).

$$J_{sc}^{\max} = q \int_{E_g}^{+\infty} \phi_{AM1.5}(E) dE \quad (2-49)$$

$$J_0^{\min} = q \int_{E_g}^{+\infty} \frac{2\pi}{c^2 h^3} E^2 \exp\left(-\frac{E}{kT}\right) dE \approx \frac{2\pi q}{c^2 h^3} E_g^2 kT \exp\left(-\frac{E_g}{kT}\right) \quad (2-50)$$

$$V_{oc}^{\max} \approx \frac{E_g}{q} + \frac{kT}{q} \ln \left(\frac{c^2 h^3 J_{sc}^{\max}}{2\pi q E_g^2 kT} \right) \quad (2-51)$$

The J - V curve is described by

$$J(V) = J_0^{\min} \left(\exp \left(\frac{qV}{kT} \right) - 1 \right) - J_{sc}^{\max} \quad (2-52)$$

Maximum power $P = J \cdot V$ occurs when

$$\frac{d(JV)}{dV} = 0 \quad (2-53)$$

This gives a relation between V_{oc} and the voltage V_m at which the maximum power is obtained.

$$\frac{qV_{oc}^{\max}}{kT} = \frac{qV_m}{kT} + \ln \left(1 + \frac{qV_m}{kT} \right) \quad (2-54)$$

If V_{oc} is known, this relation must be numerically solved in order to obtain V_m . We can now numerically calculate the FF under these conditions. It is a function of V_m only. Knowledge of the maximum J_{sc} , V_{oc} and the corresponding FF allows calculation of the maximum attainable efficiency η_{\max} of a single absorber, single junction photovoltaic device in function of the bandgap E_g . This is shown in Figure 2-8.

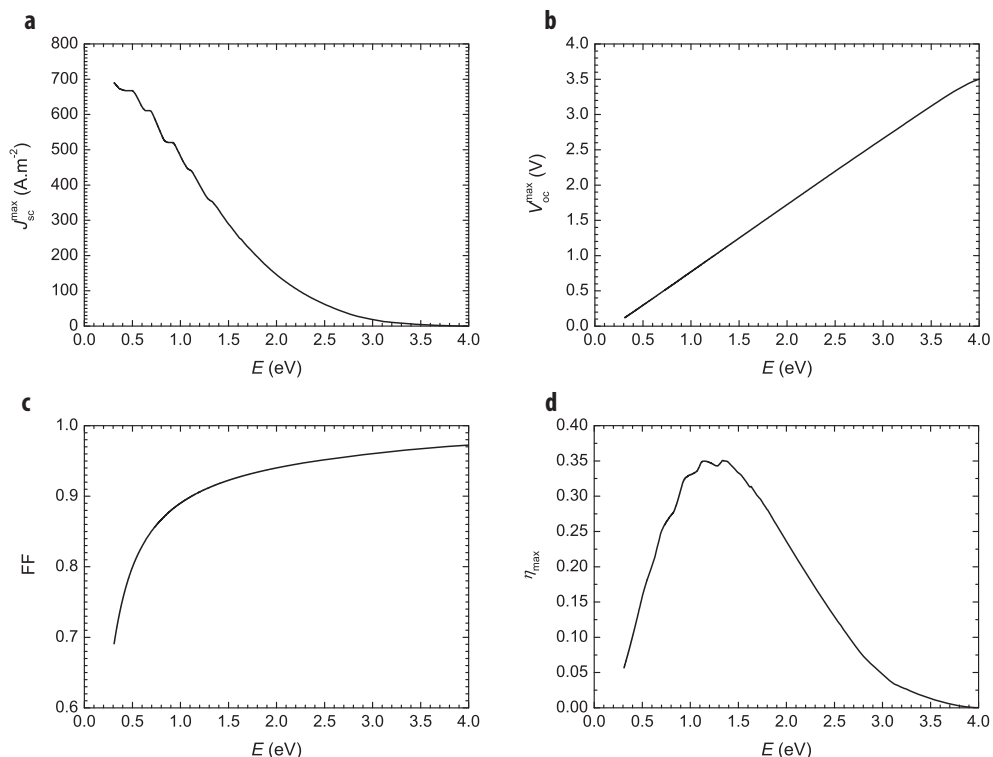


Figure 2-8: The Shockley-Queisser limit for (a) the short circuit-current, (b) the open-circuit voltage, (c) the fill factor and (d) the power conversion efficiency. Maximum efficiency is obtained for a bandgap between 1.1 and 1.4 eV.

The maximum efficiency of this idealized photovoltaic device under standardized solar illumination is obtained in the range $1.1 \text{ eV} < E_g < 1.4 \text{ eV}$. For $E_g < 1.1 \text{ eV}$, a high J_{sc} can be achieved, but at the cost of a low V_{oc} . High V_{oc} can be achieved if $E_g > 1.4 \text{ eV}$, however this will unavoidably result in low J_{sc} . Note that V_{oc} varies linearly with qE_g in the 0.5 - 3.5 V range, but that it is even under these ideal conditions not equal to qE_g . The difference between both is about 0.25-0.30 V.

A similar calculation, under similar assumptions can be made for the maximum obtainable photovoltaic parameters for organic donor/acceptor based solar cells. Hereby the maximum efficiency is not a function of the bandgap of the main absorber only, but also a function of CT state properties. This is described in paper E.¹⁴

References

- 1 Information about the sun can be found online, in the form of a sun fact sheet at: <http://nssdc.gsfc.nasa.gov/planetary/factsheet/sunfact.html>
- 2 The AM0 solar spectrum and more information about it can be found at: <http://rredc.nrel.gov/solar/spectra/am0/>
- 3 Information about the solar constant can be obtained, for example at: <http://en.wikipedia.org/wiki/Sunlight>
- 4 The AM1.5 and AM1.5g solar spectrum and more information about them can be found at: <http://rredc.nrel.gov/solar/spectra/am1.5/>
- 5 Information about the solar simulator used in this work is available online: http://www.newport.com/file_store/Supporting_Documents/e5712_Oriel-Class-A-Solar-Simulators.pdf
- 6 P. Würfel, *J. Phys. C: Solid state Phys.* **15**, 3967 (1982)
- 7 R. C. Hilborn, *Am. J. Phys.* **50**, 982 (1982), can be found online at: <http://arxiv.org/ftp/physics/papers/0202/0202029.pdf>
- 8 U. Rua, *Phys. Rev. B* **76**, 085303 (2007)
- 9 T. Kirchartz, U. Rau, *phys. stat. sol. (a)* **205**, 2737 (2008)
- 10 V. D. Mihailetchi, L. J. A. Koster, J. C. Hummelen, P. W. M. Blom, *Phys. Rev. Lett.* **93**, 216601 (2004)
- 11 P. W. M. Blom, V. D. Mihailetchi, L. J. A. Koster, D. E. Markov, *Adv. Mater.* **19**, 1551 (2007)
- 12 C. L. Braun, *J. Chem. Phys.* **80**, 4157 (1984)
- 13 W. Shockley, H. J. Queisser, *J. Appl. Phys.* **32**, 510 (1961)
- 14 K. Vandewal, A. Gadisa, K. Tvingstedt, O. Inganäs, J. V. Manca, unpublished (2009)

3 Fourier-Transform Photocurrent Spectroscopy

This chapter focuses on the working principles of the fast and highly sensitive technique named Fourier-Transform Photocurrent Spectroscopy (FTPS). In contrast to the classical monochromatic techniques, is FTPS a dispersive technique, meaning that the sample is illuminated by light of several photon-energies at the same time. The different methods for obtaining a spectrum by a monochromatic or dispersive technique are explained and summarized in this chapter. Two modes of FTPS are discussed, the continuous scan mode (CS-FTPS) and the amplitude modulated step scan mode (AM-FTPS). For CS-FTPS, a correction procedure for the correct interpretation of the CS-FTPS measurements as photocurrent spectra is described.

3.1 Introduction

Fourier-Transform Photocurrent Spectroscopy (FTPS) is a very powerful technique, able to measure EQE_{PV} and photocurrent spectra of photovoltaic devices over several orders of magnitude. This high sensitivity is sufficient to detect new absorption features below the optical gap of the investigated photovoltaic material. One of the goals in this work is to implement this technique and apply it to organic photovoltaic devices.

The ordinate axis of the graphs produced by FTPS will always be in units of photon energy E , wavelength λ or wavenumber σ . It is useful to be able to quickly recalculate from one of these units to the other. Therefore the relation between these quantities is given in Table 3-1. Usually, E is given in the unit eV, λ in nm and σ in cm^{-1} .

Table 3-1: Relations between E , λ and σ .

$E = h \frac{c}{\lambda}$	$E = hc\sigma$	$\sigma = \frac{1}{\lambda}$
$E[\text{eV}] = \frac{1240}{\lambda[\text{nm}]}$	$E[\text{eV}] = \frac{\sigma[\text{cm}^{-1}]}{8065}$	$\sigma[\text{cm}^{-1}] = \frac{10^7}{\lambda[\text{nm}]}$

Classically, spectral resolution of a quantity, such as photocurrent, EQE_{PV} or absorption into one of the units above, occurs by a *monochromatic* technique. In this case, the quantity is measured separately for each photon energy in the spectral region of interest. However, a more innovative and sensitive way of obtaining spectral information is to make use of so called *dispersive* techniques. In these techniques, light containing all photon energies of interest, is used to illuminate the sample. Spectral information is obtain by a special modulation of this white light. FTPS is an example of such a dispersive technique. Before the

working principle of FTPS is addressed in paragraph 3.3 , first a comparison of the working principles of monochromatic and dispersive techniques is made in the following paragraph 3.2.

3.2 Monochromatic versus dispersive techniques

The simplest and most intuitive way to spectrally resolve a quantity is to illuminate a sample or photovoltaic device with monochromatic light, perform a measurement of the quantity, and then scan to the next wavelength. In order to obtain such a monochromatic light beam, a white light source is used to illuminate a diffraction grating which unweaves the white light into a rainbow of colors (see figure in Table 3-2). With the aid of a slit, the right wavelength is selected. With a band pass filter, higher order diffracted wavelengths are filtered out. Due to the size of the slit, the selection of exactly one photon energy is never perfect. A spectral band, of certain bandwidth, centered on the wavelength of interest is transmitted through the system. The spectral resolution $\Delta\lambda$ is proportional to the width of the slit. However, the total amount of power which passes through the monochromating system is also proportional to the slit width. The use of a monochromator thus results in an exchange between spectral resolution and signal to noise ratio.

This can in particular be a problem when one wants to spectrally resolve very sharp peaks due to molecular vibrations or rotations in the infrared. The dispersive technique, Fourier-transform infrared spectroscopy (FTIR), based on an interferometer instead of a monochromator, provides a solution to this problem. In this technique, a white light source illuminates a Michelson interferometer.¹ In the interferometer, the light beam is split into two by a beamsplitter. A path length difference $\delta=2d$ between the beams is created, before both beams are joined back together (see figure in Table 3-2). Depending on δ , constructive or destructive interference occurs, and the intensity of the throughput light for a given wavenumber σ is

$$s(\sigma)(1 + \cos(2\pi\sigma\delta)) \quad (3-1)$$

Hereby is $s(\sigma)$ the input white light irradiance spectrum. When this intensity is measured by a detector with a response $d_{PC}(\sigma)$, the photocurrent $I(\delta)$ measured by the detector is

$$I(\delta) = \int_0^{+\infty} d_{PC}(\sigma) s(\sigma) (1 + \cos(2\pi\sigma\delta)) d\sigma \quad (3-2)$$

This is a Fourier cosine transform. The inverse Fourier-transform of the measured interferogram $I(\delta)$ gives us our desired result $d_{PC}(\sigma)s(\sigma)$.

$$d_{PC}(\sigma)s(\sigma) = 4 \int_0^{+\infty} \left(I(\delta) - \frac{1}{2} I(0) \right) \cos(2\pi\sigma\delta) d\delta \quad (3-3)$$

However, practically the integral in equation (2-3) cannot be calculated exactly. It will be approximated by a summation of values taken at intervals $\Delta\delta$. Furthermore, there will be a maximum mirror distance $\delta_{\max} < +\infty$. Both restrictions will have consequences for the maximum obtainable spectral bandwidth and resolution.

The result of the finite resolution $\Delta\delta$ is that only signals with a finite spectral bandwidth σ_{\max} can be exactly measured.²

$$\sigma_{\max} = \frac{1}{2\Delta\delta} \quad (3-4)$$

In practical FTIR spectrometers, a red HeNe laser ($\sigma_{\text{HeNe}} = 15798 \text{ cm}^{-1}$) is sent through the interferometer along with the white light.² The interferogram of the laser is a cosine, of which the zeros are used for equidistant sampling. This results in two samples per period of the HeNe laser interference pattern, and thus $\sigma_{\max} = \sigma_{\text{HeNe}}$. Some FTIRs also allow sampling at the maxima and minima of the HeNe laser interference pattern, resulting in a bandwidth $\sigma_{\max} = 2\sigma_{\text{HeNe}}$, or 31596 cm^{-1} (3.9 eV). This bandwidth is higher than the bandwidth of most used lightsources, detectors and beamsplitters.

The spectral resolution is set by the maximum path length difference δ_{\max} .²

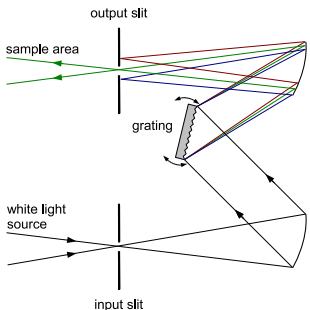
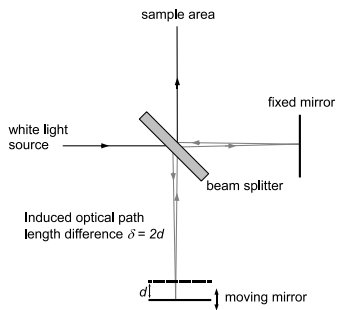
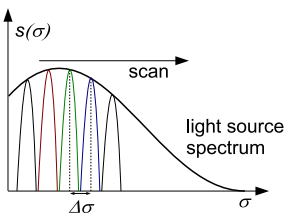
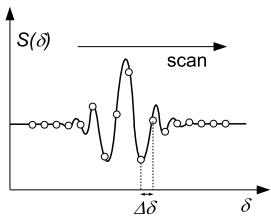
$$\Delta\sigma = \frac{1}{2\delta_{\max}} \quad (3-5)$$

If the distance δ_{\max} over which the moving mirror is scanned, is longer, the spectral resolution, but also the measurement time, will increase. In monochromatic techniques spectral resolution is exchanged with signal to noise ratio. Here a major advantage of the Fourier-transform technique becomes clear. It allows to measure at very fine spectral resolutions (down to 0.125 cm^{-1} for a δ_{\max} of 4 cm), while maintaining high signal to noise ratio.

In Table 3-2 the comparison of the dispersive Fourier-transform technique with monochromatic techniques is summarized. The FTIR used in this work is a research grade Thermo Electron Nicolet 8700 FTIR, with a spectral resolution down to 0.125 cm^{-1} and a maximum bandwidth of 31596 cm^{-1} .³ For experiments in the visible and near infrared (IR) area of the spectrum a quartz beam splitter

is used. CaF₂ and KBr beamsplitters are also available, with increased transmittivity in the near infrared and far infrared region.

Table 3-2: Comparison between monochromatic and dispersive Fourier-transform techniques.

	MONOCHROMATIC TECHNIQUE	FOURIER-TRANSFORM TECHNIQUE
Essential part	monochromator	Michelson interferometer
Scanning part	rotating grating	linearly moving mirror
Schematic representation of working principle		
Signal power at the sample area	$s(\sigma)$	$\int s(\sigma)(\cos(2\pi\sigma\delta)+1)d\sigma$
Graph of signal available on the sample area		
Main restriction	finite monochromatic bandwidth ↓ finite spectral resolution $\Delta\sigma$	finite sample spacing $\Delta\delta$ ↓ finite spectral bandwidth

3.3 Measurement of photocurrent spectra

3.3.1 Setup with monochromator

The classical and most straightforward way for measuring photocurrent spectra is to illuminate the sample with monochromatic light of photon energy E and measure the corresponding photocurrent density $J_{\text{ph}}(E)$. In order to correctly measure the photocurrent spectrum, the current induced by the monochromatic light must only be a small perturbation on the total photocurrent. Therefore, a white bias light source is used, with the monochromatic light being only a small perturbation as compared to the bias. To distinguish the monochromatic light from the bias light, it is chopped at a certain frequency f . The induced photocurrent at the frequency f is detected with a lock-in amplifier. If the chopping frequency is sufficiently low, the photocurrent spectrum measured in this way can be interpreted as the DC photocurrent spectrum.

3.3.2 Fourier-Transform Photocurrent Spectroscopy

a Introduction

The dispersive technique Fourier-Transform Photocurrent Spectroscopy (FTPS) was only recently (2002) introduced as a fast characterization technique for solar cells by Vanecek et al.⁴ FTPS uses a FTIR with external detector option. A photocurrent spectrum of a photovoltaic device is obtained by using this device as the external detector. The spectrum $S(\sigma, \delta)$ of the FTIR's output light beam, incident on the device is a function of the optical path length difference δ (see also section 0).

$$S(\sigma, \delta) = s(\sigma)(1 + \cos(2\pi\sigma\delta)) \quad (3-6)$$

Hereby is $s(\sigma)$ the lamp irradiance spectrum. If the photovoltaic device has a linear photocurrent response $d_{\text{pc}}(\sigma)$ (in A/W), a photocurrent in function of δ is produced

$$J_{\text{pc}}(\delta) = \int d_{\text{pc}}(\sigma)s(\sigma)(1 + \cos(2\pi\sigma\delta))d\sigma \quad (3-7)$$

This signal is fed back to the FTIR. The machine software performs the Fourier-transform. This gives us:

$$d_{\text{pc}}(\sigma)s(\sigma) \quad (3-8)$$

The lamp spectrum $s(\sigma)$ can be obtained by performing a measurement with a calibrated detector.

Two FTPS measurement modes exist, each with their specific advantages and disadvantages. They will be discussed below, in paragraphs b and d.

b Continuous scan FTPS

In continuous scan FTPS (CS-FTPS), the mirror is continuously moving at a constant velocity v . In this way, the optical path length difference δ becomes an explicit function of time t .

$$\delta = 2d = 2vt \tag{3-9}$$

The device is illuminated by a time varying illumination irradiance signal

$$S(\sigma, t) = s(\sigma)(\cos(2\pi ft) + 1) \tag{3-10}$$

Hereby is the modulation frequency f equal to

$$f = 2v\sigma \tag{3-11}$$

This means that, for every σ , the signal is modulated with a different frequency f , given by equation (3-11). In the CS-FTPS mode, wavenumbers are thus converted into modulation frequencies. This is illustrated in Figure 3-1.

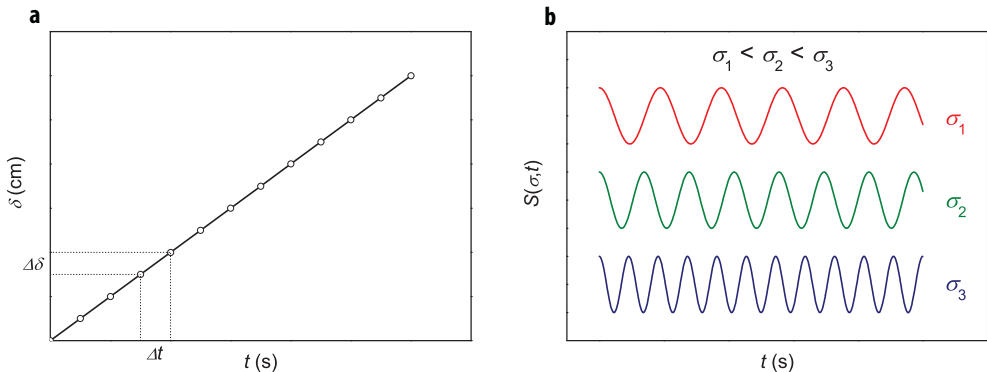


Figure 3-1: (a) In CS-FTPS, the optical path length difference δ is a linear function of time. Sampling occurs at a resolution Δt , resulting in a resolution $\Delta\delta$. (b) Illustration of the illumination signal incident on the device. For different σ , the signal is modulated with a different frequency, according to equation (3-11).

The incident signal $S(\sigma, t)$ contains also a DC part, equal to $s(\delta)$ (equation (3-10)). Bias light is thus inherently present in CS-FTPS. However, if needed, the sample can be illuminated by additional bias light.

A schematic drawing of the FTPS setup in continuous scan mode is shown in Figure 3-2. The modulated light beam is focussed onto the photovoltaic device

mounted in a sampleholder. In this work a sampleholder which can be cooled by liquid nitrogen, with a temperature control between 78 K and 350 K, was used. The electrical signal of the device is amplified and fed back into the FTIR where it is processed. A bandpass optical filter, passing only the spectral region of interest, can be placed into the light beam path. This is useful to distinguish between photo-induced signal and signal due to ground-state absorption.

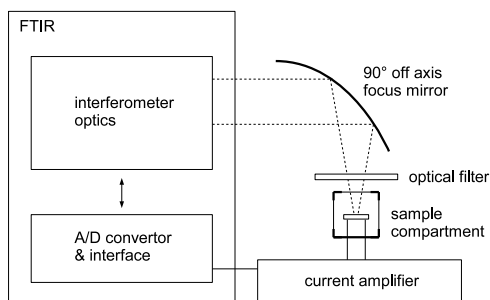


Figure 3-2: Schematic drawing of the FTPS setup in continuous scan mode.

The lowest mirror speed available in commercial FTIRs in continuous scan mode is $0.1581 \text{ cm}\cdot\text{s}^{-1}$, converting the laser wavenumber $\sigma_{\text{HeNe}} = 15798 \text{ cm}^{-1}$ to a frequency of 5 kHz. To obtain a typical spectral resolution $\Delta\sigma$ of 32 cm^{-1} , ($4 \times 10^{-3} \text{ eV}$) a distance δ_{max} of 0.016 cm is scanned (see also paragraph 0). This gives a measurement time of 50 ms per scan. A full, high resolution spectrum is thus obtained very quickly. Such a fast measurement allows for mediation of multiple scans (e.g. 1000 mediations), increasing the signal to noise ratio, while maintaining a reasonable measurement time.

A drawback, however of such fast measurement and consequently high modulation frequencies (around 5 kHz) is, that it can only be used on samples with fast photoresponses. The photo-induced current must be able to follow the kHz range light modulation. In other words, the modulation frequency response of the photodetector in the kHz region should be spectrally flat in order to obtain a correct photocurrent spectrum by CS-FTPS. If the frequency response is not flat, the photocurrent spectrum is deformed, because every σ corresponds to a different f . However, a correction procedure, correcting for the “non-flatness” of the frequency response is possible and is described in the next section. Even worse is the case if the cut-off frequency of the photodetector is below $\sim 1 \text{ kHz}$. In this case, no signal will be obtained at all, and a different FTPS mode must be used. This is described in paragraph d.

c Correction procedure for CS-FTPS spectra

We assume that the total detector response $d_{pc}(\sigma, f)$ can be written as the product of a function $a(\sigma)$, which only depends on σ and a function $b(f)$ which only depends on f .

$$d_{pc}(\sigma, f) = a(\sigma)b(f) \quad (3-12)$$

Because $f = 2\nu\sigma$, the spectrum $d_{pc}(\sigma, f)$ is deformed by $b(f)$ if $b(f)$ is not a constant over the range of mirror speed induced frequencies.

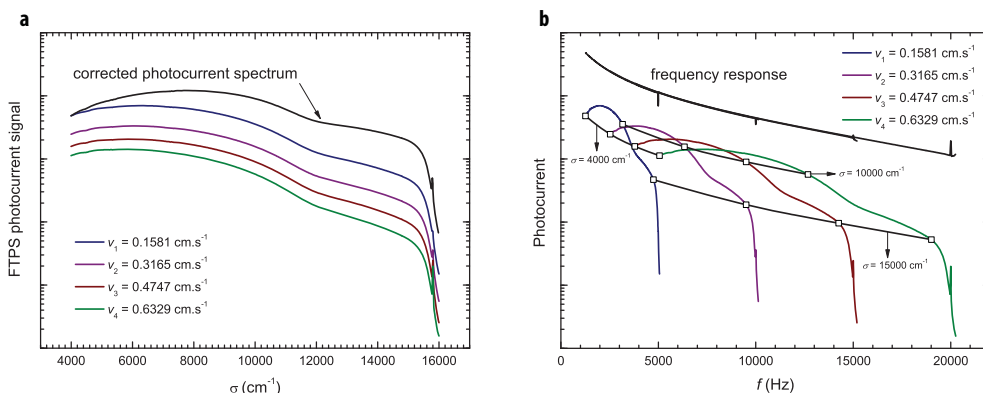


Figure 3-3: (a) FTSP spectra for 4 different mirror velocities. (b) conversion to the frequency domain. The frequency response can be deduced as indicated in the text.

To correct for this, measurements are performed at n mirror speeds v_1, v_2, \dots, v_n . This introduces frequencies $f_1 = 2\sigma v_1, f_2 = 2\sigma v_2, \dots, f_n = 2\sigma v_n$. In Figure 3-3 (a), an example of a spectrum measured by the FTIR internal detector is shown for 4 mirror speeds. In Figure 3-3 (b), the same spectra are plotted, but now σ is converted to its corresponding f by using $f = 2\nu\sigma$. For a fixed $\sigma = \sigma_1$ we can obtain the frequency response $b(f)$, multiplied by a constant $a(\sigma_1)$ in n points.

We can do this for several σ , equal to $\sigma_1, \sigma_2, \dots, \sigma_m$, each giving us the modulation frequency response in n points, in a different frequency region, multiplied with $a(\sigma_1), a(\sigma_2), \dots, a(\sigma_m)$. In Figure 3-3 (b) this is shown for 3 values of σ . The shape of the frequency response over the whole spectral region of interest can be obtained, by matching the frequency response curves in their overlapping frequency region.

Once $b(f)$ is known, the modulation frequency independent spectral response $a(\sigma)$ can be calculated, from equation (3-12).

d Amplitude Modulated Step scan FTPS

For photovoltaic devices with a very strong frequency dependency the signal can be very low for modulation frequencies higher than 1 kHz. This makes it impossible to use CS-FTPS to obtain a photocurrent spectrum. For this type of photovoltaic devices a slow measurement must be performed. This is possible, if the FTIR is used in step-scan mode.

In step-scan mode, the moving mirror is not moved continuously, but in steps. The waiting time in between the steps can be chosen to be sufficiently slow to make all the electrical processes in the photovoltaic device relax. So for every δ_i , the device is allowed to reach its equilibrium, before a photocurrent measurement is performed. To increase the signal to noise ratio, the interferometer light beam is chopped at a frequency f_0 , and the photocurrent signal is measured by a lock-in amplifier. f_0 should always be chosen to be lower than the devices cut-off frequency. This mode is called amplitude modulated step scan FTPS (AM-FTPS). The major difference with CS-FTPS is that in AM-FTPS every σ is modulated with the same frequency f_0 , while for CS-FTPS every σ is modulated with a different frequency f , given by equation (3-11). This implies that for AM-FTPS, no corrections are needed.

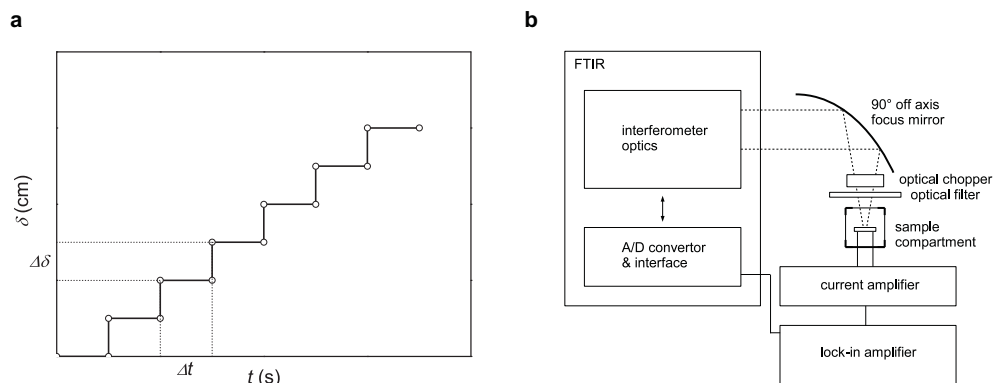


Figure 3-4: (a) In AM-FTPS, the optical path length difference δ is not an explicit function of time anymore. The time interval Δt is chosen to be longer than all relaxation processes in the sample. (b) Schematic drawing of the FTPS setup in amplitude modulated, step scan mode.

For the polymer:fullerene solar cells studied in this work, CS-FTPS with the correction procedure was used. The corrections that had to be made however are quite small. For other types of solar cells, such as dye-sensitized solar cells,⁵ however, CS-FTPS does not produce any useful signal. For this type of solar cells, AM-FTPS is useful. This is described in paper A.⁶

References

- 1 A. A. Michelson, *Phil. Mag.* **31**, 256 (1891)
- 2 P. R. Griffiths, J. A. deHasseth, "Fourier Transform Infrared Spectroscopy", John Wiley & Sons, New York (1986)
- 3 A product description of the FTIR used in this work can be found online: <http://www.thermo.com/com/cda/product/detail/1,,1000001344729,00.html>
- 4 M. Vaněček, A. Poruba, *Appl. Phys. Lett.* **80**, 719 (2002)
- 5 B. O'Regan, M. Graetzel, *Nature* **353**, 737 (1991)
- 6 K. Vandewal, L. Goris, I. Haeldermans, M. Nesladek, K. Haenen, P. Wagner, J. V. Manca, *Thin Solid Films* **516**, 7135 (2008).

4 Guide to the papers

The core of this thesis is a collection of 6 papers written in the period 2007-2009. For each paper the innovative aspect, motivation, content and relation to other work is summarized below.

Paper A

Fourier-Transform Photocurrent Spectroscopy for a fast and highly sensitive spectral characterization of organic and hybrid solar cells

K. Vandewal, L. Goris, I. Haeldermans, M. Nesladek, K. Haenen, P. Wagner, J. V. Manca, *Thin Solid Films* **516**, 7135 (2008)

In this paper, the highly sensitive technique Fourier-Transform Photocurrent Spectroscopy (FTPS) is introduced in the field of organic, dye-sensitized and hybrid solar cells. For organic and hybrid photovoltaic devices, the continuous scan mode is applicable and allows a fast and sensitive characterization. For dye sensitized solar cells (DSSC), the continuous scan mode is not suitable, due to the long photocurrent response times of this type of solar cells. To overcome this problem, the step-scan mode is introduced, enabling FTPS characterization of also DSSCs. In contrast to the fully organic solar cells, however no sub-gap absorption could be detected for this type of solar cells.

For the fully organic solar cells it was already shown in previous work by our group, that FTPS and also photo-thermal deflection spectroscopy can be used to detect the formation of a charge transfer complex between polymer and fullerene.^{1,2} The involvement of the excited CTC or charge-transfer (CT) state in the production of photocurrent was discussed in a subsequent paper.³ The absence of a sub-gap CT band in a certain polymer:fullerene combination was accompanied by the absence of charge carrier formation resulting in poor device performance. This indicates that efficient population of the CT state thus seems to be crucial for obtaining high photocurrent producing polymer:fullerene solar cells.

However, at the time it was not clear if CTC formation also affected photovoltaic parameters, other than the photocurrent. Therefore, we focused in the following papers on the open-circuit voltage (V_{oc}) in particular.

Paper B

The relation between open-circuit voltage and the onset of photocurrent generation by charge-transfer absorption in polymer: fullerene bulk heterojunction solar cells

K. Vandewal, A. Gadisa, W. D. Oosterbaan, S. Bertho, F. Banishoeib, I. Van Severen, L. Lutsen, T. J. Cleij, D. Vanderzande, J. V. Manca, *Adv. Funct. Mater.* **18**, 2064 (2008)

Organic bulk heterojunction solar cells comprising various donor polymers blended with PCBM were prepared and studied with FTPS. A linear correlation of the onset of the CT absorption band and V_{oc} was made. It was furthermore observed that for a certain polymer:PCBM combination, changes in the active layer preparation conditions resulted in small changes in the spectral position of the CT band, accompanied by changes in V_{oc} .

Independent from our work, D. Veldman et al.⁴ observed a similar linear correlation between V_{oc} and the peak of the CT band in the photoluminescence spectrum of a polyfluorene:PCBM comprising different polymer to PCBM weight ratios. Potscavage et al.⁵ also suggested an involvement of CTC formation determining V_{oc} for small molecule/ C_{60} bilayer devices.

Further, several other papers exist,^{6,7,8} correlating V_{oc} with the difference between the highest occupied molecular orbital of the donor and the lowest unoccupied molecular orbital of the acceptor. From early studies of donor/acceptor CTCs it is known that the spectral position of the CT band correlates also with this energetic level difference.^{9,10}

The correlations between V_{oc} and the spectral position of the CT band, found in this paper, indicate an involvement of donor/acceptor material interaction in the determination of V_{oc} . A physical theory, revealing the exact origin of V_{oc} , and the precise involvement of CTC formation, however is still missing.

Paper C

On the origin of the open-circuit voltage of polymer:fullerene solar cells

K. Vandewal, K. Tvingstedt, A. Gadisa, O. Inganäs, J. V. Manca, *Nature Mater.* **8**, 904 (2009)

In this work a rational explanation, why the correlations between V_{oc} and the spectral position of the CT band, as discussed in paper B, are observed is provided. In order to achieve this, we use an established theory based on thermodynamics, already shown to be valid for inorganic solar cells and DSSCs. The basics of this theory are given in paragraphs 2.3 and 2.4.

In order to make sure that the basic assumptions made in this theory are correct, the validity of the reciprocity relations between photovoltaic and electroluminescent actions (paragraph 2.4.1) must be checked. In our lab we specialize in obtaining highly sensitive measurements of the EQE_{PV} . Sensitive measurements of the reciprocal action, i.e. electroluminescence were performed in collaboration with Kristofer Tvingstedt and Olle Inganäs at the University of Linköping in Sweden.

We found that the electroluminescence spectra of commonly used polymer:fullerene combinations for photovoltaic applications, is dominated by CT emission.¹¹ The EQE_{EL} of CT emission, however is low, in the range 10^{-9} to 10^{-6} . The reciprocity relation between EQE_{PV} and the electroluminescence spectrum was confirmed for these devices. This allows us to reproduce the CT dominated emission spectrum from the knowledge of the EQE_{PV} spectrum. Further it allows us to calculate V_{oc} (see paragraph 0). V_{oc} calculated in this way is compared to the experimentally measured V_{oc} . Excellent correspondence is obtained, for a whole range of polymer:fullerene combinations. This shows that the assumption of quasi-equilibrium and the reciprocity relation is valid, at least when a charge density comparable to solar conditions is present in the device.

We have thus shown that the classical theory, explaining V_{oc} works, also for organic polymer:fullerene solar cells, but only on the condition that the sub-gap absorption and emission due to the CT states is taken into account.

Paper D

Relating the open-circuit voltage to interface molecular properties of donor:acceptor bulk heterojunction solar cells

K. Vandewal, A. Gadisa, K. Tvingstedt, O. Inganäs, J. V. Manca, *Phys. Rev. B*, submitted (2009)

The above paper C relates three measurable quantities, i.e. V_{oc} , EQE_{PV} and the EL spectrum to each other. These relations are derived, based on thermodynamic assumptions, and no assumptions about the internal working mechanisms of the device are needed. In this paper, we fit the CT bands in the EQE_{PV} and EL spectrum using a function derived by applying Marcus theory of electron transfer.¹² This allows us to experimentally obtain parameters used in this theory, providing information about the internal absorption and emission mechanism. Important parameters are: the energy difference between the CTC ground state and excited CT state, abbreviated E_{CT} , the reorganization energy λ and the electronic coupling constant, proportional to the strength of the coupling between donor and acceptor.

We obtain an analytical formula for V_{oc} depending on the internal interfacial molecular parameters, but also on temperature (T) and illumination intensity. Only in the limit of T approaching 0 K, V_{oc} is equal to E_{CT} .

This formula is shown to be valid for several polymer:fullerene devices. In evaluating the equation however it must be taken into account that EQE_{EL} can depend on the charge density present in the device. This is the origin of the ideality factor, often used in the description of dark current voltage curves of organic photovoltaic devices.

Paper E

The ultimate efficiency of organic donor/acceptor single junction solar cells

K. Vandewal, A. Gadisa, K. Tvingstedt, O. Inganäs, J. V. Manca, unpublished (2009)

An important question for every new photovoltaic technology is its maximum theoretically obtainable conversion efficiency. The classical Shockley-Queisser limit for a single absorber material assumes that EQE_{PV} equals 1 above the bandgap E_g and 0 below it. Further it assumes that there is no non-radiative recombination present ($EQE_{EL} = 1$). This allows for the calculation of a maximum efficiency in function of the E_g .¹³

For donor/acceptor solar cells having a weak donor/acceptor coupling, a maximum efficiency can also be calculated. Here it is assumed that EQE_{PV} equals 1 above the optical gap of the main absorber and that the only emission present is CT emission with $EQE_{EL} = 1$. Under these assumptions, the maximum efficiency does not depend only on the bandgap of the main absorber, but also on the number of CTCs present in the device, the donor/acceptor coupling and the energy of the CT state (E_{CT}).

Calculating these maximum efficiency limits allows us to compare different photovoltaic technologies. More than 50 years of research on inorganic solar cells have brought them close to their fundamental thermodynamic limit. They have reached above 90 % of their maximum obtainable short-circuit current and fill factor and about 80 % of their maximum obtainable open-circuit voltage. The relatively young technology of organic polymer:fullerene solar cells is far away from the Shockley-Queisser thermodynamic limits. While it is possible to obtain high photocurrents above 80 % of their thermodynamic limit, the main source of energy loss is at V_{oc} . This is due to the large difference between E_{CT} and E_g of present day devices exhibiting large photocurrents. The presence of non-radiative recombination mechanisms, causing EQE_{EL} to be smaller than 10^{-6} , causes even more additional loss in real devices.

Paper F

Varying polymer crystallinity in nanofiber poly(3-alkylthiophene):PCBM solar cells: Influence on charge transfer state energy and open-circuit voltage

K. Vandewal, W. D. Oosterbaan, S. Bertho, V. Vrindts, A. Gadisa, L. Lutsen, D. Vanderzande, J. V. Manca, *Appl. Phys. Lett.* **95**, 123303 (2009)

Papers D and E show the importance of the energy of the interfacial CT state E_{CT} . This energy is mainly, but not exclusively, determined by the difference between the highest occupied molecular orbital of the donor and the lowest unoccupied molecular orbital of the acceptor. In paper B it was already shown that the spectral position of the CT band depends on several preparation conditions, such as annealing and donor/acceptor stoichiometry.

In this paper we investigate the influence of donor polymer crystallinity on E_{CT} . Dispersions of crystalline nanofibers of poly(3-butylthiophene), poly(3-pentylthiophene) and poly(3-hexylthiophene) are prepared by Wibren Oosterbaan. He is able to determine and control the crystalline nanofiber to total polymer weight fraction between $\sim 10\%$ and $\sim 90\%$. This makes it possible to perform a systematic study of the influence of the crystalline poly(3-alkylthiophene) content on E_{CT} .

We observe that for all three poly(3-alkylthiophene) polymers, E_{CT} decreases about ~ 0.2 eV, when varying the crystalline fraction from 0 to 100%. V_{oc} follows roughly the same trend. This work indicates that changes in active layer morphology induced for example by aging or thermal annealing of photovoltaic devices do not only affect the short-circuit current, but also the open-circuit voltage.

References

- 1 L. Goris, K. Haenen, M. Nesladek, P. Wagner, D. Vanderzande, L. de Schepper, J. d'Haen, L. Lutsen, J. V. Manca, *J. Mater. Sci.* **40**, 1413 (2005)
- 2 L. Goris, A. Poruba, L. Hod'akova, M. Vanecek, K. Haenen, M. Nesladek, P. Wagner, D. Vanderzande, L. de Schepper, J. V. Manca, *Appl. Phys. Lett.* **88**, 052113 (2006)
- 3 J. J. Benson-Smith, L. Goris, K. Vandewal, K. Haenen, J. V. Manca, D. Vanderzande, D. D. C. Bradley, J. Nelson, *Adv. Funct. Mater.* **17**, 451 (2007)
- 4 D. Veldman, O. Ipek, S. C. J. Meskers, J. Sweelssen, M. M. Koetse, S. C. Veenstra, J. M. Kroon, S. S. van Bavel, J. Loos, R. A. J. Janssen, *J. Am. Chem. Soc.* **130**, 7721 (2008)
- 5 W. J. Potscavage, S. Yoo, B. Kippelen, *Appl. Phys. Lett.* **93**, 193308 (2008)
- 6 C. J. Brabec, A. Cravino, D. Meissner, N. S. Sariciftci, M. T. Rispens, L. Sanchez, J. C. Hummelen, T. Fromherz, *Thin Solid Films* **403**, 368 (2002)
- 7 A. Gadisa, M. Svensson, M. R. Andersson, O. Inganäs, *Appl. Phys. Lett.* **84**, 1609 (2004)
- 8 M. C. Scharber, D. Muhlbacher, M. Koppe, P. Denk, C. Waldauf, A. J. Heeger, C. J. Brabec, *Adv. Mater.* **18**, 789 (2006)
- 9 R. Foster, "Organic Charge-Transfer Complexes", Academic Press, New York (1969)
- 10 P. Panda, D. Veldman, J. Sweelssen, J. J. A. M. Bastiaansen, B. M. W. Langeveld-Voss, S. C. J. Meskers, *J. Phys. Chem.* **111**, 5076 (2007)
- 11 K. Tvingsedt, K. Vandewal, A. Gadisa, F. Zhang, J. Manca, O. Inganäs, *J. Am. Chem. Soc.* **131**, 11819 (2009)
- 12 R. A. Marcus, *J. Phys. Chem.* **93**, 3078 (1989)
- 13 W. Shockley and H. J. Queisser, *J. Appl. Phys.* **32**, 510 (1961)

5 Conclusion

For an efficient conversion of a flux of solar photons into an electric current by organic materials, the presence of a material interface between an electron donating and electron accepting material is crucial. Most successful active layers for organic solar cells comprise a blend of conjugated polymers as electron donors and fullerenes as electron acceptors, exhibiting power conversion efficiencies higher than 6%, nowadays. In order to find pathways to increase this efficiency further, properties of the electronic states at the donor/acceptor interface and their role in determining the overall power conversion efficiency, are investigated in this work.

To probe these interfacial properties, the fast and highly sensitive technique Fourier-Transform Photocurrent Spectroscopy (FTPS) is used to detect the weak absorption caused by ground state interaction of polymers and fullerenes, forming a charge transfer complex (CTC). Optical excitation of this donor/acceptor CTC by light with photon energies lower than the optical gap of both the donor and acceptor materials, results in the creation of a charge transfer (CT) exciton or CT state, comprising an electron in the acceptor phase, coulombically bound to a hole on the donor phase.

In our study, such a CT transition within the optical gap of both pure materials was detected in *all* polymer:fullerene solar cells exhibiting a significant photovoltaic effect. In these cases, the energy of the CT state is lower than the energy of the excited states of the pure blend constituents, and can efficiently be populated. The competition between geminate recombination and field dependent dissociation of CT excitons can still limit photocurrent production in some polymer:fullerene material combinations.

The origin of the open-circuit voltage

It is further shown that next to the free charge carrier and photocurrent generation, the open-circuit voltage (V_{oc}) is also affected by donor/acceptor CTC formation. V_{oc} is determined by the balance between free carrier generation and recombination processes in the active layer. These recombination processes can proceed through the formation of a CT exciton with subsequent emission of low energy photons, a process that is visible in electroluminescence experiments. Although the electroluminescence spectrum is dominated by this CT emission, the external quantum efficiency of this process is very low, in the 10^{-6} to 10^{-9} range.

In order to quantitatively investigate the role of CTC formation on the photovoltage production in polymer:fullerene solar cells, a reciprocity relation between V_{oc} and the photovoltaic and electroluminescent actions of a

generalized solar cell is used. This theory is established for various types of both inorganic and dye sensitized solar cells. In this work, it is shown to be valid, also in the case of polymer:fullerene solar cells, on the condition that the sub-gap absorption and emission due to the CT states is taken into account. Because both absorption and emission can only be detected by highly sensitive techniques, this has been overlooked in the first ten years of research on polymer:fullerene photovoltaics.

As predicted by the reciprocity relations, a linear correlation between V_{oc} and the spectral position of the CT band is observed for a range of polymer:fullerene blends, comprising different donor polymers. The energy of the CT state (E_{CT}) is known to correlate with the difference between the HOMO energy of the polymer donor and the LUMO energy of the fullerene acceptor. This explains the widely observed correlation between V_{oc} , measured under solar conditions, and this energetic difference.

Influence of polymer:fullerene stoichiometry and crystallization on E_{CT} and V_{oc}

We also investigate the influence of the preparation conditions on E_{CT} and thus V_{oc} . Increasing the concentration of the fullerene derivative PCBM from 5 % to 80 % in MDMO-PPV:PCBM photovoltaic devices, results in a redshift of the CT band, of ~ 0.15 eV. The reason for these redshift could be due to an increasing degree of PCBM crystallinity upon increasing the PCBM content. However, the slight increase in overall dielectric constant of the blend upon increasing the PCBM content, could also cause the observed redshift. The relative contributions of dielectric constant changes and crystallinity changes however, are not determined yet, and will be the subject of future work.

The effect of the donor polymer crystallinity on the spectral position of the CT band has been investigated in more detail for polythiophene:PCBM solar cells. The crystalline fiber to total polymer weight ratio in the polythiophene:PCBM blends was varied between ~ 0.1 and ~ 0.9 . We observed that E_{CT} decreases about ~ 20 meV, when increasing the fiber to total polymer weight ratio by 0.1. It was also found that V_{oc} always follows roughly the same trend as E_{CT} .

Energetic losses between qV_{oc} and E_{CT}

For the solar cells investigated in this work an energetic difference between E_{CT} and qV_{oc} measured under solar illumination conditions of ~ 0.6 eV is found. The origin of this difference is twofold. One part is energetic loss due to the radiative recombination through the CT state and can be reduced by reducing the number of CT states present in the device or by reducing the electronic coupling between donor and acceptor, changing the CT absorption cross section, but also the CT emission rate constant. For the investigated devices, this radiative loss is ~ 0.25 eV. The second part of the loss, about 0.35 eV is due to non-radiative

recombination mechanisms. Further investigations, identifying these non-radiative recombination paths, are necessary in order to find possible pathways to minimize this part of the energetic loss.

Additionally, V_{oc} was investigated under conditions different from solar conditions. Also E_{CT} was determined at different temperatures, between 150 K and 300 K. For the investigated polymer:fullerene blends, it was found that the difference between E_{CT} and qV_{oc} decreases linearly with decreasing temperature and logarithmically with decreasing illumination intensity. Furthermore, irrespective of the used illumination intensity, the extrapolation of qV_{oc} to 0 K equals the extrapolation of E_{CT} to 0 K.

Upper limits for power conversion efficiency of organic donor/acceptor solar cells

Upper limits of attainable power conversion efficiency for organic donor/acceptor photovoltaics are derived for AM1.5 conditions at room temperature. The obtained maximum efficiency values are a function of two parameters: The optical gap of the main absorber E_g and the energetic losses due to the presence of the CT state. This efficiency limit is between 25 % and 33 %, if the optical gap of the main absorber is in the 1.2-1.7 eV region and if the losses through the CT state are below 0.2 eV. However, best performing polymer:fullerene solar cells nowadays have power conversion efficiency of 6 %. In these devices, EQE_{PV} values of 70-80 % are reached above the optical gap of the polymer. The main source of energy loss in the best device lies thus in the low values of V_{oc} as compared to the upper limit.

6 Future work

In this chapter, future experiments in order to find factors limiting the device performance of photovoltaic devices based on donor/acceptor interfaces are proposed. The difficulty in increasing the power conversion efficiency of this type of solar cells lies in the contradicting material requirements for obtaining a high photocurrent and a high V_{oc} within the same device.

To attain a high V_{oc} , it is beneficial if E_{CT} is as close as possible to the optical gap of the main absorbing material. However, in order to obtain a high photocurrent, the CT state should be still efficiently populated and dissociated. These processes seem to become easier if the difference between E_{CT} and the optical gap of the main absorber is large.^{1,2} However, other factors such as the electron and hole mobility of respectively the acceptor and the donor phase,^{3,4} will also have an impact on the quantum yield for free charge carrier generation. Additionally, the presence of a dipole layer at the donor/acceptor interface due to partial charge transfer ($\sim 0.1e^-$)⁵ in the ground-state, inherent to CTC formation, is argued also to have an influence.⁶

Recently photovoltaic devices based on a promising material combination comprising a low bandgap alternating polyfluorene blended with PCBM, were discussed. This blend combines a low E_g of about 1.4 eV,⁷ with a very small difference between E_g and E_{CT} (80 meV)⁸ resulting in a V_{oc} slightly higher than 0.8 V.⁷ The potential power conversion efficiency of this material combination based on the calculation in paper E is very high. However the currently achieved external quantum efficiency in the range of polymer absorption is only modestly high, peaking at 20 % in the range of polymer absorption. Further studies must indicate if there is a fundamental limitation, preventing the EQE_{PV} to be increased even higher.

The dissociation efficiency of relaxed CT excitons

An important unanswered question is thus: What is the minimum difference between E_{CT} and E_g , which still allows efficient exciton dissociation into free charge carriers with large quantum yields approaching unity? Is the excess energy $E_g - E_{CT}$ used to dissociate the charge carriers?

In order to answer this question it would be interesting to know the dissociation yield of thermally relaxed CT excitons, and compare it to the dissociation yield of pure phase excitons generated close to the interface. After all, when CT excitons are generated by direct excitation in the weak CT absorption band, less excess energy is dissipated upon relaxation to the lowest energy CT state than in the case of pure material excitation.

This study can be performed by comparing highly sensitive EQE_{PV} measurements with highly sensitive measurements of the absorption spectrum, in order to determine the internal quantum efficiency for both the CT transition and pure phase excitations. A technique to sensitively measure the absorptivity is photothermal deflection spectroscopy.⁹ This technique is available in our lab at IMO/Uhasselt and was recently upgraded in order to perform measurements on ~ 100 nm thin films such as used in polymer photovoltaic devices.

Determination of the binding energy of CT excitons

In order to find out why the presence of a donor/acceptor interface facilitates the dissociation of pure phase excitons reaching this interface, a measurement of the CT exciton binding energy could be very helpful. Moreover, understanding of the effect of morphology, crystallization, interface dipoles, $E_g - E_{CT}$ energetic difference, etc..., on the CT exciton binding energy could help reducing it further for better organic solar cells.

Determination of the binding energy of CT excitons can be done via comparing the optical gap of the CT transition (E_{CT}) with the electrochemical gap, i.e. the difference between the HOMO level of the donor and the LUMO level of the acceptor. This electrochemical gap however, should then be measured for the solid-state material blend, prepared under similar conditions as the blend for which E_{CT} was measured.

Another method to determine the CT exciton binding energy is via field dependent quenching of the CT emission in photoluminescence experiments. The possibility of this approach has already been demonstrated for MDMO-PPV:PCBM blends, where a binding energy of the CT exciton of 0.13 eV was found using this method.¹⁰

Highly sensitive measurements of the absorption spectrum as morphological characterization tool

A highly sensitive measurement of the absorption spectrum, revealing the interfacial CT transition can also be used as to obtain information about the blend morphology, and the amount of active interface present within the blend. In order to determine the number of CTCs, or the amount of interface, in a bulk heterojunction device, the absorption cross-section of the CT transition should be determined. Bilayer devices with a well defined interfacial CTC could be used in order to achieve this.

Further, wanted and unwanted changes in crystallinity and degree of clustering of donor and acceptor phases, due to device treatment or thermal aging can induce spectral shifts of pure phase or CT absorption bands (paper B and F). When a fast characterization technique such as FTPS, which is directly applicable to photovoltaic devices, is used, these changes can be measured in situ. This

makes FTPS very suitable as electrical (EQE_{PV}) and morphological quality control tool.

Alternative acceptor materials

Up to now fullerenes and more specifically the fullerene derivative PCBM, are the most used and successful acceptor materials. However, attempts are made to use conjugated polymers¹¹ or inorganic nanoparticles^{12,13} such as metal oxides, as new electron accepting materials. In this quest for alternative acceptors, it is important to find the morphological, molecular and energetic properties, which make PCBM such a successful acceptor. More specifically the ability of PCBM to form nanocrystalline phases could be a crucial property for a good acceptor material for organic solar cells.

CTC formation between these alternative acceptor materials and conjugated polymer donors has not been studied very extensively yet. Recently, we have demonstrated CTC formation between P3HT and amorphous TiO_2 .¹⁴ For polymer/polymer interfaces several reports (for example ref 15 or 16) exist on interfacial emission, usually termed exciplex emission. However, ground-state interaction resulting in interfacial CT absorption has been less extensively studied in these material systems.

Tuning of the CTC properties in order to increase the solar cell efficiency

From this work, it is clear that V_{oc} is limited by the donor/acceptor material interaction. Tuning of CTC properties however, can result in a minimization of the introduced losses.

The most straightforward parameter to tune is E_{CT} , as it correlates with the HOMO level of the donor and the LUMO level of the acceptor. Tuning of these levels by chemical modifications, in order to increase V_{oc} is already applied, on both the donor⁷ and the acceptor^{17,18} side.

However, other parameters can also be tuned. The amount of CTCs or their transition strength can also be changed. The question however is, if CT absorption should be increased or decreased. Increasing the CT absorption could make it participate much more in sunlight absorption, however, at the cost of an increased radiative decay rate.

One could try to find ways to increase the CT absorption by increasing the number of CTCs or their absorption cross-section to that extend that CT absorption becomes very efficient, making it contribute to J_{sc} . The absorption-cross section can in principle be tuned by an increased wave-function overlap between donor and acceptor. This would demand bringing donor and acceptor molecules closer together, or linking them with chemical bridges. The question when using this approach however is, if the increased radiative decay rate,

unavoidably related to the increased absorption, will not hamper free charge carrier generation. The increased decay rate can become comparable to, or exceed the dissociation rate, which is determined by the exciton binding energy. This will result in an increased geminate recombination.

Therefore, another approach is to decrease the CT exciton decay rate by decreasing the total CT absorption. This can be accomplished by decreasing the CTC absorption cross-section or the total number of CTCs, for example by decreasing the donor/acceptor wavefunction overlap, or by using the bilayer concept. Also V_{oc} will benefit from such actions, because it depends logarithmically on the total amount of CT absorption.

Study of the non-radiative, non-geminate recombination mechanisms

It is stated in this work and also in a recent publication by Kirchartz et al.,¹⁹ that the non-radiative recombination limits substantially the overall device performance through limitation of V_{oc} . Reducing the number of non-radiative decay rate by a factor of 10 will result in an increase of V_{oc} by $kT\ln(10) = 59$ mV. However, not much is known about these non-radiative decay paths and therefore further research should also focus on identification and removal of this recombination, if possible.

references

- 1 H. Ohkita, S. Cook, Y. Astuti, W. Duffy, S. Tierney, W. Zhang, M. Heeney, I. McCulloch, J. Nelson, D. D. C. Bradley, J. R. Durrant, *J. Am. Chem. Soc.* **130**, 3030 (2008)
- 2 T. M. Clarke, A. M. Ballantyne, J. Nelson, D. D. C. Bradley, J. R. Durrant, *Adv. Funct. Mater.* **18**, 4029 (2008)
- 3 D. Veldman, O. Ipek, S. C. J. Meskers, J. Sweelssen, M. M. Koetse, S. C. Veenstra, J. M. Kroon, S. S. van Bavel, J. Loos, R. A. J. Janssen, *J. Am. Chem. Soc.* **130**, 7721 (2008)
- 4 C. Deibel, T. Strobel, V. Dyakonov, *Phys. Rev. Lett.* **103**, 036402 (2009)
- 5 Y. Kanai, J. C. Grossman, *Nano Lett.* **7**, 1967 (2007)
- 6 V. I. Arkhipov, P. Heremans, H. Bassler, *Appl. Phys. Lett.* **82**, 4605 (2003)
- 7 F. L. Zhang, J. Bijleveld, E. Perzon, K. Tvingstedt, S. Barrau, O. Inganäs, M. R. Andersson, *J. Mater. Chem.* **18**, 5468 (2008)
- 8 Y. Zhou, K. Tvingstedt, F. Zhang, C. Du, W.-X. Ni, M. R. Andersson, O. Inganäs, *Adv. Funct. Mater.* **19** 3293 (2009)
- 9 L. Goris, K. Haenen, M. Nesladek, P. Wagner, D. Vanderzande, L. de Schepper, J. d'Haen, L. Lutsen, J. V. Manca, *J. Mater. Sci.* **40**, 1413 (2005)
- 10 M. Hallermann, S. Haneder, E. Da Como, *Appl. Phys. Lett.* **93**, 053307 (2008)
- 11 S. C. Veenstra, J. Loos, J. M. Kroon, *Prog. Photovolt: Res. Appl.* **15**, 727 (2007)
- 12 W. J. E. Beek, M. M. Wienk, R. A. J. Janssen, *Adv. Mater.* **16**, 1009 (2004)
- 13 W. J. E. Beek, L. H. Slooff, M. M. Wienk, J. M. Kroon, R. A. J. Janssen, *Adv. Funct. Mater.* **15**, 1703 (2005)
- 14 I. Haeldermans, K. Vandewal, W. D. Oosterbaan, A. Gadisa, J. D'Haen, M. K. Van Bael, J. V. Manca, J. Mullens, *Appl. Phys. Lett.* **93**, 223302 (2008)
- 15 A. C. Morteani, A. S. Dhoot, J. S. Kim, C. Silva, N. C. Greenham, C. Murphy, E. Moons, S. Cina, J. H. Burroughes, R. H. Friend, *Adv. Mater.* **15**, 1708 (2003)
- 16 A. C. Morteani, P. Sreearunothai, L. M. Herz, R. H. Friend, C. Silva, *Phys. Rev. Lett.* **92**, 247402 (2004)
- 17 M. Lenes, G.-J. A. H. Wetzelaer, F. B. Kooistra, S. C. Veenstra, J. C. Hummelen, P. W. M. Blom, *Adv. Mater.* **20**, 2116 (2008)

Chapter 6

- 18 R. B. Ross, C. M. Cardona, D. M. Guldi, S. G. Sankaranarayanan, M. O. Reese, N. Kopidakis, J. Peet, B. Walker, G. C. Bazan, E. Van Keuren, B. C. Holloway, M. Drees, *Nature Mater.* **8**, 208 (2009)
- 19 T. Kirchartz, K. Taretto, U. Rau, *J. Phys. Chem. C* **113**, 17958 (2009)

Nederlandstalige samenvatting

Voor een efficiënte omzetting van een stroom van zonlicht fotonen in een elektrische stroom door organische materialen, is de aanwezigheid van een grensvlak tussen een elektron accepterend en elektron donerend materiaal cruciaal. De meest succesvolle actieve lagen voor organische zonnecellen bestaan dan ook uit een mengsel van geconjugeerde polymeren als elektron donor en fullereen derivaten als elektron acceptor. Met deze materiaalsystemen kunnen vandaag vermogen omzettingsefficiënties hoger dan 6 % behaald worden. Om strategieën te vinden die deze efficiëntie verder kunnen verhogen, worden de eigenschappen van de elektronische toestanden aan het donor/acceptor grensvlak, en hun rol in het bepalen van de efficiëntie, onderzocht in dit werk.

Een innovatieve, snelle en hooggevoelige techniek, genaamd Fourier-transform photocurrent spectroscopy (FTPS) wordt gebruikt om de zwakke absorptie veroorzaakt door materiaal-interactie tussen de polymeren en fullerenen te onderzoeken. Het geheel van op elkaar inwerkend polymeer en fullereen wordt een ladingsoverdracht complex (charge transfer complex, CTC) genoemd. Optische excitatie van een CTC, door licht met foton energieën lager dan de optische bandkloof van beide donor en acceptor materiaal, resulteert in de creatie van een ladingsovergedragen (charge transfer, CT) exciton, bestaande uit een elektron op het accepterende materiaal en een gat op het donerende materiaal. Elektron en gat zijn hierbij echter nog steeds gebonden door Coulomb krachten.

In deze studie werd zulk een CT transitie in de optische bandkloof van beide pure materialen gedetecteerd voor alle polymeer:fullereen zonnecellen die een substantieel fotovoltaisch effect vertoonden. In deze gevallen is de energie van de ladingsovergedragen toestand lager dan de energie van de geëxciteerde toestanden in de pure materiaalfasen van het mengsel. En kan dus efficiënt bezet worden. Veldafhankelijk dissociatie, in competitie met verval naar de grondtoestand van dit CT exciton, limiteert de lichtstroom in bepaalde polymeer:fullereen materiaal combinaties.

De oorsprong van de open-keten spanning

Naast vrije ladingsdragersgeneratie en fotostroom generatie, wordt ook the open-keten spanning V_{oc} beïnvloed door donor/acceptor CTC vorming. Omdat er bij een open keten geen stroom vloeit, wordt V_{oc} bepaald door de balans tussen vrije ladingsdragers generatie en recombinatie processen in de actieve laag. De recombinatieprocessen kunnen plaatsvinden met de vorming van een CT exciton met vervolgens emissie van de corresponderende lage energie fotonen. Dit proces is zichtbaar in elektroluminescentie experimenten. Hoewel de

elektroluminescentie spectra gedomineerd worden door deze CT emissie, is de externe kwantum efficiëntie van dit proces erg laag, in het 10^{-6} – 10^{-9} bereik.

Om kwantitatief de rol van CTC vorming op de productie van fotovoltage in polymeer:fullereen zonnecellen te onderzoeken, werd een reciprociteitrelatie tussen V_{oc} en de fotovoltaïsche en elektroluminescente acties van een gegeneraliseerde zonnecel gebruikt. De gebruikte theorie is reeds gevestigd voor een reeks van types van inorganische en zogenaamde kleurstof (dye-sensitized) zonnecellen. In dit werk wordt aangetoond dat deze relaties ook geldig zijn in het geval van polymeer:fullereen zonnecellen, op voorwaarde dat rekening gehouden wordt met de zwakke absorptie en emissie van de ladingsovergedragen toestanden. Omdat beide enkel gedetecteerd kunnen worden met hooggevoelige technieken, werd dit over het hoofd gezien in de tien eerste jaren van het onderzoek op dit type zonnecellen.

Zoals voorspeld door de reciprociteitrelaties, wordt een lineaire correlatie tussen V_{oc} en de spectrale positie van de CT band geobserveerd voor een hele reeks polymeer:fullereen zonnecellen bestaande uit verschillende polymeren en fullereen derivaten. Het is geweten dat de energie van de ladingsovergedragen toestand (E_{CT}) correleert met het energetisch verschil tussen het hoogste, bezette moleculaire orbitaal van de donor en het laagste, onbezette moleculair orbitaal van de acceptor. Dit verklaart de alom geobserveerde correlatie tussen dit energetisch verschil en V_{oc} , gemeten onder zonnebelichtingscondities.

De invloed van polymeer:fullereen gewichtsverhouding en kristallisatie op E_{CT} en V_{oc}

Verder werd de invloed van de zonnecel fabricatie condities op E_{CT} en dus V_{oc} bestudeerd. Wanneer de concentratie van het fullereen derivaat PCBM in MDMO-PPV:PCBM zonnecellen verhoogd wordt van 5% tot 80 %, resulteert dit in een roodverschuiving van de CT band van ongeveer 0.15 eV. De exacte oorzaak van deze roodverschuiving is nog onbekend. Ze kan deels verklaard worden door een verhoogde graad van PCBM kristallisatie wanneer er een hogere concentratie van PCBM in het mengsel aanwezig is. Echter, de lichte verhoging van de effectieve diëlektrische constante door het toevoegen van PCBM aan het polymeer zou de veroorzaakte roodverschuiving ook kunnen verklaren.

Het effect van de graad van kristallisatie van het donor polymeer op de spectrale positie van de CT band werd in meer detail onderzocht voor polythiofeen:PCBM zonnecellen. De kristallijne vezel tot totale polymeer gewichtsverhouding in dit type zonnecellen werd gevarieerd tussen ~ 0.1 en ~ 0.9 . In dit gebied daalt E_{CT} met ongeveer 20 meV, per verhoging met 0.1 vande de vezel tot totale polymeer gewichtsverhouding. In alle gevallen volgt V_{oc} ruwweg dezelfde trend als E_{CT} .

De energetische verliezen tussen qV_{oc} en E_{CT}

Voor de zonnecellen onderzocht in dit werk, werd steeds een energetisch verschil tussen E_{CT} en qV_{oc} van ongeveer 0.6 eV gevonden, met hierbij V_{oc} gemeten onder zonnebelichtingscondities. De oorzaak van dit energetisch is tweeërlei. Een deel wordt veroorzaakt door energetisch verlies wegens radiatieve recombinatie via de CT toestand. Dit deel van het energetisch verlies kan gereduceerd worden door het totaal aantal CTCs in het mengsel te verminderen of door de elektronische koppeling tussen donor en acceptor te reduceren. Dit vermindert de werkzame CT absorptie doorsnede maar ook de vervalsnelheid van de CT toestanden. Voor de onderzochte zonnecellen vertegenwoordigt dit deel ongeveer ~ 0.25 eV van het energieverlies tussen qV_{oc} en E_{CT} . Het tweede deel van het energieverlies, ongeveer ~ 0.35 eV, wordt veroorzaakt door niet-radiatieve recombinatie mechanismen. Verder onderzoek om deze niet-radiatieve paden te identificeren is nodig om mogelijke strategieën te vinden die dit verlies minimaliseren.

Beide V_{oc} en E_{CT} werden ook gemeten onder andere belichtingscondities dan kamertemperatuur en zonnebelichting. Ze werden bepaald voor verschillende temperaturen tussen 150 K en 300 K. Er werd gevonden dat voor de onderzochte polymeer:fullereen zonnecellen, het verschil tussen E_{CT} en qV_{oc} lineair daalde met dalende temperatuur, en logaritmische daalde met dalende lichtintensiteit. Verder, ongeacht de gebruikte belichtingsintensiteit, is de extrapolatie van qV_{oc} tot 0 K gelijk aan de extrapolatie van E_{CT} tot 0 K.

Bovengrens van de vermogensomzettingsefficiëntie van organische donor/acceptor zonnecellen

Een bovengrens voor de bereikbare vermogen omzettingsefficiëntie van organische donor/acceptor zonnecellen, voor gestandaardiseerde AM1.5g belichtingscondities, werd afgeleid. De efficiëntielimiet werd verkregen als functie van twee parameters: de optische bandkloof van de het meest absorberende materiaal E_g , en de radiatieve energetische verliezen veroorzaakt door de aanwezigheid van donor/acceptor materiaal interactie. Deze efficiëntielimiet ligt net boven de 25 % wanneer de optische bandkloof van het sterkst absorberende materiaal in de 1.2 – 1.7 eV regio ligt, en de radiatieve verliezen door de CT toestand beneden de 0.2 eV blijven. Vandaag halen de beste polymeer:fullereen zonnecellen een efficiëntie van 6 %. In deze zonnecellen worden fotonvoltaïsche externe kwantum efficiënties behaald van 70 % tot 80 % voor fotonen met fotonenergie hoger dan de bandkloof van het polymeer. De hoofdbron van energieverlies in deze beste zonnecellen moet men dus zoeken in de, vergeleken met de bovenlimiet, lage waarde van V_{oc} .

Appendix: Paper A-F

Paper A

Fourier-Transform Photocurrent Spectroscopy for a fast and highly sensitive spectral characterization of organic and hybrid solar cells

K. Vandewal, L. Goris, I. Haeldermans, M. Nesladek, K. Haenen, P. Wagner, J. V. Manca, *Thin solid films* **516**, 7135 (2008)

Fourier-Transform Photocurrent Spectroscopy for a fast and highly sensitive spectral characterization of organic and hybrid solar cells

K. Vandewal^{a,*}, L. Goris^a, I. Haeldermans^a, M. Nesládek^{a,b}, K. Haenen^a,
P. Wagner^a, J.V. Manca^a

^a Institute for Materials Research, Hasselt University, and IMEC-IMOMEC, vzw, Wetenschapspark 1, B-3590, Diepenbeek, Belgium

^b LIST (CEA-Recherche Technologique)/DETECS/SSTM/LTD, Building 451, F-91191 Gif-sur-Yvette, France

Available online 14 December 2007

Abstract

Two modes of Fourier-Transform Photocurrent Spectroscopy (FTPS) are presented for a fast and sensitive determination of photocurrent spectra of organic and dye sensitized solar cells. Furthermore, FTPS allows to spectrally resolve sub-bandgap absorption phenomena in P3HT, in organic P3HT:PCBM bulk heterojunctions and in hybrid P3HT/TiO₂ solar cells. The sub-bandgap absorption in the P3HT:PCBM blend is dominated by a band due to the formation of a ground-state charge-transfer complex between the polymer and PCBM. In P3HT/TiO₂ junctions such a charge-transfer complex band is not observed. Long-lived light induced sub-bandgap states appear in pure P3HT and in P3HT/TiO₂ junctions after irradiation with $E > 1.9$ eV.

© 2007 Elsevier B.V. All rights reserved.

Keywords: Organic solar cells; Dye sensitized solar cells; FTPS; Optical spectroscopy

1. Introduction

New types of solar cells such as organic bulk heterojunction (BHJ) solar cells and dye sensitized solar cells (DSSC) are based on three dimensional, nanoscale interpenetrating networks of different electron and hole transporting materials. At the large internal interface, excitons created upon illumination are split, resulting in separated electrons and holes, which are transported in different materials. Power conversion efficiencies up to 5% were reported for fully organic BHJ devices using a blend of the conjugated polymer poly(3-hexylthiophene) (P3HT) and the fullerene derivative [6-6]-phenyl C61 butyric acid methyl ester (PCBM) [1]. DSSCs consisting of a nanoporous TiO₂ network, a dye and an electrolyte nowadays reach power conversion efficiencies over 10% [2]. The use of conjugated polymers in DSSCs as a replacement for the liquid electrolyte as the hole transporting material can avoid encapsulation and stability problems. Because of the conjugated polymer's ability to absorb light, it is also possible to omit the dye [3]. On the other hand, the replacement of

the morphologically instable organic fullerene network [4,5] in organic BHJ devices by a metal oxide network could improve the stability of the morphology of such devices. In this way both the organic and dye sensitized solar cell evolve to hybrid organic/inorganic solar cells.

An important step in the further development of these types of solar cells is the need for a better insight in the electronic structure and density of trapped states of the used materials, and their influence on the device performance. States in the bandgap will have a strong influence on transport, recombination and trapping properties of the used materials. Fourier-Transform Photocurrent Spectroscopy already has proven to be a valuable measurement technique to study sub-bandgap features in amorphous silicon [6] and polymer/fullerene [7] photovoltaic devices. FTPS uses the output light beam of a Fourier-Transform Infrared (FTIR) spectrometer to illuminate the photovoltaic device under test [6]. The spectral dependence of the incident light is measured with a calibrated photodetector and converted to light irradiation power. In this way, a photocurrent spectrum in A/W can be obtained.

The output light beam of an FTIR spectrometer is an intensity-modulated light beam. In this work, two modes of the FTIR spectrometer are used: The Continuous Scan mode (CS-

* Corresponding author. Tel.: +32 11 26 88 70; fax: +32 11 26 88 99.
E-mail address: koen.vandewal@uhasselt.be (K. Vandewal).

FTPS) and the Amplitude Modulated step scan mode (AM-FTPS). In the CS-FTPS mode, the incident light is modulated with a different frequency f , depending on its wavenumber σ :

$$f = 2\sigma v \quad (1)$$

Hereby is v the mirror velocity of the FTIRs moving mirror [8]. In the AM-FTPS mode the output beam is modulated with a fixed chopping frequency for every wavenumber. In this mode, spectral information is extracted by measuring the photocurrent signal for different mirror retardations [8].

In this work, absolute photocurrent spectra of an organic P3HT:PCBM solar cell and a DSSC are obtained by the FTFS method. The extremely high sensitivity of this method will be demonstrated by the detection of sub-bandgap features in P3HT, PCBM, P3HT:PCBM and the hybrid P3HT/TiO₂ device.

2. Experimental details

2.1. Solar cells

Organic devices with an active layer of P3HT, PCBM and the P3HT:PCBM 1:1 blend were constructed using a standard procedure in N₂ atmosphere. A 40 nm thick poly(3,4-ethylenedioxythiophene-polystyrenesulfonate (PEDOT-PSS, Bayer) layer was spincoated from an aqueous solution onto indium tin oxide (ITO, 100 nm) coated glass. These substrates were dried for 20 min on a hotplate at 120 °C. Subsequently the active layers of the pure and blended materials were spincoated from a chlorobenzene solution (2 wt.%) on top of the PEDOT-PSS layer. Finally, the Al top electrode of 80 nm was evaporated on top of the active layer.

Hybrid, P3HT/TiO₂ devices were prepared in the following way: an aqueous citratoperoxo-Ti(IV)-gel precursor was spincoated onto SnO₂:F coated borosilicate glass (Solaronix). After a heat treatment of 1 h at 650 °C a 60 nm, thin dense layer of TiO₂ was formed [9]. On top, a Solaronix nanoxide T paste was tape casted and was given a heat treatment of 450 °C for 30 min in air. This resulted in the formation of a nanoporous TiO₂ layer with a thickness of 4 μm. Afterwards, a P3HT layer was spincoated on top from a 2 wt.% chlorobenzene solution. After spin coating, the sample was annealed for 10 min at 110 °C on a hotplate. As top electrode, a 40 nm thick layer of gold was evaporated.

Both the P3HT:PCBM and P3HT/TiO₂ devices have an active area of 0.25 cm².

A larger area DSSC (area = 70 cm²) has been purchased from Solaronix.

2.2. Measurement setup

The organic and hybrid photovoltaic devices were mounted in a N₂ filled measurement chamber. For the FTFS measurements, the modulated illumination beam of a Thermo Electron Nicolet 8700 FTIR with an external detector option was used. For the CS mode, the produced photocurrent upon illumination was amplified by a Stanford Research Systems (SRS) low noise current preamplifier (SR). When using the AM mode, an optical

chopper and a SRS SR830 lock-in amplifier were used to modulate and to measure the photocurrent. For both modes the amplified photocurrent was fed back to the FTIR. The resolution of the FTIR spectrometer was set to 32 cm⁻¹.

For the absolute photocurrent measurements, the light was filtered with an IR blocking filter with a cut-on at 1.5 eV. As reference, a calibrated silicon photodetector was used.

For the sub-bandgap absorption measurements a long wave pass filter with a cut-off frequency of 2 eV was used. The reference detector was the internal DTGS detector of the used spectrometer. Spectra were set to absolute absorption scale (cm⁻¹) by matching the high energy region with data obtained from transmission and reflection measurements. In this approach the measured absorption coefficient is the actual $\alpha(E)$ scaled with the quantum efficiency for free carrier generation, as the photocurrent in organic devices is proportional to $\alpha(E)\eta(E)$, in which η can also be spectrally dependent [10].

3. Results and discussion

3.1. Absolute photocurrent spectra

3.1.1. Organic bulk heterojunction solar cells

A high measurement speed, while maintaining a high resolution, makes CS-FTPS very interesting for a fast and accurate measurement of absolute photocurrent spectra. In Fig. 1, the photocurrent spectrum of the P3HT:PCBM device measured by FTFS is shown and is compared to the one measured with the classical technique using monochromatic light. The advantage of FTFS is that a high resolution (0.004 eV) spectrum between 800 and 400 nm is obtained in a few seconds. For the shorter wavelengths, the FTFS spectrum becomes noisier. This is due to the fast decreasing light intensity of the FTIRs light source in this spectral area.

The inset of Fig. 1 shows the modulation frequency response of the organic photovoltaic device. It was deduced by an algorithm using formula (1) and the data obtained for different mirror velocities. When a mirror velocity of 0.1581 cm s⁻¹ is used, the modulation frequencies are between 4 kHz and 8 kHz.

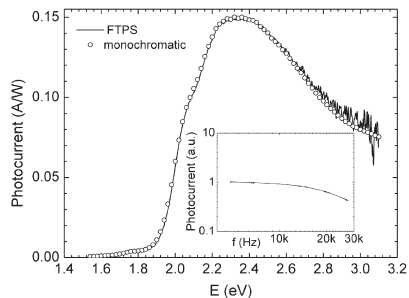


Fig. 1. The photocurrent spectrum of a P3HT:PCBM bulk heterojunction solar cell measured by the monochromatic technique and by CS-FTPS. The inset shows the modulation frequency dependence of the device.

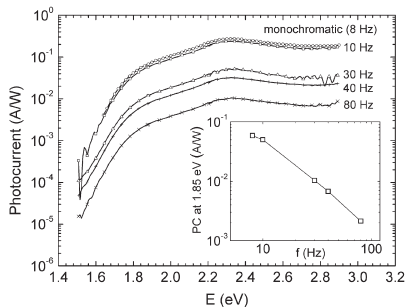


Fig. 2. The photocurrent spectrum of a dye sensitized solar cell measured by the monochromatic technique and by AM-FTPS for different frequencies. The inset shows the signal at 1.85 eV versus chopping frequency.

From the inset it is clear that for this mirror velocity, the frequency response is still in its quasi DC mode. When using this mirror velocity, the modulation frequency response will not influence the measurement.

3.1.2. Dye sensitized solar cells

The use of CS-FTPS causes problems for the measurement of DSSCs containing an electrolyte. This device usually have a cut-off frequency well below 1 kHz. The photocurrent for light modulation frequencies above 1 kHz is very low and the spectrum will undergo mayor deformations. For this kind of long response time solar cells, the use of the AM-FTPS mode at low chopping frequencies is more appropriate. In Fig. 2 the photocurrent of the DSSC obtained from Solaronix is shown for different modulation frequencies and compared with the photocurrent spectrum obtained by the monochromatic technique at a chopping frequency of 8 Hz. For this DSSC a bandgap of 1.7 eV with an Urbach slope of 52 meV can be deduced. The inset of the figure shows the photocurrent at 1.85 eV versus the modulation frequency. It is clear that the photocurrent signal decreases fast for an increasing chopping frequency, even for low frequencies.

3.2. Sub-bandgap absorption

3.2.1. Organic bulk heterojunction solar cells

Due to the extremely high sensitivity of FTPS, it is possible to measure light absorption in the low absorbing region between 1 eV and 1.9 eV, corresponding to the bandgap of the photovoltaic devices. Fig. 3 shows the measured absorption spectra on a logarithmic scale of the pure P3HT and PCBM, and the P3HT:PCBM blended devices. In the high energy part of the measurement, a bandgap of 1.9 eV for P3HT and 1.7 eV for PCBM could be deduced. Below this bandgap the absorption decreases exponentially. an Urbach slope of 33 meV and 29 meV could be deduced for respectively P3HT and PCBM.

An interesting effect is observed when examining the FTPS spectrum of the P3HT:PCBM composite. In comparison with the pure spectra, the composite one shows a new absorption

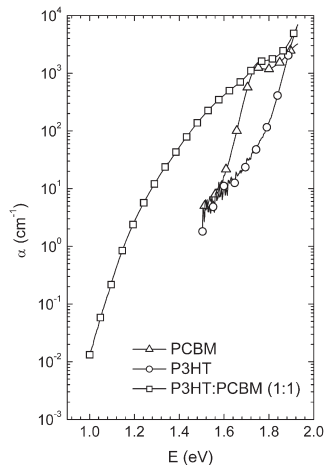


Fig. 3. Absorption coefficient below the bandgap of P3HT, PCBM and P3HT:PCBM as measured by FTPS.

band, which can be fitted by a Gaussian centred at 1.9 eV and having a width of 0.4 eV. This extra absorption band has also been previously detected for the MDMO-PPV:PCBM blend [11] and for blends of PCBM with polyfluorenes [12], and has been assigned to the formation of a charge-transfer complex (CTC) between the conjugated polymer and PCBM. The

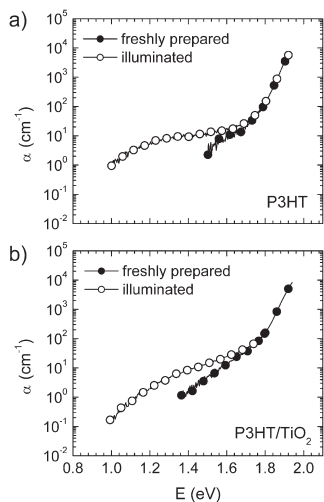


Fig. 4. The absorption coefficient below the bandgap of a freshly prepared and illuminated a) P3HT and b) P3HT/TiO₂ device.

presence of this CTC is determined by the ionization potential of the used conjugated polymer. It is argued that it has a role in charge-transfer, transport and recombination processes in these types of solar cells [12]. CS-FTPS is a suited technique to rapidly and accurately detect the presence of this CTC, directly on the solar cell device and to perform further investigation to reveal the exact influence of this extra state.

3.2.2. Illumination induced long lived states in P3HT and P3HT/TiO₂ blends

Fig. 4 a) and b) show the respective spectra of a pure P3HT and a hybrid P3HT/TiO₂ device, both before and after an illumination of 30 min with a tungsten–halogen lamp with an intensity of approximately 1 sun. For both, a low energy absorption band due to the illumination is appearing. This sub-bandgap absorption band does only appear if the illumination contains energies above 1.9 eV. When the samples are kept in the dark for 2 days, the sub-bandgap absorption decreases and disappears again. An annealing treatment at 100 °C for 5 min also eliminates the illumination-induced absorption. A similar effect of increasing sub-bandgap absorption upon above bandgap illumination was detected in the absorption spectrum of TiO₂, measured with PDS [13].

This light induced sub-bandgap absorption is caused by the presence of trapped charge carriers, created upon illumination. In the studied devices most of the photocurrent originates from excitons split at the P3HT/Al or P3HT/TiO₂ interface. The sub-bandgap photocurrent measured by FTPS after illumination is therefore attributed to carriers trapped at the interfaces. This large amount of trapped carriers will influence the interface properties such as semiconductor band bending and charge carrier generation. In reference [14] it is argued that these trapped charges have a large influence on the open circuit voltage (V_{oc}) and that the build up of charge at the P3HT/TiO₂ interface may cause the observed decrease in V_{oc} during illumination.

The broad sub-bandgap absorption band created upon illumination of P3HT/TiO₂ devices has different characteristics than the CTC band, as observed in P3HT:PCBM blends. While illumination has no measurable influence on the sub-bandgap absorption in blends of P3HT with PCBM, it has a large influence on the sub-bandgap absorption in pure P3HT and P3HT/TiO₂ devices.

4. Conclusion

In conclusion, it is shown that FTPS is a favourable technique for a fast and accurate measurement of absolute photocurrent spectra of organic bulk heterojunction and dye sensitized solar cells. The fast, continuous scan mode, produces light modulation frequencies directly proportional to the wavenumber or energy of the light source. These frequencies are practically above 1 kHz. For fast responding organic bulk heterojunction solar cells, this mode produces a photocurrent spectrum in a matter of

seconds and no corrections due to the frequency response are needed. For the measurement of long response time dye sensitized solar cells, the step scan mode is used. This mode allows lowering the modulation frequency and to measure the photocurrent spectrum for a certain, fixed frequency.

Because of the high sensitive nature of the FTPS technique, not only classical photocurrent spectra can be measured, but also photocurrent generated by sub-bandgap optical transitions can be detected. The detected low energy bands in pure P3HT and in P3HT/TiO₂ junctions appear after irradiation with $E > 1.9$ eV. This absorption may be explained by the presence of light induced, trapped charge carriers. For the P3HT:PCBM blend, the sub-bandgap absorption is dominated by a band due to the formation of a ground-state charge-transfer complex between the polymer and PCBM, and no light induced features could be detected.

Acknowledgements

This research was funded by a PhD grant of the Institute for the Promotion of Innovation through Science and Technology in Flanders (IWT-Vlaanderen), the IWI-SBO project Nanosolar, the interreg project OLED+ and the FWO project G.0252.04.

References

- [1] M. Reyes-Reyes, K. Kim, D.L. Carroll, *Appl. Phys. Lett.* 87 (2005) 083506.
- [2] J.M. Kroon, N.J. Bakker, H.J.P. Smit, P. Liska, K.R. Thampi, P. Wang, S.M. Zakeeruddin, M. Grätzel, A. Hinsch, S. Hore, U. Würfel, R. Sastrawan, J.R. Durrant, E. Palomares, H. Pettersson, T. Gruszeccki, J. Walter, K. Skupien, G.E. Tulloch, *Prog. Photovolt.: Res. Appl.* 15 (2007) 1.
- [3] D. Gebeyehu, C.J. Brabec, N.S. Sariciftci, D. Vangeneudgen, R. Kiebooms, D. Vanderzande, F. Kienberger, H. Schindler, *Synth. Met.* 125 (2002) 279.
- [4] S. Bertho, I. Haeldermans, A. Swinnen, W. Moons, T. Martens, L. Lutsen, D. Vanderzande, J.V. Manca, A. Senes, A. Bonfiglio, *Sol. Energy Mater. Sol. Cells* 91 (2007) 385.
- [5] A. Swinnen, I. Haeldermans, M. vande Ven, J. D'Haen, G. Vanhoyland, S. Aresu, M. D'Olieslaeger, J.V. Manca, *Adv. Funct. Mater.* 16 (2006) 760.
- [6] M. Vaněček, A. Poruba, *Appl. Phys. Lett.* 80 (5) (2002) 719.
- [7] L. Goris, A. Poruba, L. Hod'akova, M. Vanecek, K. Haenen, M. Nesladek, P. Wagner, D. Vanderzande, L. De Schepper, *J.V. Manca, Appl. Phys. Lett.* 88 (2006) 052113.
- [8] P.R. Griffiths, J.A. deHaseth, *Fourier Transform Infrared Spectroscopy*, Wiley, New York, 1986.
- [9] I. Truijten, M.K. van Bael, H. Van den Rul, J. d'Haen, J. Mullens, *J. Sol-Gel Sci. Technol.* 41 (2007) 43.
- [10] J. Willekens, M. Brinza, T. Aermouts, J. Poortmans, G.J. Adriaenssens, *J. Non-Cryst. Solids* 352 (2006) 1675.
- [11] L. Goris, K. Haenen, M. Nesladek, P. Wagner, D. Vanderzande, L. De Schepper, J. D'Haen, L. Lutsen, J.V. Manca, *J. Mater. Sci.* 40 (2005) 1413.
- [12] J.J. Benson-Smith, L. Goris, K. Vandewal, K. Haenen, J.V. Manca, D. Vanderzande, D.D.C. Bradley, J. Nelson, *Adv. Funct. Mater.* 17 (2007) 451.
- [13] K. Vandewal, L. Goris, K. Haenen, Y. Geerts, J.V. Manca, *Eur. Phys. J. Appl. Phys.* 36 (2006) 281.
- [14] A. Watanabe, A. Kasuya, *Thin Solid Films* 483 (2005) 358.

Paper B

The relation between open-circuit voltage and the onset of photocurrent generation by charge-transfer absorption in polymer:fullerene bulk heterojunction solar cells

K. Vandewal, A. Gadisa, W. D. Oosterbaan, S. Bertho, F. Banishoeib, I. Van Severen, L. Lutsen, T. J. Cleij, D. Vanderzande, J. V. Manca, *Adv. Funct. Mater.* **18**, 2064 (2008)

DOI: 10.1002/adfm.200800056

The Relation Between Open-Circuit Voltage and the Onset of Photocurrent Generation by Charge-Transfer Absorption in Polymer:Fullerene Bulk Heterojunction Solar Cells**

By Koen Vandewal,* Abay Gadisa, Wibren D. Oosterbaan, Sabine Bertho, Fateme Banishoeib, Ineke Van Severen, Laurence Lutsen, Thomas J. Cleij, Dirk Vanderzande, and Jean V. Manca

Photocurrent generation by charge-transfer (CT) absorption is detected in a range of conjugated polymer–[6,6]-phenyl C₆₁ butyric acid methyl ester (PCBM) based solar cells. The low intensity CT absorption bands are observed using a highly sensitive measurement of the external quantum efficiency (EQE) spectrum by means of Fourier-transform photocurrent spectroscopy (FTPS). The presence of these CT bands implies the formation of weak ground-state charge-transfer complexes in the studied polymer–fullerene blends. The effective band gap (E_g) of the material blends used in these photovoltaic devices is determined from the energetic onset of the photocurrent generated by CT absorption. It is shown that for all devices, under various preparation conditions, the open-circuit voltage (V_{oc}) scales linearly with E_g . The redshift of the CT band upon thermal annealing of regioregular poly(3-hexylthiophene):PCBM and thermal aging of poly(phenylenevinylene)(PPV):PCBM photovoltaic devices correlates with the observed drop in open-circuit voltage of high-temperature treated versus untreated devices. Increasing the weight fraction of PCBM also results in a redshift of E_g , proportional with the observed changes in V_{oc} for different PPV:PCBM ratios. As E_g corresponds with the effective bandgap of the material blends, a measurement of the EQE spectrum by FTPS allows us to measure this energy directly on photovoltaic devices, and makes it a valuable technique in the study of organic bulk heterojunction solar cells.

1. Introduction

Currently, the best performing polymer-based solar cells comprise bulk heterojunction (BHJ) polymer/acceptor interpenetrating networks characterized by a three dimensional, nanoscale morphology. The generation of photocurrent in such solar cells follows a multi-step process, namely, generation of excited electron-hole pairs (excitons), mainly in the polymer phase and the subsequent splitting of these excited states at the polymer/acceptor interface leaving free holes in the polymer phase while transferring the electrons to the electron accepting material. Such a transfer process eventually leads to two separate percolation paths for the free charge carriers.^[1,2] Successful BHJ devices have been fabricated by solution

deposition of mixtures of a soluble conjugated polymer and the fullerene derivative [6,6]-phenyl C₆₁ butyric acid methyl ester (PCBM). Among the commonly used soluble conjugated polymers are poly(phenylene vinylene) (PPV),^[3,4] polyfluorene^[5,6] and polythiophene^[7] derivatives. By controlling the BHJ nanomorphology, power conversion efficiencies up to 4–5% have been achieved.^[7,8] However, further improvements are still needed in order to obtain higher efficiencies that make polymer solar cells competitive with their inorganic counterparts.

Understanding the factors that limit photovoltaic parameters such as short-circuit current (J_{sc}) and open-circuit voltage (V_{oc}), helps to optimize material and device structures, leading to higher efficiencies. While J_{sc} is determined by the creation and subsequent dissociation of excitons at the polymer/acceptor interface followed by transport of free charge carriers towards the collecting electrodes^[9], V_{oc} is primarily determined by the effective band gap of the BHJ film.^[10,11]

As far as the exciton dissociation process is concerned, recent theories and experimental evidences indicate that an intermediate charge-transfer (CT) state exists between the excitons created upon light absorption in the polymer and the long-lived, free charge carriers. Recently, the existence of such an intermediate CT state in a BHJ consisting of a low band gap semiconducting copolymer and PCBM was inferred from analysis of its carrier recombination dynamics.^[12] Quantum chemical calculations of charge transfer in the

[*] K. Vandewal, Dr. W. D. Oosterbaan, S. Bertho, Dr. F. Banishoeib, Dr. I. Van Severen, Dr. L. Lutsen, Prof. T. J. Cleij, Prof. D. Vanderzande
Prof. J. V. Manca
Institute for Materials Research, Hasselt University
Wetenschapspark 1, 3590 Diepenbeek (Belgium)
E-mail: koen.vandewal@uhasselt.be

Dr. A. Gadisa, Dr. L. Lutsen, Prof. D. Vanderzande, Prof. J. Manca
IMEC-IMOMECE, vzw
Wetenschapspark 1, 3590 Diepenbeek (Belgium)

[**] This research was funded by the IWT-projects Nanosolar and Poly-spec, the interreg project OLED+ and the FWO projects G.0396.08 and G.0091.07. K. V. acknowledges the institute for the promotion of innovation through science and technology in Flanders (IWT-Vlaanderen) for funding. S. B. is a research assistant of the Fund for Scientific Research Flanders (FWO-Vlaanderen).

poly(3-hexylthiophene) (P3HT):PCBM material system also support the presence of an extended electronic state created upon material blending.^[13] It was shown that this state has a significant probability distribution across the donor/acceptor (D/A) interface in its lowest excited state. The existence of such intermediate bound electron-hole pairs at the D/A interface was already assumed to explain the compositional dependence of the photocurrent generation in PPV:PCBM solar cells.^[14] It was shown that the incomplete dissociation of these photo-generated bound electron-hole pairs under operating conditions is a main loss mechanism in this type of solar cells. Further optimization of polymer–fullerene based solar cells thus requires a thorough study of these interfacial intermediate states.

Highly sensitive studies of the absorption spectra of P3HT:PCBM and PPV:PCBM blends by our group, have revealed the presence of a long wavelength absorption band characteristic for a weak ground state CT complex (CTC), formed by the interaction of the lowest unoccupied molecular orbital of the fullerene acceptor LUMO(A) with the highest occupied molecular orbital of the polymer donor HOMO(D).^[15–16] Illumination with wavelengths in this CT band results in the direct creation of bound electron-hole pairs or CT excitons, as described by Foster^[17] for CTCs in solution.

CTC formation is widely observed when combining donor materials with electron acceptors such as C₆₀ and C₇₀ (see for example reference^[18] and references therein). Recently, it was shown that a whole range of π -conjugated polymers and oligomers form CT absorption bands when mixed with electron acceptors in chloroform solution.^[19] Using Photothermal Deflection Spectroscopy and photoluminescence spectroscopy, the formation of CTCs was also evidenced for solid-state blends of different types of polyfluorenes with PCBM.^[20–21]

In reference^[21] a model for the involvement of these CTCs in the photocurrent generation mechanism was proposed. It was shown that the energy of the excited CTC is critical for determining whether photocurrent is generated, or energy transfer and subsequent emission from the PCBM singlet state takes place. In previous works involving CTCs, however, no correlation between the open-circuit voltage and this CTC state has been reported.

In order to do so, we have measured the external quantum efficiency (EQE) spectra of photovoltaic devices consisting of a variety of conjugated polymers blended with PCBM by means of Fourier-transform photocurrents spectroscopy (FTPS). Originally applied to investigate subgap absorption by defects in hydrogenated microcrystalline silicon for photovoltaic devices, FTPS has a superior sensitivity^[22] as compared to monochromatic photocurrent measurement techniques. When applied to organic BHJ devices, it can be used for the determination of the device's absorption window. Moreover, FTPS has the required sensitivity to measure the low signal sub-band gap photocurrent produced by the direct creation of CT excitons upon long wavelength illumination of the CTCs.^[16]

In this paper it will be shown that the effective bandgap (E_g), determined by the onset of photocurrent generation by CT absorption, linearly correlates with the V_{oc} of the studied devices. Regardless of device type and treatment conditions such as annealing and aging a difference between the E_g and V_{oc} of about 0.43 V was observed for measurements performed at room temperature and under 1 sun illumination conditions. This investigation provides a deeper understanding of the origin of the photovoltage of polymer:PCBM based solar cells and hence may help to engineer material structures that lead to improved performance of BHJ solar cells.

2. Results and Discussion

2.1. Photocurrent Generation by CT Absorption

We have characterized various organic BHJ solar cells by measuring the EQE as a function of photon energy (E), using FTPS. The EQE is defined as the number of photo-generated electrons flowing in the external circuit at short-circuit, per incident photon.

A typical EQE spectrum of a polymer BHJ solar cell (active layer of MDMO-PPV:PCBM in a 1:4 weight ratio, sandwiched

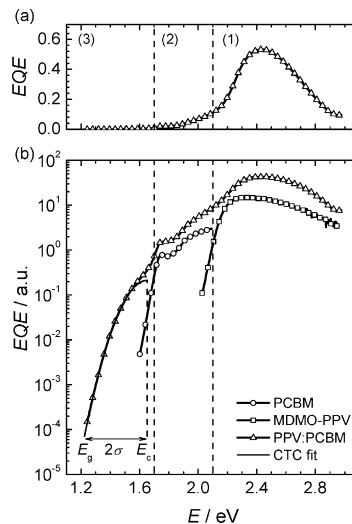


Figure 1. The external quantum efficiency (EQE) as a function of the energy (E) of the incident light of the MDMO-PPV:PCBM (1:4) photovoltaic device measured by FTPS presented on a) a linear and b) a logarithmic scale. The different spectral regions (1)–(3) are described in the text. In figure (b) the FTPS spectra of the pure materials are also represented (in arbitrary units). The non-additive CTC band can be fitted with a Gaussian function centred at E_c and with a standard deviation σ . We define the effective band gap E_g as $E_g = E_c - 2\sigma$, as shown in the figure.

between ITO/PEDOT:PSS and Ca/Al electrodes) is shown in Figure 1 on a linear (a) and on a logarithmic (b) scale.

In Figure 1(b), the photocurrent spectra of the pure materials sandwiched between ITO/PEDOT:PSS and Al are also shown (on an arbitrary scale) for comparison. The EQE spectrum depicted in Figure 1(b) shows typical features that have different origins. The rightmost region (1), with photon energies greater than 2.1 eV, corresponds to the absorption spectrum of MDMO-PPV. The photocurrent generated in this region thus mainly originates from the excited states created in the polymer. Moreover, for the MDMO-PPV:PCBM blend, high values of EQE are achieved in this region indicating that polymer absorption is the primary source of excitons. The EQE in the second region (2), located between 1.7 eV and 2.1 eV, mainly represents the absorption of the acceptor molecule PCBM. The distinct peak around 1.75 eV is due to the symmetry forbidden optical HOMO-LUMO transition in the PCBM phase.^[15] The spectrum in the leftmost region (3), with photon energies between 1.2 eV and 1.7 eV, does not overlap with the absorption spectrum of either pure MDMO-PPV or PCBM. Based on the justifications given in previous reports,^[15,16,21] we attribute this low energy band to the CTCs created at the interface of MDMO-PPV and PCBM.

The new band occurring in the EQE spectrum originates from the absorption of long wavelength photons by the CTC ground states, giving rise to a direct creation of charge-separated states. The bound electron-hole pairs created by this CT absorption are separated further, generating photocurrent. Very recently^[23] it was argued that photocurrent generation occurs more efficiently through a 'hot' CT state, than through a relaxed state. This would make the CT exciton splitting efficiency wavelength dependent. Efforts are currently underway to investigate the energetic dependence of the splitting efficiency of the CT excitons.

As the ground state interaction in a polymer:PCBM CTC is expected to be weak, the spectral position of the CT band correlates to the difference of the polymer's HOMO level and the PCBM's LUMO level.^[17,19] For MDMO-PPV this difference has been determined from cyclic voltammetry measurements to be around 1.4 eV (Table 1). This value is well below the bandgap of both MDMO-PPV (2.1 eV) and PCBM (1.7 eV), and is in the observed spectral range of the CT band (1.2–1.6 eV) in the EQE spectrum.

The absorption coefficient of the CT absorption in MDMO-PPV:PCBM blends, as determined by PDS, is well below 1000 cm^{-1} .^[15] This makes the EQE spectral shape of the CT band independent of device thickness (thicknesses of our devices are typically around 100 nm). We have also found that the spectral shape of the CT band is not affected by electrode material, and is very reproducible for devices having the same polymer:PCBM weight ratio. Furthermore, the spectral shape of the CT band can be well fitted with a Gaussian function with amplitude A_0 , centered around E_c and given by the equation $A(E) = A_0 \exp[-(E - E_c)^2 / (2\sigma^2)]$. Henceforth, we define the onset E_g of the photocurrent generation by CT absorption as:

$$E_g = E_c - 2\sigma \quad (1)$$

The difference between the onset and the maximum of the CT band, $E_g - E_c$, is related to the reorganization energy between the Franck-Condon excited state $D^+ \cdot A^-$ and the relaxed $D^+ \cdot A^-$ excited state geometry.^[24,25] In addition, the presence of CTC conformers with slightly different geometries and hence different energies of the CT state might also contribute to the width of the CT band. The CTC band gap E_g , which is much lower than the lowest band gap of the materials in the D/A blend, can be considered as the effective bandgap E_g of the BHJ films. The Gaussian fit and the involved parameters are indicated in Figure 1. By using this description of the CT band, the correlation of the energy of the lowest CT state capable of generating photocurrent, with the photovoltaic parameters of the solar cells is discussed in the next section of this paper.

The mechanism of charge dissociation, involving the CTC has previously been discussed.^[21,23] The excitons generated either in the polymer or in the PCBM phase (region (1) and (2) in Figure 1) diffuse to the interface, where the intermediate CT exciton (an excited CTC) is formed. At this stage, the CT exciton is still coulombically bound and may either decay to the CTC ground-state or be converted into a more loosely bound polaron-pair state. Upon illumination in the spectral region (3) of Figure 1, however, CT excitons are directly created. As the CTC has a much lower absorption coefficient as compared to the polymer, the contribution of the photocurrent generated by this direct CT absorption is marginal as compared to the overall photocurrent of the BHJ photovoltaic device.

Table 1. Solar cell characteristic parameters for several polymer:PCBM BHJ devices and their LUMO(A)–HOMO(D) gaps as determined by cyclic voltammetry.

Donor Polymer	D/A ratio	J_{sc} [$\text{mA} \cdot \text{cm}^{-2}$]	V_{oc} [V]	FF	$E_{\text{LUMO(A)}} - E_{\text{HOMO(D)}}$ [eV]	E_c [eV]	E_g [eV]
MDMO-PPV	1:4	3.9	0.83	0.53	1.4	1.65	1.22
OC9-PEO-PPV	1:4	2.1	0.65	0.50	1.2	1.68	1.14
RR-P3HT	1:1	7.9	0.62	0.56	1.3	1.80	1.08
Dihexyl-PTV	1:1	1.7	0.57	0.49	1.2	1.42	1.02

2.2. Influence of the HOMO Level of the Donor Polymer on E_g and V_{oc}

We have measured the photovoltaic properties of several types of solar cells with varying polymer:PCBM BHJ active films. The chemical structures of the investigated conjugated polymers are depicted in Figure 2.

We have determined the important parameters of the photovoltaic devices such as J_{sc} , V_{oc} and fill factor (FF) by measuring current-voltage characteristics under 100 mW/cm² AM1.5 solar illumination. The E_g of the corresponding blends was determined from their EQE spectra measured by FTPS, as described in the previous section. The FTPS spectra, obtained in the spectral region between 1.0 and 2.0 eV, of the photovoltaic devices consisting of different donor polymers (diHexyl-PTV, PEO-OC9-PPV, MDMO-PPV and P3HT) in their best performing polymer:PCBM ratios are depicted in Figure 3. All four polymers show CTC formation upon mixing with PCBM. CTC formation was confirmed by the presence of a low energy, Gaussian like, CT band for all devices. The presence of this sub-bandgap feature is expected in this region since the energy differences between the LUMO level of PCBM and the HOMO levels of the donor polymers (Table 1) are positioned far below the onsets of the absorption bands of the pure materials. For visibility, the fitted CT spectrum of each device is normalized.

The relation between V_{oc} and E_g is shown in the inset of Figure 3, and it is shown that V_{oc} indeed scales with E_g of the D/A material blend. J_{sc} and FF , however, do not show a clear trend as can be seen from Table 1. The latter parameters in fact depend strongly on charge transport, absorption coefficient and morphology of the active layer.

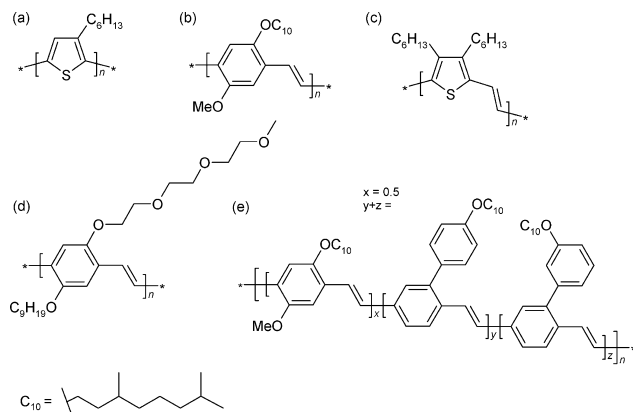


Figure 2. The chemical structure of a) P3HT, b) MDMO-PPV, c) diHexyl-PTV, d) PEO-OC9-PPV, and e) "High T_g -PPV". In this work the regiorandom and regioregular form of P3HT are used.

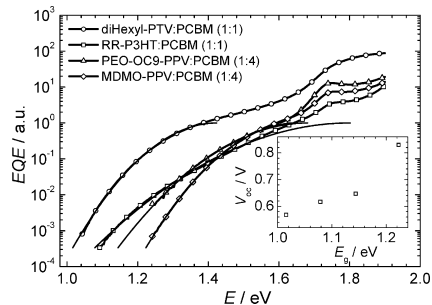


Figure 3. FTPS spectra of different types donor polymers blended with PCBM in the spectral area 1.0 eV < E < 2.0 eV. The CT absorption band was fitted with a Gaussian and the band gap was determined as described in the text. The inset shows the open-circuit voltage V_{oc} versus the effective band gap E_g .

2.3. Influence of Morphology on E_g and V_{oc}

It is well documented that the V_{oc} of P3HT:PCBM based solar cells reduces slightly upon annealing. Such changes have been attributed to morphological changes.^[26,27] Figure 4 shows the FTPS spectra of three types of solar cells: 1) regiorandom (ReRa) P3HT as electron donor, 2) non-annealed and regioregular (RR) P3HT as electron donor, 3) annealed and regioregular P3HT as electron donor.

The electron acceptor is PCBM in all cases, mixed with the polymers in a 1:1 weight ratio. In the case of RR-P3HT, it is known that an annealing procedure improves the crystallisation of the polymer phase, which improves the mobility of the charge carriers and causes a redshift in the absorption spectrum.^[27] This crystallinity enhancement results in a clear improvement of both FF and J_{sc} . In the case of ReRa-P3HT:PCBM, the morphology does not show any crystallinity at all, and therefore the solar cells exhibit a low FF and J_{sc} . These results are summarised in Table 2. From this table and Figure 4 it is clear that the improved crystallinity causes a redshift of the onset of the CT band, resulting in a proportional reduction of V_{oc} .

To investigate the effect of morphological aging on the CTC energy in more detail, photovoltaic devices were fabricated using MDMO-PPV or "High T_g -PPV" as electron donor material, blended in a 1:4 weight ratio with PCBM. Upon thermal aging at 110 °C, PCBM clusters are relatively rapidly formed in

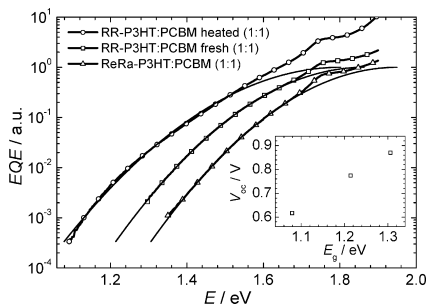


Figure 4. FTPS spectra of different types of P3HT blended with PCBM in the spectral area $1.0 < E < 2.0$ eV. The CT absorption band was fitted with a Gaussian and the effective band gap was determined as described in the text. The inset shows the open-circuit voltage V_{oc} versus the effective band gap E_g .

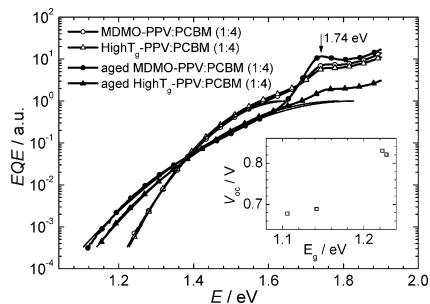


Figure 5. FTPS spectra of fresh and thermally aged MDMO-PPV:PCBM and "High T_g -PPV":PCBM photovoltaic devices in the spectral area of $1.0 < E < 2.0$ eV. The CT absorption band was fitted with a Gaussian and the band gap was determined as described in the text. The inset shows the open-circuit voltage V_{oc} versus the effective band gap E_g .

the MDMO-PPV:PCBM devices, while the morphology of the "High T_g -PPV":PCBM devices stays rather unchanged. This is due to the higher glass transition temperature T_g of "High T_g -PPV" ($T_g \approx 138$ °C) as compared to that of MDMO-PPV ($T_g \approx 12$ °C).^[28] Photovoltaic parameters for freshly prepared and for thermally aged (16 h at 110 °C) devices are given in Table 3.

From this table it is clear that J_{sc} is severely reduced by thermal aging for solar cells based on MDMO-PPV as compared to those based on "High T_g -PPV". In contrast, the V_{oc} and the onset energy of the CT band (Figure 5) degraded equally in both devices.

The formation of a more coarse phase separated morphology in thermally aged MDMO-PPV:PCBM blends^[28] can be identified in the FTPS spectra: for the aged MDMO-

PPV-PCBM device, the PCBM photocurrent peak at 1.74 eV becomes more pronounced due to the formation of PCBM aggregates. Upon aging, the amount of CTCs thus decreases, indicating less D/A material interaction, and thus a more phase separated morphology. In the case of "High T_g -PPV", the amount of complexes stays relatively unchanged upon thermal aging, indicating a more stable morphology^[28] as expected from its higher T_g .

In the case of RR-P3HT the observed redshift is explained by an increase in the polymer's HOMO level upon crystallisation. For the PPVs, it is known that a large scale crystallisation does not take place upon annealing. However, the formation of aggregates upon annealing of PPVs, resulting in an increased amount of polymer interchain interaction, has been observed.^[29] On the other hand, phase separation is only detected in the case of MDMO-PPV.^[28] We conclude that similarly as in the case of RR-P3HT:PCBM, the formation of aggregates created upon thermal aging of both types of PPV:PCBM based devices increases the effective HOMO level of the polymer and leads to the shift in CT energy and the corresponding drop in V_{oc} .

Table 2. Solar cell characteristic parameters for photovoltaic bulk heterojunction devices consisting of P3HT with a different degree of crystallinity.

Donor Polymer	Heat treatment	J_{sc} [$\text{mA}\cdot\text{cm}^{-2}$]	V_{oc} [V]	FF	E_c [eV]	E_g [eV]
ReRa-P3HT	no	0.73	0.87	0.29	1.95	1.31
RR-P3HT	no	3.5	0.77	0.36	1.86	1.21
RR-P3HT	yes	7.9	0.62	0.56	1.80	1.08

Table 3. Solar cell characteristic parameters for fresh and thermally aged photovoltaic bulk heterojunction devices consisting of MDMO-PPV and "High- T_g -PPV".

Donor Polymer	Aged	J_{sc} [$\text{mA}\cdot\text{cm}^{-2}$]	V_{oc} [V]	FF	E_c [eV]	E_g [eV]
MDMO-PPV	no	3.9	0.83	0.53	1.65	1.22
"High T_g -PPV"	no	3.1	0.82	0.40	1.63	1.23
MDMO-PPV	yes	1.7	0.68	0.34	1.83	1.11
"High T_g -PPV"	yes	2.8	0.69	0.39	1.79	1.14

2.4. Influence of the Composition Ratio on E_g and V_{oc}

In previous reports it was demonstrated that V_{oc} varies with the polymer:PCBM composition ratio. In the case of MDMO-PPV it was shown that V_{oc} decreases with increasing PCBM content.^[30] To verify if this effect can also be attributed to a change in E_g , FTPS was performed on four solar cells of MDMO-PPV with different weight percentages of PCBM (5, 10, 50 and 80%).

The results are summarized in Table 4 and shown in Figure 6. Again, V_{oc} and E_g follow the same trend. Upon increasing PCBM concentration, a redshift of the CT band and a proportional decrease in V_{oc} are observed.

Table 4. Solar cell characteristic parameters for photovoltaic BHJ devices consisting of freshly prepared MDMO-PPV:PCBM blends with a different weight fractions of PCBM.

PCBM weight fraction [%]	J_{sc} [$\text{mA}\cdot\text{cm}^{-2}$]	V_{oc} [V]	FF	E_c [eV]	E_g [eV]
5	0.062	0.97	0.23	1.87	1.34
10	0.13	0.91	0.23	1.83	1.32
50	2.6	0.88	0.30	1.69	1.27
80	3.9	0.83	0.53	1.65	1.22

These results indicate that the addition of PCBM in MDMO-PPV:PCBM blends stabilizes the CT state, possibly by dipole-induced dipole interactions and/or by lowering the effective LUMO-level of PCBM due to the formation of PCBM clusters. The exact influence of both effects on the spectral position of the CT band is currently under investigation.

2.5. Relation between E_g and V_{oc}

Figure 7 summarises the overall results of the studies. It depicts the relation between E_g and V_{oc} of the polymer:PCBM devices at room temperature.

The excellent correlation found clearly indicates that the energy E_g , as defined in Equation (1), determines V_{oc} . Upon applying a linear fit, we obtain:

$$V_{oc} \approx \frac{E_g}{e} - 0.43\text{V} \quad (2)$$

The onset of 0.43 V is expected to be illumination and temperature dependent. It can mainly be attributed to voltage losses at the ITO/PEDOT:PSS and Ca/Al ohmic contacts. The band bending at these ohmic contacts reduces V_{oc} at room

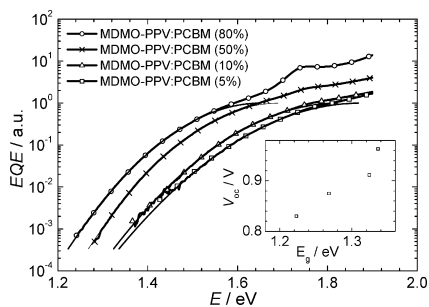


Figure 6. FTPS spectra of MDMO-PPV blended with different weight fractions of PCBM in the spectral area $1.2 < E < 2.0$ eV. The CT absorption band was fitted with a Gaussian and the effective band gap was determined as described in the text. The inset shows the open-circuit voltage V_{oc} versus the effective band gap E_g .

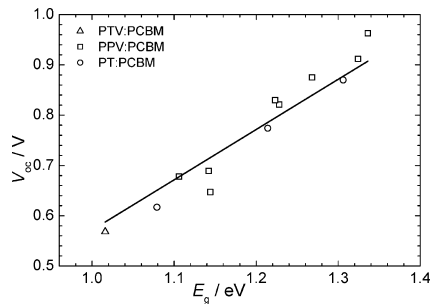


Figure 7. The effective band gap E_g versus V_{oc} of all the studied photovoltaic devices.

temperature and under 1 sun illumination by typically 0.2 V for each contact.^[31]

3. Conclusions

We have observed the formation of ground state CTCs in blends of a range of PPVs, regiorandom and regioregular P3HT and a soluble PTV derivative, all blended with PCBM. Due to its high sensitivity, FTPS enables the measurement of the photocurrent generated by the direct long wavelength absorption of the CTC, which typically has a very low absorption coefficient. The CT photocurrent band can be fitted with a Gaussian function and from the onset of the band, an effective band gap E_g for the blend can be determined. The size of E_g not only depends on the tabulated energetic position of the LUMO(A) - HOMO(D) energy differences, but also on the PCBM weight fraction and on the morphological and electronic effect of thermal annealing and aging procedures.

While the band gap of the polymer determines the spectral overlap with the solar spectrum and thus the maximum obtainable J_{sc} , we have found that there is a linear correlation between E_g as determined from the onset of the photocurrent generated by CT absorption and the V_{oc} of the solar cells. These findings go one step further than the widely accepted correlation of the open-circuit voltage with the LUMO(A) - HOMO(D) difference, as it is shown that our proposed correlation can also explain variations in V_{oc} , observed for different preparation and aging conditions of the same polymer:PCBM material system.

EQE measurement by FTPS proves to be a valuable technique because it can determine both maximum obtainable short-circuit photocurrent and maximum obtainable open-circuit voltage for a given polymer:PCBM combination in one single, fast measurement. These findings may open up new research windows that help engineering next generation solar cell organic materials.

4. Experimental

Materials: PCBM was purchased from Solenne, P3HT (ReRa and RR) from Rieke Metals and MDMO-PPV and “High T_g - PPV” [32] from Merck. Synthesis of PEO-OC9-PPV [33] and diHexyl-PTV [34] were described elsewhere.

Device Construction: Organic devices with an active layer of MDMO-PPV, PCBM and the polymer:PCBM blends were constructed using a standard procedure in N_2 atmosphere. First, a 40 nm thick poly(3,4-ethylenedioxythiophene:polystyrenesulfonate (PEDOT:PSS, Bayer) layer was spincoated from an aqueous solution onto indium tin oxide (ITO, 100 nm) coated glass. These substrates were dried for 20 min on a hotplate at 120 °C. Subsequently the active layers of the pure and blended materials were spincoated from a chlorobenzene solution on top of the PEDOT:PSS layer. Finally, 20 nm of Ca and 60 nm of Al was evaporated through a shadow mask as top electrode. All devices have an active area of 25 mm².

Device Measurement: All measurements were performed in N_2 atmosphere.

The IV-characteristics were measured under illumination with an Oriol solar simulator equipped with a Xenon Short Arc lamp with a power of 150W, using a home built setup with a Keithley 2004 current voltage source meter.

Thin film electrochemical properties were measured using a conventional three electrode cell with an Ag/Ag⁺ reference electrode, a platinum counter electrode and an ITO coated glass substrate as working electrode. Cyclic voltamograms were recorded at 50 mV/s under N_2 atmosphere.

For the FTPS measurements, the modulated illumination beam of a Thermo Electron Nicolet 8700 FTIR with an external detector option was used. For the absolute photocurrent or EQE measurements via FTPS, a calibrated silicon photodetector was used as reference detector. More experimental details involving the FTPS setup are described in [35].

Received: January 11, 2008

Revised: March 13, 2008

- [1] S. Günes, H. Neugebauer, N. S. Saricifti, *Chem. Rev.* **2007**, *107*, 1324.
- [2] B. C. Thompson, J. M. J. Fréchet, *Angew. Chem. Int. Ed.* **2008**, *47*, 58.
- [3] S. Shaheen, C. J. Brabec, N. S. Saricifti, F. Padinger, T. Fromherz, J. C. Hummelen, *Appl. Phys. Lett.* **2001**, *78*, 841.
- [4] T. Munters, T. Martens, L. Goris, V. Vrindts, J. V. Manca, L. Lutsen, W. De Ceuninck, D. Vanderzande, L. De Schepper, J. Gelan, N. S. Saricifti, C. J. Brabec, *Thin Solid Films* **2002**, *403-404*, 247.
- [5] O. Inganäs, M. Svensson, F. Zhang, A. Gadisa, N. K. Persson, X. Wang, M. R. Anderson, *Appl. Phys. A* **2004**, *79*, 31.
- [6] A. Gadisa, W. Mammo, L. M. Andersson, S. Admassie, F. Zhang, M. R. Anderson, O. Inganäs, *Adv. Funct. Mater.* **2007**, *17*, 3836.
- [7] W. L. Ma, C. Yang, X. Gong, K. Lee, A. J. Heeger, *Adv. Funct. Mater.* **2005**, *15*, 1617.
- [8] J. Peet, J. Y. Kim, N. E. Coates, W. L. Ma, D. Moses, A. J. Heeger, G. C. Bazan, *Nat. Mater.* **2007**, *6*, 497.
- [9] P. W. M. Blom, V. D. Mihailetchi, L. J. A. Koster, D. E. Markov, *Adv. Mater.* **2007**, *19*, 1551.
- [10] A. Gadisa, M. Svensson, M. R. Andersson, O. Inganäs, *Appl. Phys. Lett.* **2004**, *84*, 1609.
- [11] M. C. Scharber, D. Mühlbacher, M. Koppe, P. Denk, C. Waldauf, A. J. Heeger, C. J. Brabec, *Adv. Mater.* **2006**, *18*, 789.
- [12] I.-W. Hwang, C. Soci, D. Moses, Z. Zhu, D. Waller, R. Gaudiana, C. J. Brabec, A. J. Heeger, *Adv. Mater.* **2007**, *19*, 2307.
- [13] Y. Kanai, Y. C. Grossman, *Nano Lett.* **2007**, *7*, 1967.
- [14] V. D. Mihailetchi, L. J. A. Koster, P. W. M. Blom, C. Melzer, B. de Boer, J. K. J. van Duren, R. A. J. Janssen, *Adv. Funct. Mater.* **2005**, *15*, 795.
- [15] L. Goris, K. Haenen, M. Nesladek, P. Wagner, D. Vanderzande, L. De Schepper, J. D'Haen, L. Lutsen, J. V. Manca, *J. Mater. Sci.* **2005**, *40*, 1413.
- [16] L. Goris, A. Poruba, L. Hod'akova, M. Vanecek, K. Haenen, M. Nesladek, P. Wagner, D. Vanderzande, L. De Schepper, J. V. Manca, *Appl. Phys. Lett.* **2006**, *88*, 052113.
- [17] R. Foster, in: *Organic Charge-Transfer Complexes*, Academic Press, New York **1969**.
- [18] D. V. Konarev, R. N. Lyubovskaya, N. V. Drihko, V. N. Semkin, A. Graja, *Russ. Chem. Bull.* **1999**, *48*, 3.
- [19] P. Panda, D. Veldman, J. Sweelssen, J. J. A. M. Bastiaansen, B. M. W. Langeveld-Voss, S. C. J. Meskers, *J. Phys. Chem.* **2007**, *111*, 5076.
- [20] M. A. Loi, S. Toffanin, M. Muccini, M. Forster, U. Scherf, M. Scharber, *Adv. Funct. Mater.* **2007**, *17*, 2111.
- [21] J. J. Benson-Smith, L. Goris, K. Vandewal, K. Haenen, J. V. Manca, D. Vanderzande, D. D. C. Bradley, J. Nelson, *Adv. Funct. Mater.* **2007**, *17*, 451.
- [22] M. Vaněček, A. Poruba, *Appl. Phys. Lett.* **2002**, *80*, 719.
- [23] H. Ohkita, S. Cook, Y. Astuti, W. Duffy, S. Tierney, W. Zhang, M. Heeney, I. McCulloch, J. Nelson, D. D. C. Bradley, J. R. Durrant, *J. Am. Chem. Soc.* **2008**, *130*, 3030.
- [24] R. A. Marcus, *J. Phys. Chem.* **1989**, *93*, 3078.
- [25] R. A. Marcus, *J. Phys. Chem.* **1990**, *94*, 4963.
- [26] M. Reyes-Reyes, K. Kim, D. L. Carroll, *Appl. Phys. Lett.* **2005**, *87*, 083506.
- [27] P. Vanlaeke, A. Swinnen, I. Haeldermans, G. Vanhoyland, T. Aernouts, D. Cheyns, C. Deibel, J. D'Haen, P. Heremans, J. Poortmans, J. V. Manca, *Sol. Energy Mater. Sol. Cells* **2006**, *90*, 2150.
- [28] S. Bertho, I. Haeldermans, A. Swinnen, W. Moons, T. Martens, L. Lutsen, D. Vanderzande, J. V. Manca, A. Senes, A. Bonfiglio, *Sol. Energy Mater. Sol. Cells* **2007**, *91*, 385.
- [29] T. Q. Nguyen, I. B. Martini, J. Liu, B. J. Schwartz, *J. Phys. Chem. B* **2000**, *104*, 237.
- [30] J. K. J. Van Duren, X. Yang, J. Loos, C. W. T. Bulle-Lieuwma, A. B. Sieval, J. C. Hummelen, R. A. J. Janssen, *Adv. Funct. Mater.* **2004**, *14*, 425.
- [31] V. D. Mihailetchi, P. W. M. Blom, J. C. Hummelen, M. T. Rispens, *J. Appl. Phys.* **2003**, *94*, 6849.
- [32] H. Becker, H. Spreitzer, W. Kreuder, E. Kluge, H. Schenk, I. Parker, Y. Cao, *Adv. Mater.* **2000**, *12*, 42.
- [33] M. Bresselge, I. Van Severen, L. Lutsen, P. Adriaensens, J. Manca, D. Vanderzande, T. Cleij, *Thin Solid Films* **2006**, *511-512*, 328.
- [34] F. Banishoeib, S. Fourier, T. J. Cleij, L. Lutsen, D. Vanderzande, *Eur. Phys. J. Appl. Phys.* **2007**, *37*, 237.
- [35] K. Vandewal, L. Goris, I. Haeldermans, M. Nesladek, P. Wagner, J. V. Manca, *Thin Solid Films* **2007**, in press

Paper C

On the origin of the open-circuit voltage of polymer:fullerene solar cells

K. Vandewal, K. Tvingstedt, A. Gadisa, O. Inganäs, J. V. Manca, *Nature Mater.* **8**, 904 (2009)

On the origin of the open-circuit voltage of polymer–fullerene solar cells

Koen Vandewal^{1*}, Kristofer Tvingstedt², Abay Gadisa¹, Olle Inganäs² and Jean V. Manca¹

The increasing amount of research on solution-processable, organic donor–acceptor bulk heterojunction photovoltaic systems, based on blends of conjugated polymers and fullerenes has resulted in devices with an overall power-conversion efficiency of 6%. For the best devices, absorbed photon-to-electron quantum efficiencies approaching 100% have been shown. Besides the produced current, the overall efficiency depends critically on the generated photovoltage. Therefore, understanding and optimization of the open-circuit voltage (V_{oc}) of organic solar cells is of high importance. Here, we demonstrate that charge-transfer absorption and emission are shown to be related to each other and V_{oc} in accordance with the assumptions of the detailed balance and quasi-equilibrium theory. We underline the importance of the weak ground-state interaction between the polymer and the fullerene and we confirm that V_{oc} is determined by the formation of these states. Our work further suggests alternative pathways to improve V_{oc} of donor–acceptor devices.

The most successful solution-processable organic solar cells use a C_{60} or C_{70} fullerene derivative as an electron acceptor blended with a conjugated polymer^{1–3}. In the field, attempts have been made to derive upper limits for the efficiency of this type of polymer–fullerene photovoltaic device, albeit with empirical arguments related to the details of the origin of the open-circuit voltage^{4–5} (V_{oc}). However, as energy is converted from one form (radiation) to another (electrical), fundamental losses should be taken into account and it should be possible to derive an upper limit for V_{oc} , purely on the basis of thermodynamic considerations. For single absorber materials, this fundamental question was answered in 1961 in a seminal paper by Shockley and Queisser⁶. Their analysis was based on the detailed balance of absorption and emission events from the solar cell, a ‘grey’ body at the surface of the Earth, illuminated by the Sun, a black body of much higher temperature. This allowed the derivation of an expression for V_{oc} as a function of the material’s bandgap. It was found that V_{oc} is maximal for the ideal case in which the charges can recombine only radiatively.

According to this reasoning, it is clear that the V_{oc} of polymer–fullerene devices has not reached its thermodynamic maximal value yet. This value would be reached if the only recombination mechanism at open-circuit conditions is a radiative one⁶. As a result of the severe luminescence quenching in material blends yielding a substantial charge generation, it is clear that radiative recombination is just a small fraction of the total recombination, and a reduction of the maximum obtainable V_{oc} is expected. In fact, no correlations of V_{oc} with the optical gap of any of the blend constituents, as predicted by Shockley and Queisser⁶, are observed. Instead, V_{oc} is found to scale with the difference between the highest occupied molecular orbital energy of the donor and the lowest unoccupied molecular orbital energy of the fullerene acceptor^{4,7}. This leads to the conclusion that in this type of solar cell, the V_{oc} is determined by recombination at the donor/acceptor interface^{8–12}.

Recently, for some polymer–fullerene blends, radiative interface recombination was observed. The presence of a weak emission signal, redshifted compared to the pure components, was detected in the photoluminescence and electroluminescence spectra and

was assigned to the emission of interface electron–hole pairs or charge-transfer excitons^{13–17}. The signature of this emitting state is also present in the absorption spectrum as a new, weak subgap absorption band in several polymer–fullerene blends used for photovoltaic applications^{18–20}. Such absorption bands are typical for the formation of a ground-state charge-transfer complex (CTC) between the polymer and the fullerene. Furthermore, good correlations between the open-circuit voltage and the spectral position of the charge-transfer absorption²⁰, photoluminescence¹⁵ or electroluminescence¹⁷ could be made.

Here, we show that the electroluminescence and photovoltaic external quantum efficiency spectra in the low-energy, charge-transfer region are related to each other as predicted by the detailed balance approach. Furthermore, it is shown that at V_{oc} , the photocurrent generated by the absorption of sunlight balances with the recombination current, resulting in emission of photons by the excited CTCs. This confirms previous suggestions^{10,15,20}, that V_{oc} is determined by the CTC formation between the polymer and the fullerene.

To validate the generality of the detailed balance treatment for polymer–fullerene solar cells, blends of five different donor polymers and two fullerene derivatives, that is, [6,6]-phenyl C61 butyric acid methyl ester (PC₆₁BM) and [6,6]-phenyl C71 butyric acid methyl ester (PC₇₁BM), were investigated. The polymers belong to different conjugated polymer material families, comprising different conjugated backbones. These conjugated polymers are representative of the donor polymers used in polymer–fullerene solar cells explored in the community at present. Their chemical structures are shown in Fig. 1.

Devices based on poly[2-methoxy-5-(30,70-dimethyloctyloxy)-1,4-phenylene vinylene] (MDMO-PPV) and poly[2,7-(9-di-octylfluorene)-alt-5,5-(4',7'-di-2-thienyl-2',1',3' benzothiadiazole)] (APFO3) were prepared using different polymer/fullerene stoichiometries. Optimal devices were obtained using a 1:4 polymer/fullerene weight ratio, resulting in a power conversion efficiency of ~2% and ~2.5% respectively. At a lower fullerene content, the photogenerated current becomes lower and the

¹IMEC-IMOMECE, vzw, Institute for Materials Research, Hasselt University, Wetenschapspark 1, 3590 Diepenbeek, Belgium, ²Biomolecular and Organic Electronics, Center of Organic Electronics (COE), Department of Physics, Chemistry and Biology, Linköping University, 58183 Linköping, Sweden.
*e-mail: koen.vandewal@uhasselt.be.

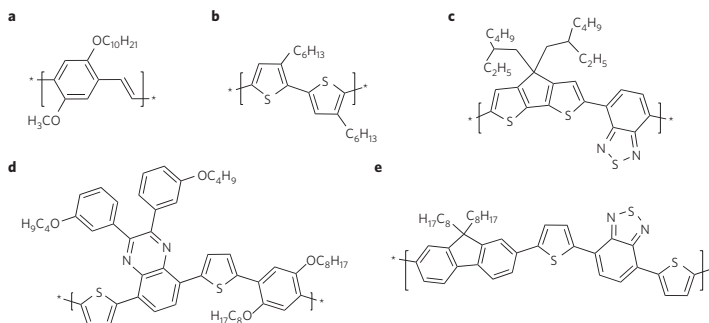


Figure 1 | The chemical structures of the donor polymers used. a, MDMO-PPV. b, P3HT. c, PCPDTBT. d, LBPP5. e, APFO3.

Table 1 | Measured J_{sc} , V_{oc} and calculated J_0 for all of the devices studied in this work.

Material	J_{sc} ($A\ m^{-2}$)	V_{oc} (V)	J_0 ($A\ m^{-2}$)
P3HT-PC ₆₁ BM (1:1)			
annealed	81 (± 8)	0.62 (± 0.01)	1.3 (± 0.9) E-9
as prepared	35 (± 8)	0.76 (± 0.03)	5.6 (± 3.0) E-12
PCPDTBT-PC ₆₁ BM (1:2)			
with octyldithiols	100 (± 5)	0.64 (± 0.01)	1.9 (± 1.1) E-9
without octyldithiols	66 (± 7)	0.67 (± 0.01)	6.7 (± 5.3) E-11
LBPP5-PC ₇₁ BM (1:3)			
	45 (± 9)	0.73 (± 0.015)	5.4 (± 2.1) E-12
MDMO-PPV-PC ₆₁ BM			
1:4	34 (± 7)	0.83 (± 0.02)	2.2 (± 0.8) E-13
1:1	14 (± 2)	0.88 (± 0.01)	1.1 (± 0.4) E-14
4:1	3 (± 0.6)	0.92 (± 0.02)	3.8 (± 2.2) E-15
APFO3-PC ₆₁ BM			
1:4	45 (± 5)	1.02 (± 0.01)	1.6 (± 0.6) E-16
1:1	28 (± 4)	1.08 (± 0.015)	2.7 (± 1.0) E-18
4:1	10 (± 1)	1.16 (± 0.01)	1.3 (± 0.8) E-19
APFO3-PC ₇₁ BM			
1:4	35 (± 5)	0.98 (± 0.01)	1.5 (± 0.3) E-16
1:1	30 (± 3)	1.00 (± 0.01)	1.0 (± 0.2) E-16
4:1	10 (± 2)	1.13 (± 0.01)	6.6 (± 4.4) E-19

J_0 was calculated using the $EQE_{PV}(E)$ and $EQE_{EL}(E)$ spectra by means of equation (3). The errors on J_{sc} and V_{oc} are experimental errors obtained by measuring different devices. For the errors on J_0 , the variation of J_0 over the spectral range of the CTC was taken into account as well as the experimental error on EQE_{EL} .

efficiency drops. However, V_{oc} increases as the fullerene content is decreased (see Supplementary Information). APFO3-based devices were prepared with both PC₆₁BM and PC₇₁BM. For the poly[3-hexylthiophene] (P3HT)-PC₆₁BM blends, ordering of the polymer phase, for example, induced by annealing, has been proven to have a major influence on the device performance²¹. Therefore, in this study, as-prepared and annealed devices were characterized. For this material system, typical conversion efficiencies of 3.5% were reached. However, higher efficiencies for P3HT-PC₆₁BM devices of up to 5% have been reported²². A polymer of particular interest is poly[2,6-(4,4-bis-(2-ethylhexyl)-4H-cyclopenta[2,1-b;3,4-b']-dithiophene)-alt-4,7-(2,1,3-benzothiadiazole)] (PCPDTBT), as it has a low optical gap, close to the optimum as predicted by Shockley and Queisser⁶. It was shown that the addition of thiols in a PCPDTBT-fullerene solution improves the device performance²³. We obtained for PCPDTBT-PC₆₁BM devices typically a power conversion efficiency of 3%. Efficiencies of 5.5% were reported for

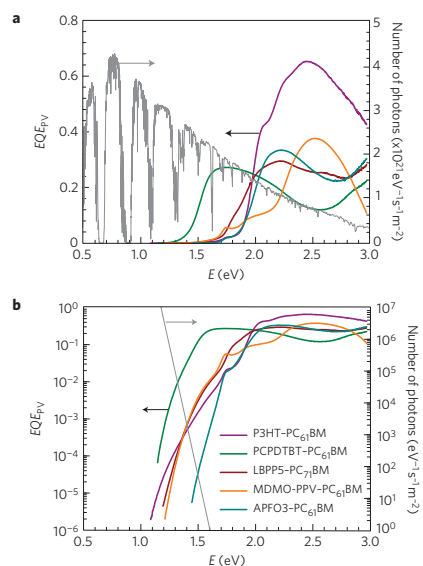


Figure 2 | The EQE_{PV} spectra of polymer-fullerene devices. The devices comprise active layers: P3HT-PC₆₁BM (1:1) (annealed), PCPDTBT-PC₆₁BM (1:2), LBPP5-PC₇₁BM (1:3), MDMO-PPV-PC₆₁BM (1:4) and APFO3-PC₆₁BM (1:4). **a**, The spectra on a linear scale. The standard AM1.5 G spectrum is shown on the right axis. **b**, The spectra on a logarithmic scale, to make the weak contribution of the low oscillator strength CTC visible. A charge-transfer band is clearly visible for all five material blends. Depending on the donor polymer, the spectral position of the charge-transfer band varies. On the right axis of **b**, the emission spectrum of a black body at room temperature is shown.

PCPDTBT-PC₇₁BM devices²³. As in this article, there is particular interest in the V_{oc} of the devices; note that the obtained V_{oc} values correspond to what is found in the literature for similar devices. An overview of the devices studied in this work and the measured short-circuit current (J_{sc}) and V_{oc} values are listed in Table 1.

In Fig. 2a, photovoltaic external quantum efficiency (EQE_{PV}) spectra are shown on a linear scale for five devices using the

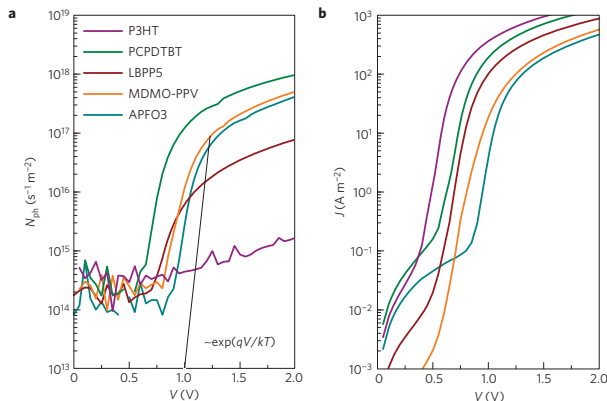


Figure 3 | Electroluminescence emission and corresponding injected current versus voltage curves of polymer–fullerene devices. The active layers of the devices are: P3HT–PC₆₁BM (1:1) (annealed), PCPDTBT–PC₆₁BM (1:2), LBPP5–PC₇₁BM (1:3), MDMO–PPV–PC₆₁BM (1:4) and APFO3–PC₆₁BM (1:4). **a**, The number of detected photons by a silicon detector versus the applied voltage over the device. The black line represents a curve proportional to $\exp(qV/kT)$. An onset proportional to this curve is measurable for all polymer–fullerene devices, except for the annealed P3HT–PC₆₁BM device, because of its low-efficiency electroluminescence. **b**, The corresponding injection current versus voltage curves.

above conjugated polymers. Spectra for further devices using different preparation conditions are shown in the Supplementary Information. For the P3HT-, MDMO-PPV-, APFO3- and poly[1,4-(2,5-dioctyloxybenzene)-alt-5,5'-(5',8'-di-2-thienyl-2',3'-di-(3'-butoxyphenyl)quinoxaline)] (LBPP5)-based devices, the fullerene has the lowest optical gap of the blend constituents (1.7 eV). For the PCPDTBT–PC₆₁BM device however, the lowest optical gap is the polymer bandgap (1.4 eV). From these EQE_{PV} spectra, the total photogenerated current can be calculated, by integrating the EQE_{PV} spectrum over the solar spectrum, shown on the right axis of Fig. 2a. From this figure, it is clear that the photocurrent under solar illumination for these five devices is dominated by polymer absorption. In this respect, the use of a C₇₀ fullerene derivative is beneficial, as it aids in absorbing a substantially greater part of the sunlight than the C₆₀ derivative²⁴.

Polymer–fullerene ground-state material interaction and CTC formation is characterized by the presence of a new absorption band, owing to an optical transition in which an electronic charge is transferred from the donor-conjugated polymer to the fullerene acceptor. The low oscillator strength of this transition and hence low absorption coefficient however, forces us to use specialized techniques to detect charge-transfer bands in the $EQE_{PV}(E)$ spectra. Therefore, the sensitive detection method Fourier-transform photocurrent spectroscopy^{20,25} (FTPS) is also used to collect the very low photocurrent signals generated by excitation of the CTCs. These signals become visible in the $EQE_{PV}(E)$ spectra, shown in Fig. 2b on a logarithmic scale. For all five material combinations shown in the figure and the combinations shown in the Supplementary Information, the lowest energy excitation is due to a charge-transfer optical transition. Depending on the donor polymer, this subgap charge-transfer band has an onset ranging from 1 to 1.5 eV.

In Fig. 3, the total number of photons N_{ph} emitted by electroluminescence and detected by a silicon detector, versus voltage, and the corresponding injected current $J_{inj}(V)$ for the five material combinations are shown. It can be seen that the electroluminescence emission onset is proportional to $\exp(qV/kT)$. Here, k is the Boltzmann constant, T is the absolute room temperature and q is the elementary electron charge. This onset

is lower than the voltage onset of the electroluminescence of the pure materials¹⁷. At high voltages, the electroluminescence and injected current are space-charge and/or series-resistance limited and deviate from the exponential. Owing to the low quantum efficiency of the charge-transfer emission of annealed P3HT–PC₆₁BM devices and the limited detection range of the Si photodiode, the exponential part in the electroluminescence versus voltage curves could not be resolved for this device.

To spectrally resolve the electroluminescence spectra with a sufficiently high signal, they were measured with a sensitive set-up using injection currents corresponding to a charge density present in the device comparable to 1–10 sun conditions. As the total number of photons emitted by electroluminescence scales with the injected current, we choose to show the electroluminescence external quantum efficiency (EQE_{EL}), calculated as the number of emitted photons divided by the number of injected electrons. These spectra are shown in Fig. 4a. In contrast to the $EQE_{PV}(E)$ spectra in Fig. 2, the $EQE_{EL}(E)$ spectra are dominated by charge-transfer emission, and substantially redshifted as compared with the emission of the pure components^{15–17}. The overall, integrated EQE_{EL} for all samples is very low, ranging from 10^{-9} to 10^{-6} .

We will now use the principle of detailed balance to make a connection between the low-energy, charge-transfer-dominated part of the $EQE_{PV}(E)$ and $EQE_{EL}(E)$ spectra, and to relate these spectra to V_{oc} . In this respect, Würfel derived a generalized Planck law for systems in quasi-equilibrium, including a chemical potential of radiation equal to the splitting of the quasi-Fermi levels²⁶. It was shown to be valid for inorganic solar cells²⁷ and dye-sensitized solar cells²⁸. Similar approaches were used to relate photoluminescence spectra to the absorption spectra of organic materials²⁹ and to calculate the free energy available in photosynthetic systems³⁰. Extensions were made for third-generation photovoltaics³¹. A useful equation, similar to Würfel's generalized Planck law, was recently introduced by Rau, relating the photovoltaic and electroluminescent actions of solar cells³².

$$\phi_{EL}(E, V) = EQE_{PV}(E) \phi_{BB}(E) \left(\exp\left(\frac{qV}{kT}\right) - 1 \right) \quad (1)$$

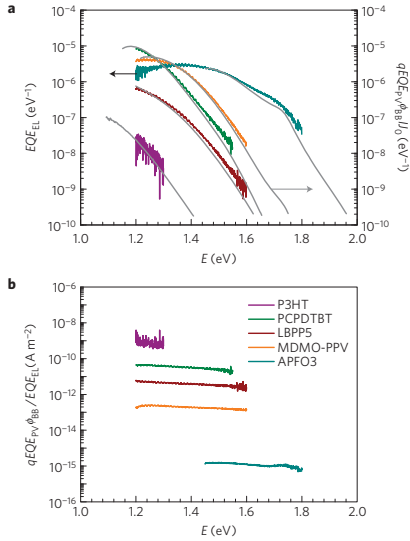


Figure 4 | Comparison of the measured EQE_{EL} with the product of the EQE_{PV} spectrum with the black-body spectrum at room temperature. a. Left axis: The EQE_{EL} spectra devices based on the material blends P3HT- $PC_{61}BM$ (1:1) (annealed), PCPDTBT- $PC_{61}BM$ (1:2), LBPP5- $PC_{71}BM$ (1:3), MDMO-PPV- $PC_{61}BM$ (1:4) and APFO3- $PC_{61}BM$ (1:4). These EQE_{EL} were obtained using injection currents in the range (1–10) times J_{sc} . Right axis: EQE_{EL} spectra, proportional to the product of the EQE_{PV} spectrum with the black-body spectrum at room temperature. **b.** The ratio of the EQE_{PV} and EQE_{EL} multiplied by the black-body spectrum at room temperature. This value is fairly constant over the low-energy spectral region and equals J_0 .

Here, $\phi_{EL}(E, V)$ is the excess electroluminescence spectral photon flux and $\phi_{BB}(E)$ is the black-body spectrum at 300 K, integrated over all possible incidence angles. The $\phi_{BB}(E)$ spectrum is shown on the right axis of Fig. 2b. Note that this is an exponentially decreasing function with increasing photon energy, making only the low-energy part of $EQE_{PV}(E)$ important in the evaluation of equation (1). For a low-mobility organic metal–insulator–metal, it was recently shown that relation (1) becomes only approximately valid³³. However, the deviations are expected to be within one order of magnitude.

A simple relationship between $EQE_{EL}(E)$ and $EQE_{PV}(E)$ can be deduced if the ideal diode equation is used to describe the injected current $J_{inj}(V)$:

$$J_{inj}(V) = J_0 \left(\exp\left(\frac{qV}{kT}\right) - 1 \right) \quad (2)$$

Here, J_0 is the dark saturation current. We can deduce the following relationship between the EQE_{PV} and EQE_{EL} spectra:

$$J_0 EQE_{EL}(E) = q EQE_{PV}(E) \phi_{BB}(E) \quad (3)$$

Here, J_0 is assumed to be implicitly voltage dependent, to maintain the generality of equation (2) for the description of dark I – V curves of polymer–fullerene devices. Typically, J_0 is determined

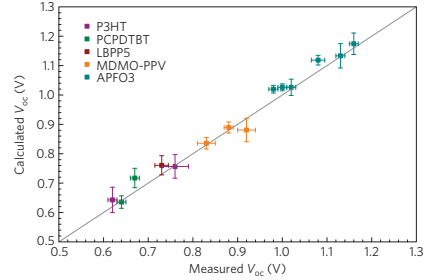


Figure 5 | The V_{oc} obtained by means of the detailed balance approach versus the measured V_{oc} . The different colours indicate devices based on different donor polymers: P3HT- $PC_{61}BM$ (1:1), PCPDTBT- $PC_{61}BM$ (1:2), LBPP5- $PC_{71}BM$ (1:3), MDMO-PPV- $PC_{61}BM$, APFO3- $PC_{61}BM$ and APFO3- $PC_{71}BM$. Measured and calculated V_{oc} values were obtained for freshly prepared and annealed P3HT-based devices. For MDMO-PPV- $PC_{61}BM$, APFO3- $PC_{61}BM$ and APFO3- $PC_{71}BM$, the stoichiometry was changed (4:1, 1:1, 1:4). PCPDTBT- $PC_{61}BM$ (1:2) was studied with and without the addition of octyldithiols in the solution. The grey line is a one-to-one correspondence. Experimental errors on the measured V_{oc} were obtained by measuring different samples. Error bars on the V_{oc} calculated by means of detailed balance were obtained by using the errors on the calculated J_0 and the absolute value of the measured EQE_{EL} .

by injection and recombination mechanisms of the free carriers³⁴. For polymer–fullerene blends, diode equations with ideality factors between one and two are often used³⁵. In the notation used here, J_0 is in that case exponentially dependent on voltage. See the Supplementary Information for further details regarding J_0 and the ideality factor.

Equation (3) relates the shape of the $EQE_{PV}(E)$ spectrum to the shape of the $EQE_{EL}(E)$ spectrum. The validity of this simple relation for polymer–fullerene solar cells is shown in Fig. 3a. It can be seen that multiplying $EQE_{PV}(E)$ by the ambient black-body spectrum $\phi_{BB}(E)$, the charge-transfer-dominated $EQE_{EL}(E)$ of all photovoltaic devices comprising our five different donor polymers is obtained within acceptable limits. Note that these relations are valid also for large Stokes shifts between the charge-transfer absorption and emission.

Furthermore, using equation (3), a value for J_0 can be deduced, by taking the ratio between $qEQE_{PV}(E)\phi_{BB}(E)$ and $EQE_{EL}(E)$. Here, EQE_{EL} is measured under injection conditions equivalent to 1–10 suns, whereas $EQE_{PV}(E)$ was measured under short-circuit conditions. Note that J_0 obtained in this way is fairly constant over the range of overlapping $EQE_{PV}(E)$ and $EQE_{EL}(E)$. Only a slight decrease of J_0 with increasing photon energy is observed. This is at least partly due to the fact that during the EQE_{EL} measurements, current is injected into the device, causing the effective temperature of the devices to increase as compared with room temperature. This heating slightly broadens the emission bands and causes the observed small slope. Further experimental errors on J_0 originate from the experimental errors on the absolute EQE_{EL} . The obtained J_0 values for all investigated photovoltaic devices with their experimental errors are listed in Table 1.

Integrating equation (3) yields the following expression for J_0 :

$$J_0 = \frac{q}{EQE_{EL}} \int EQE_{PV}(E) \phi_{BB}(E) dE \quad (4)$$

Here, EQE_{EL} is the overall electroluminescence external quantum efficiency, obtained by integrating $EQE_{EL}(E)$ over all photon

energies. The essential contribution of $EQE_{PV}(E)$ to the integral in equation (4) is in fact only the low-energy charge-transfer part, as ϕ_{BB} is exponentially decreasing with increasing photon energy. This is in correspondence with the suggestion made by Potscavage *et al.*¹⁰ that the dark current originates from thermal excitations of ground-state charge-transfer complexes.

At open circuit, the injected current $J_{inj}(V)$ causing the low-quantum-efficiency charge-transfer emission equals J_{sc} ; hence, by reforming equation (2), we obtain a commonly used equation for V_{oc} :

$$V_{oc} = \frac{kT}{q} \ln \left(\frac{J_{sc}}{J_0} + 1 \right) \quad (5)$$

Note that this formula for V_{oc} does not contain a parameter related explicitly to any optical gap. Spectral band positions are present in the equation implicitly in the term J_0 through equation (3). Note that, as both J_0 and J_{sc} are proportional to respectively $\phi_{BB}(E)$ and the AM1.5 spectrum integrated over $EQE_{PV}(E)$, their ratio is determined by the spectral shape of $EQE_{PV}(E)$ alone, which was measured at short circuit in this work. Furthermore, this formula is expected to be valid if the injected current is diode-like, as it is for the devices investigated in this work at voltages comparable to V_{oc} (Fig. 3).

To check the validity of equation (5), J_0 is obtained as described above. J_{sc} is obtained by integrating the EQE_{PV} spectrum over the solar spectrum or by measuring it directly under solar illumination. Experimental errors on J_{sc} were obtained by comparing the calculated data with the measured data of several devices on different solar simulators. The used J_{sc} values with their experimental errors of all the devices studied in this work are listed in Table 1.

The V_{oc} values calculated by means of detailed balance versus the measured V_{oc} values are shown in Fig. 5 for all studied devices comprising the five investigated polymers, using different preparation conditions. An overview of all preparation conditions is shown in the Supplementary Information. Excellent correspondence of the measured V_{oc} with the calculated V_{oc} is observed and differences in V_{oc} on changing preparation conditions, such as stoichiometry alterations and annealing, are accurately reproduced. These differences in V_{oc} are interpreted as being mainly caused by the spectral shifts of the charge-transfer bands on changing the preparation conditions^{13,18}.

The obtained new insights reveal pathways to increase the V_{oc} of polymer–fullerene devices. From equation (4) it is clear that, because of the exponential nature of $\phi_{BB}(E)$ a blueshift of the charge-transfer band results in an exponential decrease of J_0 through the term $EQE_{PV}(E)\phi_{BB}(E)$. Owing to the logarithmic dependence of V_{oc} on J_0 (equation (5)), V_{oc} depends linearly on the spectral position of the charge-transfer band. This results in the good correlations of V_{oc} with the onset of the charge-transfer band²⁰ or the peak of charge-transfer emission^{15,17}.

The spectral position of the charge-transfer band is mainly determined by the energetic difference between the highest occupied molecular orbital of the donor polymer to the lowest unoccupied molecular orbital of the electron acceptor^{36–38}. The presented theoretical approach explains the widely observed correlation between V_{oc} and this energy level difference. However, there are other factors influencing the spectral position of the charge-transfer band, such as the binding energy of the charge-transfer exciton and its electrostatic environment^{36–38}.

Up to now, increasing the lowest unoccupied molecular orbital level of the fullerene^{39,40} or using donor polymers with optimized energetic levels⁴¹, have been the most followed pathways for increasing the V_{oc} of polymer–fullerene solar cells. From equation (5) however, other pathways for increasing V_{oc} become apparent. Reducing the electronic coupling between the polymer

and the fullerene will suppress the charge-transfer band oscillator strength and will reduce J_0 , and thus increase V_{oc} . The fact that V_{oc} can also depend on the coupling between donor and acceptor material, was recently shown by Perez and colleagues⁴².

In the devices studied here, the recombination rate exceeds many times the charge-transfer emission rate, hence the low EQE_{EL} in the studied devices. At solar illumination conditions, values of EQE_{EL} are of the order of 10^{-6} or 10^{-9} . Increasing EQE_{EL} , by eliminating the extra non-radiative pathways and thus improving the carrier lifetime, will result in a decrease of J_0 (formula (5)) and therefore an increase in V_{oc} .

The theoretical maximum V_{oc} will be obtained at EQE_{EL} equals unity. This means that all non-radiative pathways are eliminated, resulting in a maximum charge-carrier lifetime, only determined by radiative recombination. Note that even in this case V_{oc} does not necessarily equal the optical gap of the material blend, as fundamental thermodynamic losses owing to entropy creation will always cause the potential of the device to be lower than the energy of the relaxed charge-transfer exciton. From equations (4) and (5), we can deduce that, increasing EQE_{EL} by a factor of 10 will result in an increase in V_{oc} of ~ 58 mV at room-temperature conditions. This means that for polymer–fullerene solar cells, for which $EQE_{EL} \sim 10^{-9}$ – 10^{-6} , 0.5–0.3 V is still to be gained, by eliminating the non-radiative recombination pathways, if this is possible. Therefore, to improve V_{oc} , the exact origin of these non-radiative recombination pathways should be investigated in future works.

Methods

The devices were manufactured by spin-coating the active-layer blend solutions on top of electronic-grade poly(3,4-ethylenedioxythiophene) poly(styrenesulphonate) (Clevis P VP Al 4083) coated indium tin oxide/glass slides. For the P3HT-, PCPDTBT- and MDMO-PPV-based devices, chlorobenzene solutions were used. For the APFO3 and LBPP5 devices, chloroform was used as a solvent. All devices are finalized by thermal sublimation of 0.7 nm LiF or 20 nm of Ca, finalized by a 70 nm Al top electrode. The active areas of the cells range from 0.25 to 1 cm² and thicknesses are between 80 and 150 nm. P3HT was obtained from Merck, MDMO-PPV from Aldrich, PCPDTBT from Konarka and PC₆₁BM and PC₇₁BM from Solenne. APFO3 and LBPP5 were synthesised at Chalmers University. 1,8-octanedithiol, used for the PCPDTBT-based devices, was obtained from Aldrich. Device annealing of P3HT–PC₆₁BM devices was carried out after electrode deposition.

Photovoltaic devices were characterized by measurement of the I - V curve under solar illumination. J_{sc} and V_{oc} were extracted from these measurements. Error bars were obtained by measuring several different devices with two different solar simulators. V_{oc} is typically very stable (± 0.01 V). For J_{sc} however, considerable deviations can be observed. Values for all devices are listed in Table 1.

For the electroluminescence measurements, an Oriol optical liquid light guide was located as close to the biased cell as possible and connected to the entrance slit of the spectrometer. A Newton electron-multiplying CCD (charge-coupled device) Si array detector cooled to -60 °C in conjunction with a Shamrock sr 303i spectrograph from Andor Technology served as the emission-detection system. The system was wavelength-calibrated by an argon lamp to a resolution better than 0.5 nm. The transmission of the entire fibre-monochromator–CCD system was further radiometrically calibrated by an Optronic OL245M standard spectral irradiance lamp. The CCD detector is ‘back illuminated’, which increases the sensitivity but unfortunately also gives rise to some interference effects at wavelengths between 850 and 1,000 nm. Absolute values of the EQE_{EL} spectrum could be obtained by measuring the total number of emitted photons in the 300–1,100 nm wavelength range with a homebuilt system using a large-area calibrated Si photodiode from Oriol.

For the FTPS measurements, the modulated illumination beam of a Thermo Electron Nicolet 8700 FTIR with an external detector option was used. For the scaling to absolute EQE_{PV} , a calibrated silicon photodiode was used as a reference detector.

Received 4 June 2009; accepted 15 September 2009;
published online 11 October 2009

References

1. Thompson, B. C. & Fréchet, J. M. J. Polymer-fullerene composite solar cells. *Angew. Chem. Int. Ed.* **47**, 58–77 (2008).
2. Park, S. H. *et al.* Bulk heterojunction solar cells with internal quantum efficiency approaching 100%. *Nature Photon.* **3**, 297–302 (2009).
3. Denzler, G., Scharber, M. C. & Brabec, C. J. Polymer-fullerene bulk-heterojunction solar cells. *Adv. Mater.* **13**, 1323–1338 (2009).

4. Scharber, M. C. *et al.* Design rules for donors in bulk-heterojunction solar cells—towards 10% energy-conversion efficiency. *Adv. Mater.* **18**, 789–794 (2006).
5. Veldman, D., Meskers, S. C. J. & Janssen, R. A. J. The energy of charge-transfer states in electron donor–acceptor blends: Insight into the energy losses in organic solar cells. *Adv. Funct. Mater.* **19**, 1939–1948 (2009).
6. Shockley, W. & Queisser, H. Detailed balance limit of efficiency of p–n junction solar cells. *J. Appl. Phys.* **32**, 510–519 (1961).
7. Gadisa, A., Svensson, M., Andersson, M. R. & Inganäs, O. Correlation between oxidation potential and open-circuit voltage of composite solar cells based on blends of polythiophenes/fullerene derivative. *Appl. Phys. Lett.* **84**, 1609–1611 (2004).
8. Nelson, J., Kirkpatrick, J. & Ravirajan, P. Factors limiting the efficiency of molecular photovoltaic devices. *Phys. Rev. B* **69**, 035337 (2004).
9. Rand, B. P., Burk, D. P. & Forrest, S. R. Offset energies at organic semiconductor heterojunctions and their influence on the open-circuit voltage of thin-film solar cells. *Phys. Rev. B* **75**, 115327 (2007).
10. Potsavage, W. J., Yoo, S. & Kippelen, B. Origin of the open-circuit voltage in multilayer heterojunction organic solar cells. *Appl. Phys. Lett.* **93**, 193308 (2008).
11. Kirchartz, T., Mattheis, J. & Rau, U. Detailed balance theory of excitonic and bulk heterojunction solar cells. *Phys. Rev. B* **78**, 235320 (2008).
12. Benson-Smith, J. J. *et al.* Formation of a ground-state charge-transfer complex in polyfluorene/[6,6]-phenyl-C-61 butyric acid methyl ester (PCBM) blend films and its role in the function of polymer/PCBM solar cells. *Adv. Funct. Mater.* **17**, 451–457 (2007).
13. Loi, M. A. *et al.* Charge transfer excitons in bulk heterojunctions of a polyfluorene copolymer and a fullerene derivative. *Adv. Funct. Mater.* **17**, 2111–2116 (2007).
14. Hallermann, M., Haneder, S. & Da Como, E. Charge-transfer states in conjugated polymer/fullerene blends: Below-gap weakly bound excitons for polymer photovoltaics. *Appl. Phys. Lett.* **93**, 053307 (2008).
15. Veldman, D. *et al.* Compositional and electric field dependence of the dissociation of charge transfer excitons in alternating polyfluorene copolymer/fullerene blends. *J. Am. Chem. Soc.* **130**, 7721–7735 (2008).
16. Kim, H. *et al.* Electroluminescence in polymer–fullerene photovoltaic cells. *Appl. Phys. Lett.* **86**, 183502 (2005).
17. Tvingstedt, K. *et al.* Electroluminescence from charge transfer states in polymer solar cells. *J. Am. Chem. Soc.* **131**, 11819–11824 (2009).
18. Goris, L. *et al.* Absorption phenomena in organic thin films for solar cell applications investigated by photothermal deflection spectroscopy. *J. Mater. Sci.* **40**, 1413–1418 (2005).
19. Goris, L. *et al.* Observation of the subgap optical absorption in polymer–fullerene blend solar cells. *Appl. Phys. Lett.* **88**, 052113 (2006).
20. Vandewal, K. *et al.* The relation between open-circuit voltage and the onset of photocurrent generation by charge-transfer absorption in polymer: fullerene bulk heterojunction solar cells. *Adv. Funct. Mater.* **18**, 2064–2070 (2008).
21. Campoy-Quiles, M. *et al.* Morphology evolution via self-organization and lateral and vertical diffusion in polymer: fullerene solar cell blends. *Nature Mater.* **7**, 158–164 (2008).
22. Ma, W. L., Yang, C. Y., Gong, X., Lee, K. & Heeger, A. J. Thermally stable, efficient polymer solar cells with nanoscale control of the interpenetrating network morphology. *Adv. Funct. Mater.* **15**, 1617–1622 (2005).
23. Peet, J. *et al.* Efficiency enhancement in low-bandgap polymer solar cells by processing with alkane dithiols. *Nature Mater.* **6**, 497–500 (2007).
24. Wienk, M. M. *et al.* Efficient methano[70]fullerene/MDMO-PPV bulk heterojunction photovoltaic cells. *Angew. Chem. Int. Ed.* **42**, 3371–3375 (2003).
25. Vanecek, M. & Poruba, A. Fourier-transform photocurrent spectroscopy of microcrystalline silicon for solar cells. *Appl. Phys. Lett.* **80**, 719–721 (2002).
26. Würfel, P. The chemical potential of radiation. *J. Phys. C* **15**, 3967–3985 (1982).
27. Schick, K., Daub, E., Finkbeiner, S. & Würfel, P. Verification of a generalized Planck law for luminescence radiation from silicon solar cells. *Appl. Phys. A* **54**, 109–114 (1992).
28. Trupke, T., Würfel, P., Uhlendorf, I. & Lauer, I. Electroluminescence of the dye-sensitized solar cell. *J. Phys. Chem. B* **103**, 1905–1910 (1999).
29. Band, Y. B. & Heller, D. F. Relationships between absorption and emission of light in multilevel systems. *Phys. Rev. A* **38**, 1885–1895 (1988).
30. Ross, R. T. & Calvin, M. Thermodynamics of light emission and free-energy storage in photosynthesis. *Biophys. J.* **7**, 595–614 (1967).
31. Green, M. A. *Third Generation Photovoltaics: Advanced Solar Energy Conversion* (Springer, 2006).
32. Rau, U. Reciprocity relation between photovoltaic quantum efficiency and electroluminescent emission of solar cells. *Phys. Rev. B* **76**, 085303 (2007).
33. Kirchartz, T. & Rau, U. Detailed balance and reciprocity in solar cells. *Phys. Status Solidi A* **205**, 2737–2751 (2008).
34. Bruan, D. Electron injection and conduction processes for polymer devices. *J. Polym. Sci. Part B: Polym. Phys.* **41**, 2622–2629 (2003).
35. Waldauf, C., Scharber, M. C., Schillings, P., Hauch, J. A. & Brabec, C. J. Physics of organic bulk heterojunction devices for photovoltaic applications. *J. Appl. Phys.* **99**, 104503 (2006).
36. Panda, P. *et al.* Charge transfer absorption for pi-conjugated polymers and oligomers mixed with electron acceptors. *J. Phys. Chem. B* **111**, 5076–5081 (2007).
37. Foster, R. *Organic Charge-Transfer Complexes* (Academic, 1969).
38. Pope, M. & Swenberg, C. E. *Electronic Processes in Organic Crystals and Polymers* (Oxford Univ. Press, 1999).
39. Ross, R. B. *et al.* Endohedral fullerenes for organic photovoltaic devices. *Nature Mater.* **8**, 208–212 (2009).
40. Lenes, M. *et al.* Fullerene bisadducts for enhanced open-circuit voltages and efficiencies in polymer solar cells. *Adv. Mater.* **20**, 2116–2119 (2008).
41. Zhang, F. *et al.* High photovoltage achieved in low band gap polymer solar cells by adjusting energy levels of a polymer with the LUMOs of fullerene derivatives. *J. Mater. Chem.* **18**, 5468–5474 (2008).
42. Perez, M. D., Borek, C., Forrest, S. R. & Thompson, M. E. Molecular and morphological influences on the open circuit voltages of organic photovoltaic devices. *J. Am. Chem. Soc.* **131**, 9281 (2009).

Acknowledgements

K.V., A.G. and J.V.M. acknowledge the institute for the promotion of science and technology in Flanders (IWT-Vlaanderen) the IWT-project polyspec, the FWO project nano-fibres and the European project solar-n-type. K.T. and O.I. thank the Swedish Energy Agency for funding through the programme Tandem. All authors acknowledge M.R. Andersson at Chalmers University for supplying APFO3 and LBPP5 and Markus Scharber for supplying PCPDTBT. D. Vanderzande, W. D. Oosterbaan, P. Adriaensens and S. Chambon are thanked for valuable discussions.

Author contributions

K.V. and A.G. prepared the devices and carried out FTPS measurements in Hasselt. K.T. and K.V. prepared devices and carried out the electroluminescence measurements in Linköping. K.V. wrote the paper. All authors provided comments on the manuscript. J.V.M. and O.I. directed the research.

Additional information

Supplementary information accompanies this paper on www.nature.com/naturematerials. Reprints and permissions information is available online at <http://npg.nature.com/reprintsandpermissions>. Correspondence and requests for materials should be addressed to K.V.

Supplementary information for:

On the origin of the open-circuit voltage of polymer:fullerene solar cells

Koen Vandewal, Kristofer Tvingstedt, Abay Gadisa, Olle Inganäs and Jean V. Manca

The additional information consists of 3 parts. In part 1 $EQE_{PV}(E)$ and $EQE_{EL}(E)$ spectra and their relation are shown for all investigated devices, with particular focus on the impact of various preparation conditions. In Part 2, a comparison is made between the J_0 values obtained by analysis of the $EQE_{PV}(E)$ and $EQE_{EL}(E)$ spectra, as explained in the main text and J_0 as obtained directly from the IV curves. In part 3, additional information relating the equation (4) used in the main text to calculate V_{oc} is provided.

1. Determination of J_0 by analysis of $EQE_{PV}(E)$ and $EQE_{EL}(E)$ for devices using various preparation conditions

For one particular polymer:fullerene combination, the open-circuit voltage (V_{oc}) can depend on the preparation conditions. Therefore, this supplementary information contains photovoltaic external quantum efficiency (EQE_{PV}), electroluminescence external quantum efficiency (EQE_{EL}) spectra and the J_0 values for additional devices, using various preparation conditions. The J_0 values were obtained from the EQE_{PV} and EQE_{EL} spectra, as described in the main text. For the MDMO-PPV and APFO3 based devices, 3 different polymer:fullerene stoichiometries were investigated. APFO3 was blended with PC₆₁BM and PC₇₁BM. For the devices using PCPDTBT as donor polymer, the effect of the additive 1,8-octanedithiol in the blend solution was studied. For P3HT:PC₆₁BM spectra were obtained for the annealed and unannealed devices.

For the MDMO-PPV:PC₆₁BM, APFO3:PC₆₁BM and APFO3:PC₇₁BM devices, polymer:fullerene ratios of 20:80, 50:50 and 80:20 were used, shown in respectively **additional figure 1**, **additional figure 2** and **additional figure 3**. Upon increasing the fullerene content, a redshift of the CT band in both the EQE_{PV} and EQE_{EL} spectrum can be observed. A Redshift of the CT band upon increasing the fullerene content was observed previously in FTPS [1], photoluminescence [2] and electroluminescence [3]

studies. This redshift is the main cause of the increasing J_0 with increasing fullerene content. At this point it is difficult to see a trend in the absolute EQE_{EL} values as function of varying fullerene content. EQE_{EL} will depend on many parameters, including the used contacts and the quality of the contact of the used metal with the active layer.

The addition of additives to the PCPDTBT:fullerene solution has been shown to be beneficial for the overall power conversion efficiency of the photovoltaic device. This is due to an increase in fillfactor and short circuit current. The V_{oc} however, drops slightly [4]. Also in this case, the drop in V_{oc} and increasing J_0 upon adding 1,8-octanedithiol is caused by a redshift of the CT band (**additional figure 4**).

Annealing of P3HT:PC₆₁BM devices results in a higher efficiency device, but again, a lower V_{oc} , as in the unannealed case. Again the origin is the redshift of the CT band upon annealing, due to the annealing induced order (**additional figure 5**) [5].

2. Relating J_0 obtained by analysis of $EQE_{PV}(E)$ and $EQE_{EL}(E)$ to J_0 obtained by analysis of the IV curves

In equation (2) of the main paper a diode equation was used, having the form

$$J_{inj} = J_0 \left(\exp\left(\frac{qV}{kT}\right) - 1 \right) \quad (A11)$$

As emphasized in the main text, for polymer:fullerene devices, it should be taken into account that J_0 is not constant and depends on the number of charges present in the device. Therefore it is important in our analysis that EQE_{EL} is measured as close as possible to 1 sun conditions. Due to the limited sensitivity of the detector, we could measure EQE_{EL} for injection currents corresponding to 1-10 times J_{sc} , depending on the material system.

For dark IV curves of polymer:fullerene solar cells, the following function, including an ideality factor n is often used to fit the diodelike part of the curve:

$$J_{inj} = J_{0,n} \left(\exp\left(\frac{qV}{nkT}\right) - 1 \right) \quad (A12)$$

In this case $J_{0,n}$ is a constant. It is the intercept with the 0 V line of an exponential fit of the injected current $J_{inj}(V)$. values for n and $J_{0,n}$ for the 5 example material systems are determined from the dark IV curves shown in **additional figure 6** and are listed in **additional table 1**.

A relation between J_0 , as defined in the main paper, and $J_{0,n}$ can be deduced by equating (A11) and (A12):

$$J_0 \left(\exp\left(\frac{qV}{kT}\right) - 1 \right) = J_{0,n} \left(\exp\left(\frac{qV}{nkT}\right) - 1 \right)$$

At voltages V exceeding several times nkT , we can neglect the -1 term on both sides of the equation

$$J_0 \exp\left(\frac{qV}{kT}\right) = J_{0,n} \exp\left(\frac{qV}{nkT}\right)$$

$$J_0 = J_{0,n} \exp\left(\frac{(1-n)qV}{nkT}\right)$$

Or, in function of J_{inj} :

$$J_0 = J_{0,n}^n J_{inj}^{1-n}$$

At ideality factors $n > 1$ it is necessary to evaluate J_0 under the right conditions. As the papers deals with 1 sun conditions, we must evaluate this expression at $J_{inj} = J_{ph}$. We get the following expression for J_0 in function of IV curve parameters.

$$J_0 = \frac{J_{0,n}^n}{J_{sc}^n} J_{sc} \quad (A13)$$

It is now possible to compare J_0 determined by the approach presented in the main paper with J_0 evaluated using equation (A13). Their comparison is shown in **additional figure 7**.

Paper C

The agreement between J_0 obtained via EQE_{PV} and EQE_{EL} and the J_0 obtained from the IV curves is reasonable, and a trend is clearly visible. However, J_0 obtained via EQE_{PV} and EQE_{EL} seems to be a slight overestimation of the J_0 obtained via IV curves. This is because J_0 was evaluated from the EQE_{PV} (E) spectra obtained at short-circuit and not at injection conditions at a voltage comparable to V_{oc} . Due to the field dependent photocurrent in some material systems the EQE_{PV} under injection conditions can be lower than the EQE_{PV} at short circuit, resulting in an overestimation of J_0 via the method presented in the main paper. However this overestimation of J_0 does not affect our calculation of V_{oc} , as explained in the next section of this additional information.

3. Relating J_0 to V_{oc}

At V_{oc} the produced photocurrent J_{ph} balances with the injected current J_{inj} , and we get the following formula for V_{oc} from equation (A11) or equation (2) of the main paper.

$$V_{oc} = \frac{kT}{q} \ln \left(\frac{J_{ph}}{J_0^*} + 1 \right)$$

Hereby are J_{ph} and J_0^* evaluated by integrating the product of $EQE_{PV}(E)$ with respectively the AM1.5 spectrum and $\phi_{BB}(E)$. If there is a voltage dependence of the photocurrent J_{ph} , $EQE_{PV}(E)$ will also depend on voltage and for the evaluation of J_{ph} and J_0^* , $EQE_{PV}(E)$ should be measured under injection conditions, at voltages comparable to V_{oc} . Assuming that the spectral shape of $EQE_{PV}(E)$ does not depend on the injection conditions than the J_{ph}/J_0^* ratio depends only on the spectral shape of the $EQE_{PV}(E)$ spectrum and we can replace J_{ph}/J_0^* with J_{sc}/J_0 . Hereby are J_{sc} and J_0 evaluated by integrating the product of the $EQE_{PV}(E)$ spectrum measured at short circuit with respectively the AM1.5 spectrum and $\phi_{BB}(E)$, as described in the main paper.

We obtain thus equation (5) of the main paper

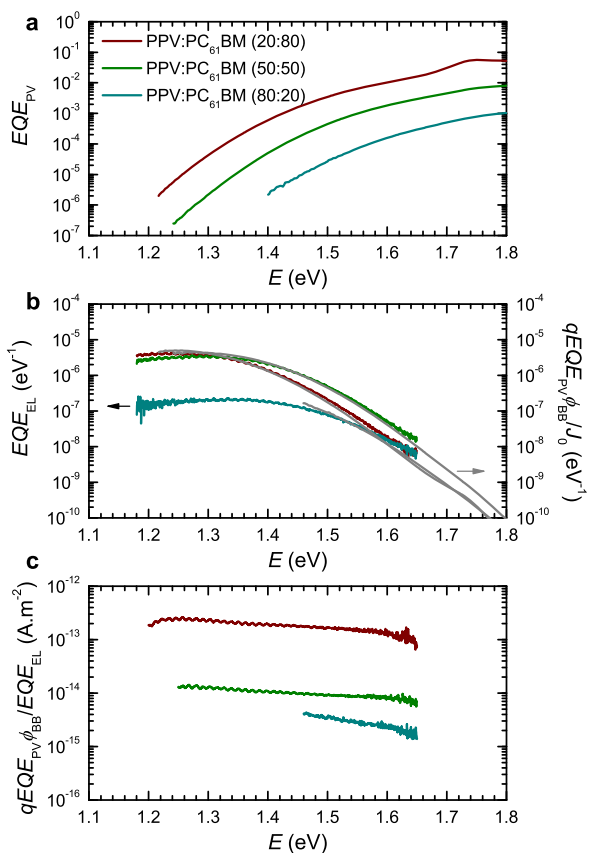
$$V_{oc} = \frac{kT}{q} \ln \left(\frac{J_{sc}}{J_0} + 1 \right)$$

Hereby should J_0 be evaluated as in the main paper, with $EQE_{PV}(E)$ measured at short-circuit.

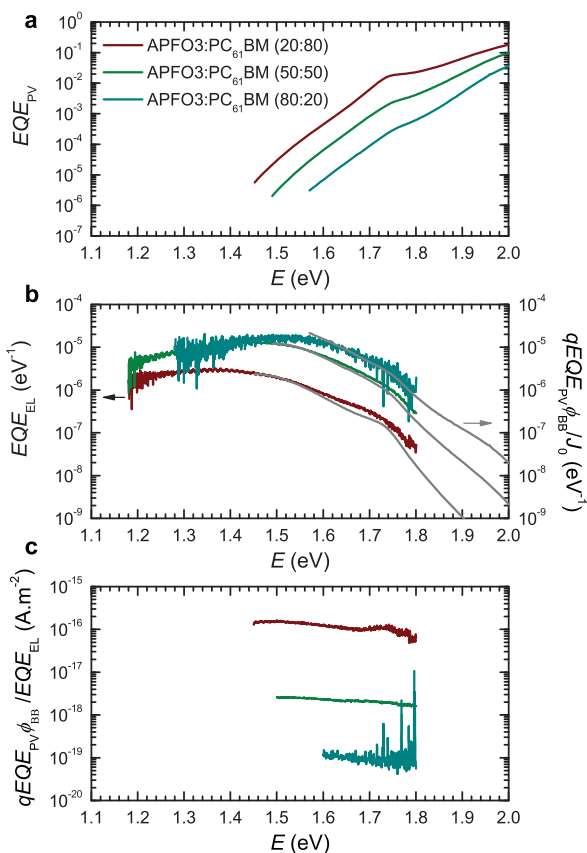
References

- _[1] Vandewal K. *et al.* The relation between open-circuit voltage and the onset of photocurrent generation by charge-transfer absorption in polymer: fullerene bulk heterojunction solar cells. *Adv. Funct. Mater.* **18**, 2064-2070 (2008).
- _[2] Veldman D. *et al.* Compositional and electric field dependence of the dissociation of charge transfer excitons in alternating polyfluorene copolymer/fullerene blends. *J. Am. Chem. Soc.* **130**, 7721-7735 (2008).
- _[3] Tvingstedt K. *et al.* Electroluminescence from charge transfer states in polymer solar cells. *J. Am. Chem. Soc.* **article ASAP** (online August 4) (2009).
- _[4] Peet J. *et al.* Efficiency enhancement in low-bandgap polymer solar cells by processing with alkane dithiols. *Nat. Mater.* **6**, 497-500 (2007).
- _[5] Campoy-Quiles M. *et al.* Morphology evolution via self-organization and lateral and vertical diffusion in polymer: fullerene solar cell blends. *Nat. Mater.* **7**, 158-164 (2008).

Figures



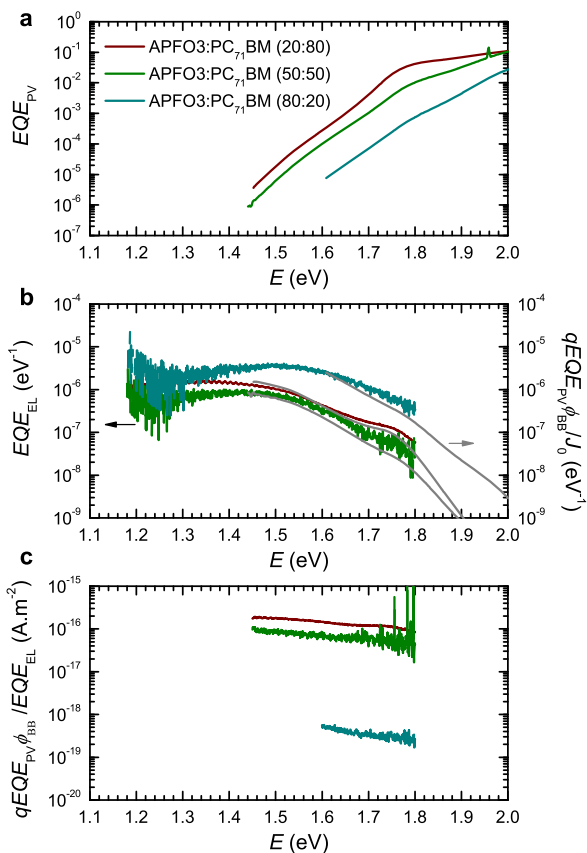
Additional figure 1: $EQE_{PV}(E)$, $EQE_{EL}(E)$ and J_0 for MDMO-PPV:PC₆₁BM in 3 different stoichiometries. The used polymer:fullerene ratios are 20:80 (blue), 50:50 (green) and 80:20 (red). Panel (a) shows the EQE_{PV} spectra. EQE_{EL} and the product of EQE_{PV} with the blackbody spectrum at room temperature are shown in panel (b). Panel (c) shows J_0 , calculated using formula (3) of the main text.



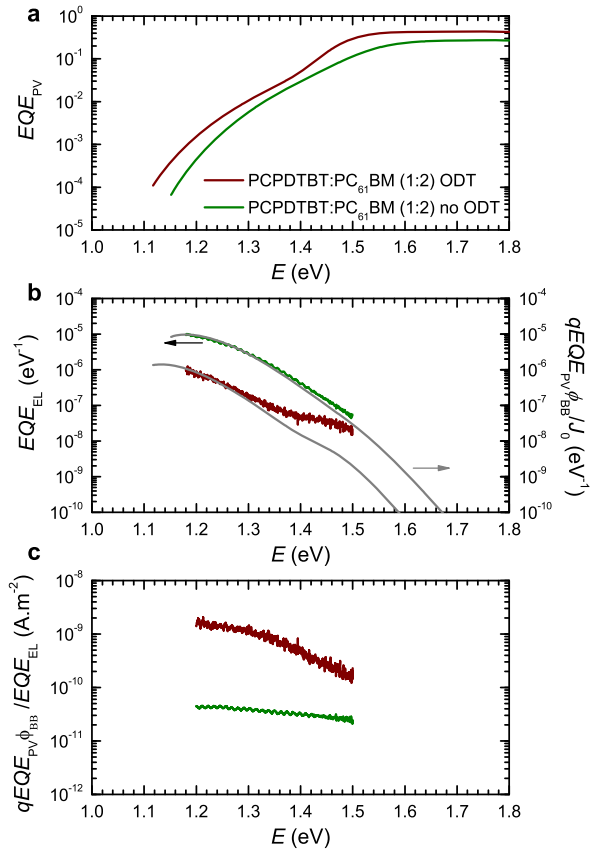
Additional figure 2: $EQE_{PV}(E)$, $EQE_{EL}(E)$ and J_0 for APFO3:PC₆₁BM in 3 different

stoichiometries. The used polymer:fullerene ratios are 20:80 (blue), 50:50 (green) and 80:20 (red).

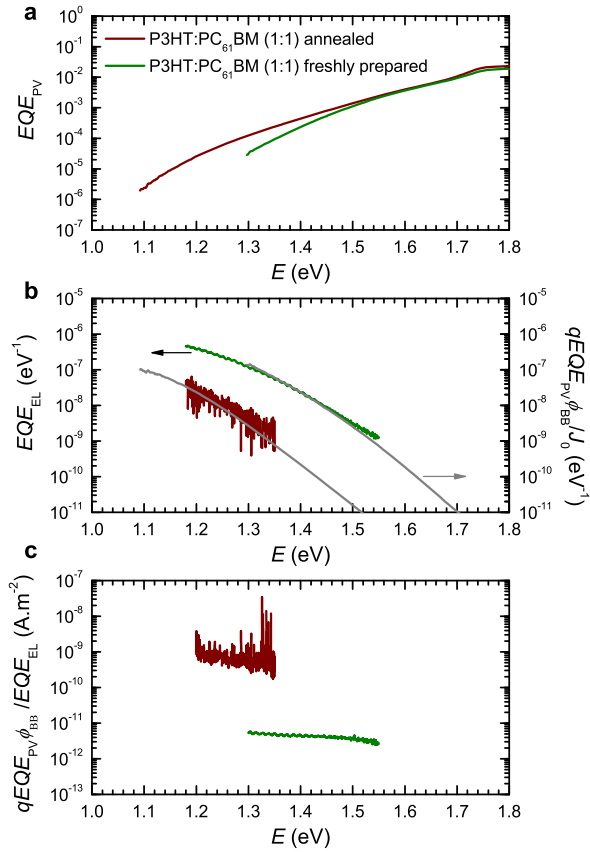
Panel (a) shows the EQE_{PV} spectra. EQE_{EL} and the product of EQE_{PV} with the blackbody spectrum at room temperature are shown in panel (b). Panel (c) shows J_0 , calculated using formula (3) of the main text.



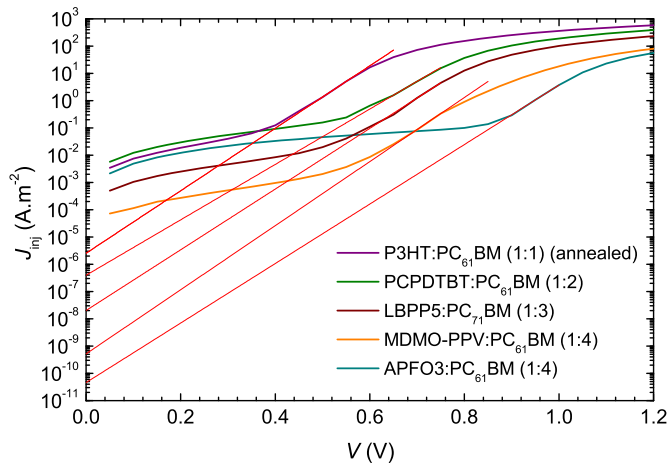
Additional figure 3: $EQE_{PV}(E)$, $EQE_{EL}(E)$ and J_0 for APFO3:PC₇₁BM in 3 different stoichiometries. The used polymer:fullerene ratios are 20:80 (blue), 50:50 (green) and 80:20 (red). Panel (a) shows the EQE_{PV} spectra. EQE_{EL} and the product of EQE_{PV} with the blackbody spectrum at room temperature are shown in panel (b). Panel (c) shows J_0 , calculated using formula (3) of the main text.



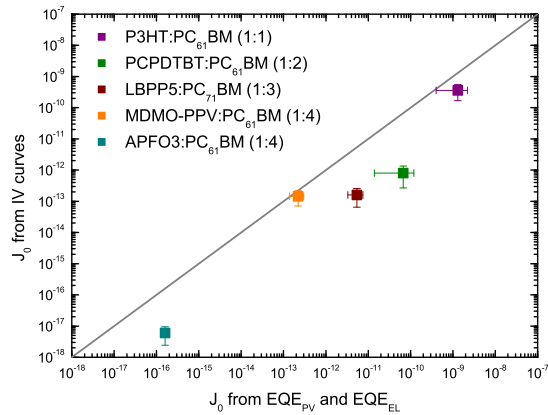
Additional figure 4: $EQE_{PV}(E)$, $EQE_{EL}(E)$ and J_0 for PCPDTBT:PC₆₁BM devices, with and without the use of 1,8-octanedithiol. The spectrum in green is the as prepared device, the spectrum in red is with the use of 1,8-octanedithiol (ODT). Panel (a) shows the EQE_{PV} spectra. EQE_{EL} and the product of EQE_{PV} with the blackbody spectrum at room temperature are shown in panel (b). Panel (c) shows J_0 , calculated using formula (3) of the main text.



Additional figure 5: $EQE_{PV}(E)$, $EQE_{EL}(E)$ and J_0 for annealed and unannealed P3HT:PC₆₁BM devices. The unannealed device is shown in the green spectrum while the annealed device is shown in red. Panel (a) shows the EQE_{PV} spectra. EQE_{EL} and the product of EQE_{PV} with the blackbody spectrum at room temperature are shown in panel (b). Panel (c) shows J_0 , calculated using formula (3) of the main text.



Additional figure 6: The dark injected current $J_{inj}(V)$ versus voltage V for polymer:fullerene devices. Active layers of the devices are: P3HT:PC₆₁BM (1:1) (annealed) (purple), PCPDTBT: PC₆₁BM (1:2) (green), LBPP5: PC₇₁BM (1:3) (red), MDMO-PPV: PC₆₁BM (1:4) (orange) and APFO3: PC₆₁BM (1:4) (cyan). The red lines represent exponential fits, allowing determination of $J_{0,n}$ and the ideality factor n .



Additional figure 7: J_0 obtained via analysis of the $EQE_{pV}(E)$ and $EQE_{EL}(E)$ spectra, compared with J_0 obtained from $J_{0,n}$ and n . Active layers of the devices are: P3HT:PC₆₁BM (1:1) (annealed) (purple), PCPDTBT: PC₆₁BM (1:2) (green), LBPP5: PC₇₁BM (1:3) (red), MDMO-PPV: PC₆₁BM (1:4) and APFO3: PC₆₁BM (1:4) (cyan). The gray line represents a one to one relation.

Additional table 1: Values for $J_{0,n}$ and n obtained by fitting of the exponential part of the dark IV curves.

Material system	$J_{0,n}$ (A.m ⁻²)	n
P3HT:PCBM (1:1) annealed	2.5E-6	1.49
PCPDTBT:PCBM (1:2)	4.0E-7	1.67
LBPP5:PC70BM (1:3)	2.0E-8	1.53
MDMO-PPV:PCBM (1:4)	5.2E-9	1.45
APFO3:PCBM (1:4)	4.6E-11	1.56

Paper D

Relating the open-circuit voltage to interface molecular properties of donor:acceptor bulk heterojunction solar cells

K. Vandewal, A. Gadisa, J. V. Manca, K. Tvingstedt, O. Inganäs, *Phys. Rev. B*, submitted (2009)

Relating the open-circuit voltage to interface molecular properties of donor:acceptor bulk heterojunction solar cells

Koen Vandewal,* Abay Gadisa, and Jean V. Manca
 IMEC-IMOMECE, vzw and Institute for Materials Research,
 Hasselt University, Wetenschapspark 1, 3590 Diepenbeek (Belgium)

Kristofer Tvingstedt and Olle Inganäs
 Biomolecular and Organic Electronics, Center of Organic Electronics (COE),
 Department of Physics, Chemistry and Biology, Linköping University, 58183 Linköping (Sweden)
 (Dated: November 4, 2009)

The open-circuit voltage (V_{oc}) of polymer:fullerene bulk heterojunction solar cells is determined by the interfacial charge-transfer (CT) states between polymer and fullerene. Fourier-transform photocurrent spectroscopy and electroluminescence spectra of several polymer:fullerene blends are used to extract the relevant interfacial molecular parameters. An analytical expression linking these properties to V_{oc} is deduced, and shown to be valid for photovoltaic devices comprising three commonly used conjugated polymers blended with the fullerene derivative PCBM. V_{oc} is proportional to the energy of the CT states E_{CT} . The energetic loss $q\Delta V$ between E_{CT} and qV_{oc} , vanishes when approaching 0 K. It depends linearly on T and logarithmically on illumination intensity. Furthermore $q\Delta V$ can be reduced by decreasing the electronic coupling between polymer and fullerene or by reducing the non-radiative recombination rate. For the investigated devices we find a loss $q\Delta V$ of ~ 0.6 eV at room temperature and under solar illumination conditions, of which ~ 0.25 eV is due to radiative recombination via the CT state and ~ 0.35 eV is due to non-radiative recombination.

I. INTRODUCTION

Research in organic photovoltaics has advanced over the latest years. Currently power conversion efficiencies of 5-6 %, with external quantum efficiencies of 70-80 %¹⁻³ and internal quantum efficiencies approaching 100 %³ are achieved for polymer:fullerene photovoltaic devices. This indicates that in these high quantum efficiency cases, nearly all photons absorbed by the polymer are converted into collected electrons at short-circuit, and hence, that the achieved short-circuit currents are close to their predicted maximum. Power conversion efficiency, however, does not only depend on the production of photocurrent but also on the photovoltage. Optimization and understanding of the fundamental limits of the open-circuit voltage (V_{oc}) therefore is as important as the optimization of the short-circuit current (J_{sc}).

V_{oc} has been shown to depend on the donor/acceptor material combination^{4,5}, the electrode material⁶, as well as light intensity and temperature.⁷ Modelling of the internal field and charge distribution has successfully explained the influence of several of these parameters on V_{oc} . However, there exists also a relation between externally measurable electro-optical spectra and V_{oc} .⁸ This relation is based on the principle of detailed balance and the assumption of quasi-equilibrium conditions.^{9,10} A benefit of this approach is that it avoids description of the internal charge and field distributions in the solar cell, which are difficult to measure. With this theory, the origin of V_{oc} of polymer:fullerene solar cells can be explained in terms of ground-state charge transfer complex (CTC) formation between polymer and fullerene.⁸

Upon blending a suitable donor polymer with a fullerene acceptor, interaction between polymer and fullerene results in the formation of a ground-state CTC.¹¹⁻²⁰ Upon excitation of this new ground-state, the charge transfer (CT) exciton is created. Optical transitions from the CTC ground-state to the CT exciton are visible in the low energy region of the photovoltaic external quantum efficiency (EQE_{PV}) spectrum, if measured with sensitive techniques.¹⁶ Radiative decay of CT excitons is sometimes observed in photoluminescence measurements of polymer:fullerene blends^{12-14,17-20} and can be more easily detected in electroluminescence spectra obtained by applying a forward voltage over polymer:fullerene photovoltaic devices.¹⁹

CT excitons play a major role in the operation of polymer:fullerene solar cells.^{8,12,17,20} These weakly bound electron-hole pairs at the polymer:fullerene interface are mainly populated via a photoinduced electron transfer after excitation of polymer or fullerene. Due to the low oscillator strength of polymer:fullerene CTCs only a very small fraction of CT excitons is populated by direct optical excitation of the CTCs. The major contribution to the photocurrent originates from polymer or fullerene excitation. However, the efficiency of CT exciton formation and their dissociation into free carriers determines the photocurrent.^{12,17,20} Both formation and dissociation efficiencies depend on the blend morphology and donor:acceptor energetics. Also V_{oc} is determined by the spectral properties of the CT excitons, again being morphology dependent. In general, the spectral position of the CT exciton correlates with the difference between the Lowest Unoccupied Molecular Orbital (LUMO) of the fullerene acceptor and the Highest Occupied

Molecular Orbital (HOMO) of the donor polymer²¹, resulting in the widely observed correlation between V_{oc} and this difference.^{1,2,4,5} However, recently it has been argued that other CTC related parameters, such as the electronic coupling between donor and acceptor, also have an influence on V_{oc} .^{22,23}

In this paper we aim to describe in more detail how V_{oc} is affected by CTC properties. These properties are obtained by observing the CT optical transition bands in sensitive measurements of the photovoltaic external quantum efficiency (EQE_{PV}) spectrum and the electroluminescence spectrum. An analytical expression for V_{oc} as a function of interfacial CTC properties is deduced. V_{oc} is shown to be proportional to the energy of the interfacial CT state E_{CT} . The energetic loss between E_{CT} and qV_{oc} depends linearly on temperature and logarithmically on illumination intensity as observed also by others.^{7,24} In this work we show that this loss can be reduced by reducing the electronic coupling between polymer and fullerene and by reducing the non-radiative recombination.

The derived analytical expression is shown to be valid in a temperature range from 150 K to 300 K and under different illumination intensities, for four material systems, consisting of poly[2-methoxy-5-(30,70-dimethyloxy)-1,4-phenylene vinylene] (MDMO-PPV), poly[3-hexylthiophene] (P3HT) and poly[2,7-(9-di-octyl-fluorene)-alt-5,5-(4',7'-di-2-thienyl-2',1',3'-benzothiadiazole)] (APFO3), blended with the fullerene derivative [6,6]-Phenyl C61 butyric acid Methyl ester (PCBM). For the APFO3 based devices, APFO3:PCBM 1:4 and 1:1 stoichiometries were studied.

II. THEORY

In the framework of Marcus theory, the spectral lineshape of the CT absorption cross-section $\sigma(E)$ at photon energy E is described by^{25,26}:

$$\sigma(E)E = \frac{f_\sigma}{\sqrt{4\pi\lambda kT}} \exp\left(\frac{-(E_{CT} + \lambda - E)^2}{4\lambda kT}\right) \quad (1)$$

Hereby is k Boltzmann's constant and T the absolute temperature. E_{CT} is the free energy difference between the CTC ground state and the CT excited state and λ is a reorganisation energy associated with the CT absorption process, as shown in figure 1 (a). f_σ does not depend on E ,²⁶ and is proportional to the square of the electronic coupling matrix element. It represents a measure of the strength of the donor/acceptor material interaction. The absorption coefficient α in the spectral region of CT absorption equals σN_{CTC} , with N_{CTC} the number of CTCs per unit volume.

The emission rate I_f at photon energy E , per unit energy equals^{25,26}

$$\frac{I_f}{E} = \frac{f_{I_f}}{\sqrt{4\pi\lambda kT}} \exp\left(\frac{-(E_{CT} - \lambda - E)^2}{4\lambda kT}\right) \quad (2)$$

In analogy to f_σ , f_{I_f} does not depend on E and is proportional to the square of the electronic coupling matrix element.²⁶ The left hand side of equations (1) and (2) are called the reduced absorption and emission spectrum, respectively. They exhibit a mirror image relationship. The midpoint energy of these two spectra equals E_{CT} . λ can be deduced from the Stokes shift, or from the linewidth of the absorption or emission bands. This is visualized in the scheme shown in figure 1 (a).

Because of their low absorption coefficients, highly sensitive techniques are needed to spectrally resolve CT absorption bands in polymer:fullerene blends.²⁷ We use Fourier-transform photocurrent spectroscopy (FTPS) to measure the photovoltaic EQE_{PV} spectrum of polymer:fullerene devices over several decades. The CT bands are visible in the low energy part of the EQE_{PV} spectrum. Because of the low value of α , the total absorption in this spectral region can be approximated by $\alpha 2d$, when using a back reflecting metal cathode. The EQE_{PV} equals the total absorption $\alpha 2d$, multiplied by the absorbed-photon-to-electron internal conversion efficiency η .

$$EQE_{PV}(E) = \eta \sigma(E) N_{CTC} 2d \quad (3)$$

Using equation (1) for $\sigma(E)$ we obtain in the spectral region of CT absorption:

$$EQE_{PV}(E) = \frac{f}{E\sqrt{4\pi\lambda kT}} \exp\left(\frac{-(E_{CT} + \lambda - E)^2}{4\lambda kT}\right) \quad (4)$$

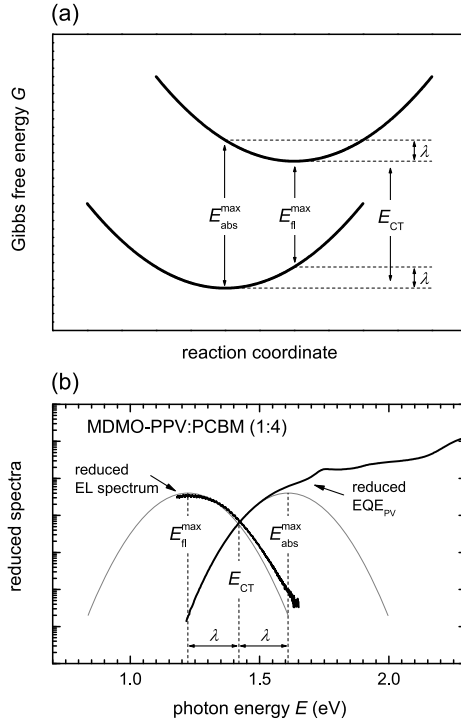


FIG. 1: (a) Free energy diagram for the ground state and lowest excited state of the CTC as a function of a generalized coordinate. (b) Reduced EQE_{PV} and electroluminescence spectra for a MDMO-PPV:PCBM (1:4) photovoltaic device. The gray curves are fits of the EQE_{PV} and electroluminescence spectra using formula (1) and (2), using the same E_{CT} and λ values. These parameters, together with the maxima of absorption E_{abs}^{max} and emission E_{fl}^{max} are indicated in the figure.

In this equation the prefactor f equals $\eta N_{CTC} 2df_{\sigma}$. The normalized reduced EQE_{PV} and electroluminescence emission spectra are shown in figure 1 (b) for MDMO-PPV:PCBM in a 1:4 ratio. In the figure we have indicated how the parameters E_{CT} and λ in figure 1 (a) can be deduced from figure 1 (b).

We will now relate these CTC properties to V_{oc} . In ref⁸, using the method of detailed balance we have shown that the CT states relate to the recombination current and V_{oc} . At voltages V , higher than the thermal voltage $\frac{kT}{q}$, with q the elementary charge, we use the following expression for the dark injected current J_{inj} versus voltage characteristic:

$$J_{inj} = J_0 \exp\left(\frac{qV}{kT}\right) \quad (5)$$

Following the reasoning of Rau¹⁰, J_0 is related to the electro-optical properties by:

$$J_0 = \frac{q}{EQE_{EL}} \int EQE_{PV}(E) \phi_{BB}^T dE \quad (6)$$

In this equation EQE_{EL} is the electroluminescence external quantum efficiency and ϕ_{BB}^T is the black body spectrum at temperature T . The $\phi_{BB}^T EQE_{PV}$ product should be integrated over all possible energies E . However because ϕ_{BB}^T

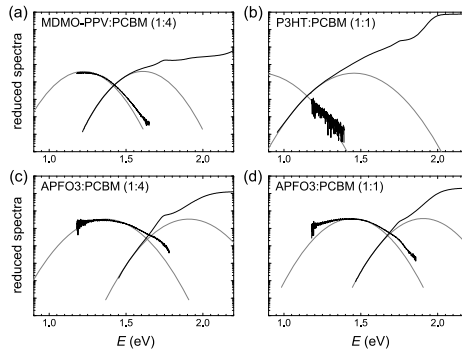


FIG. 2: Reduced EQE_{PV} and electroluminescence spectrum for (a) APFO3:PCBM (1:4), (b) APFO3:PCBM (1:1) and P3HT:PCBM (1:1) photovoltaic devices. The gray curves are fits of the EQE_{PV} and electroluminescence spectra using formula 1 and 2, with the same values for E_{CT} and λ .

is strongly decreasing with increasing energy, only the low energy, CT part of the EQE_{PV} spectrum contributes to this integral.⁸ Using formula (4) in formula (6) gives:

$$J_0 \approx \frac{q}{EQE_{EL}} f \frac{2\pi}{h^3 c^2} (E_{CT} - \lambda) \exp\left(-\frac{E_{CT}}{kT}\right) \quad (7)$$

The derivation of equation (7) is explained in more detail in the appendix. From equation (5) and (7) and the fact that, at open-circuit, the injection current J_{inj} equals the photocurrent J_{sc} , we get an analytical expression for V_{oc} as a function of EQE_{EL} and the parameters E_{CT} , λ and f :

$$V_{oc} = \frac{E_{CT}}{q} + \frac{kT}{q} \ln\left(\frac{J_{sc} h^3 c^2}{f q 2\pi (E_{CT} - \lambda)}\right) + \frac{kT}{q} \ln(EQE_{EL}) \quad (8)$$

This formula implies a linear dependence of V_{oc} on temperature and a logarithmic dependence on illumination intensity. Such dependencies are observed and described in the literature.^{7,28,29} The formulation of equation (8) however, allows us to relate measurable properties related to the molecular interface between donor and acceptor to V_{oc} . This will be further discussed in the next sections.

III. EXTRACTION OF CTC PROPERTIES

We have investigated polymer:PCBM solar cells based on 3 different donor polymers, i.e. MDMO-PPV, P3HT, APFO3. For the APFO3:PCBM blends, the polymer:fullerene 1:1 and 1:4 weight ratios are investigated. The EQE_{PV} and electroluminescence spectrum of MDMO-PPV:PCBM in a 1:4 ratio were already shown in figure 1 (b). The spectra for the APFO3 and P3HT based devices are shown in figure 2.

For all material systems, we can deduce the reorganization energy λ and E_{CT} by fitting the CT band in the EQE_{PV} spectrum with equation (4). The EL emission spectra were measured with the aid of a Si CCD camera in the spectral range above 1.2 eV. In this range, the shape of the predicted reduced emission spectrum calculated via formula (2) resembles the measured, reduced electroluminescence spectrum for all devices. This indicates that the shape of the CT bands at room temperature can be described to a fairly good approximation with formulas (1)-(4)

We have also applied formula (4) to account for the temperature dependence of the CT band. EQE_{PV} spectra were obtained between 150 and 300 K. The spectra for the 4 different material systems are shown in figure 3, together with their fits using formula (4). The obtained parameters are listed in table I. For the studied material systems, we obtain λ values, which are quite independent of temperature, in the order of 0.2-0.3 eV. The values of E_{CT} , and the values of E_{abs}^{max} however, are slightly temperature dependent. We observe a small redshift of the CT band ~ 0.1

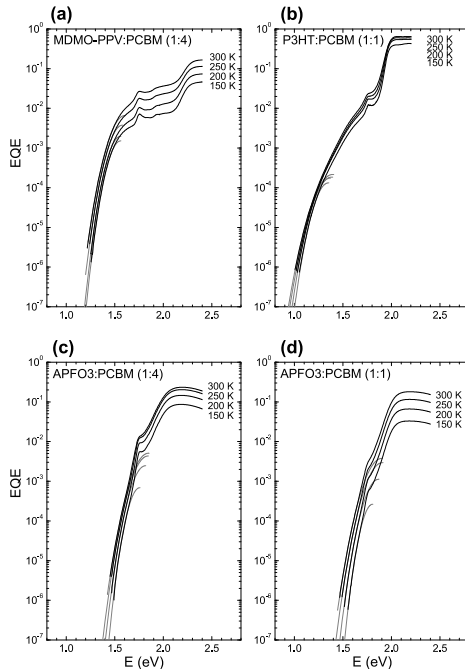


FIG. 3: EQE_{PV} spectra of (a) MDMO-PPV:PCBM (1:4), (b) P3HT:PCBM (1:1), (c) APFO3:PCBM (1:4), (d) APFO3:PCBM (1:1), measured at several temperatures. The spectra were fitted with formula (4) to obtain values for E_{CT} and λ .

eV upon cooling from 300 K to 150 K. This corresponds to what is observed for temperature dependent absorption, fluorescence and electroluminescence spectra of pure conjugated polymers^{30,31} or conjugated polymers involved in a CTC³². The origin of this phenomenon can be attributed to an increased overlapping of orbitals, due to less thermally induced disorder at lower temperatures.³²

The APFO3:PCBM blends show the highest E_{CT} , with the 1:1 stoichiometry having a slightly higher value than the 1:4 stoichiometry. The P3HT:PCBM blend has the lowest E_{CT} (table I).

IV. TEMPERATURE DEPENDENCE OF V_{oc}

In this section we investigate the temperature dependence of the dark saturation current J_0 and V_{oc} . We have already seen that E_{CT} also depends on temperature. If we approximate E_{CT} by $E_{CT}^0 + T \frac{dE_{CT}}{dT}$, then, for the investigated devices $\frac{dE_{CT}}{dT}$ is almost constant in the region from 150 K to 300 K (figure 4). In this case E_{CT}^0 is the linear extrapolation of E_{CT} to 0 K. It is also the activation energy of the dark current, for $J_0 \sim \exp\left(-\frac{E_{CT}^0 + T \frac{dE_{CT}}{dT}}{kT}\right) \sim \exp\left(-\frac{E_{CT}^0}{kT}\right)$.

We obtain the following values for E_{CT}^0 : For MDMO-PPV:PCBM (1:4) $E_{CT}^0 = 1.25$ eV and for P3HT:PCBM (1:1) $E_{CT}^0 = 0.94$ eV. These values are very close to the activation energies E_a of the dark saturation current values found in ref²⁸ for MDMO-PPV:PCBM (1:4) ($E_a = 1.25$ eV) and P3HT:PCBM (1:1) ($E_a = 0.92$ eV - 0.93 eV). For the APFO3:PCBM (1:4) and APFO3:PCBM (1:1) devices we find respectively $E_{CT}^0 = 1.45$ eV and $E_{CT}^0 = 1.51$ eV. This last example indicates that the spectral position of the CT band and E_{CT} are not only affected by the energetic levels

TABLE I: Summary of the parameters E_{CT} , λ and f obtained by fitting the CT band in the temperature dependent EQE_{PV} spectra with equation (4).

MDMO-PPV:PCBM(1:4)				P3HT:PCBM(1:1)		
T (K)	f (eV ²)	E_{CT} (eV)	λ (eV)	f (eV ²)	E_{CT} (eV)	λ (eV)
150	4.8E-4	1.31	0.25	4.1E-5	1.03	0.32
200	6.4E-4	1.36	0.20	6.0E-5	1.08	0.29
250	1.4E-3	1.39	0.19	7.2E-5	1.11	0.29
300	2.6E-3	1.42	0.19	8.8E-5	1.14	0.27

APFO3:PCBM(1:4)				APFO3:PCBM(1:1)		
T (K)	f (eV ²)	E_{CT} (eV)	λ (eV)	f (eV ²)	E_{CT} (eV)	λ (eV)
150	2.3E-4	1.54	0.22	9.0E-5	1.60	0.20
200	1.0E-3	1.58	0.24	4.9E-4	1.62	0.25
250	2.0E-3	1.61	0.24	1.5E-3	1.65	0.26
300	2.5E-3	1.64	0.21	2.0E-3	1.68	0.23

of a single donor and a single acceptor molecule, but also on polymer:fullerene stoichiometry.¹⁶

Regarding the temperature dependence of V_{oc} , Green³³ showed that if the dark recombination current is of the form of equation (8), an approximately linear temperature dependence of qV_{oc} is predicted with a 0 K intercept equal to E_{CT}^0 . In figure 4, the validity of this reasoning for the 4 polymer:fullerene solar cells investigated in this work is shown. This figure shows the temperature dependence of the E_{CT} values and V_{oc} values for different illumination intensities, between ~ 0.001 and ~ 0.1 sun. Extrapolation of temperature dependent values E_{CT} to zero Kelvin coincides very well with the extrapolation of the temperature dependent V_{oc} , for all 4 material systems and the investigated illumination intensities. For both APFO3 samples, there are some deviations from the straight line at low temperature. For inorganic solar cells, such as Si and GaAs, the same reasoning can be made for the relation between V_{oc} and the bandgap of the used inorganic material.³³ This indicates that, with respect to V_{oc} , the energy of the CT exciton E_{CT} , fulfills the same role as the bandgap does in inorganic solar cells. This confirms that E_{CT} is an appropriate definition for the gap of organic solar cells based on blends of donor and acceptor materials. Note that E_{CT} is defined differently in this work, than it is in previous work¹⁶, where we used an empirical definition for the interfacial bandgap. However, we believe that E_{CT} , as defined in the present work represents better the actual involved physical processes of CT absorption and emission.

V. ILLUMINATION INTENSITY DEPENDENCE OF V_{oc}

We can calculate EQE_{EL} using the expression (8), together with experimentally obtained values for V_{oc} , J_{sc} , E_{CT} and f . In figure 5 the calculated values are shown as a function of the short-circuit current J_{sc} of the device. It can be seen that the calculated EQE_{EL} values are in the order of 10^{-9} to 10^{-6} with the lowest EQE_{EL} values for the P3HT:PCBM (1:1) devices.

In order to compare these calculated EQE_{EL} values with experimental values we have measured EQE_{EL} as a function of injection current, using a Si photodiode. Because of the low EQE_{EL} values, good signals have only been obtained at high injection currents. Because at V_{oc} , the photocurrent and injected current balance, the EQE_{EL} obtained by using formula (8) must be compared with experimentally measured EQE_{EL} at an injection current corresponding to the short-circuit current. In figure 5, it can be seen that the experimentally obtained $EQE_{EL}(J_{inj})$ trend corresponds fairly well with the calculated $EQE_{EL}(J_{sc})$.

A dependence of EQE_{EL} on J_{inj} and thus internal charge density, is observed. We can approximate the relation of EQE_{EL} as a function of J_{inj} by a power law relationship $EQE_{EL}(J_{inj}) \approx EQE_{EL}(1)J_{inj}^\alpha$. Hereby is $EQE_{EL}(1)$ the EQE_{EL} measured at an injection current of 1 A.m⁻². Using this in equation (7) and (5) this gives:

$$J_{inj} = J_{0,n} \exp\left(\frac{qV}{nkT}\right) \quad (9)$$

Hereby $n = 1 + \alpha$ and $J_{0,n} = (J_0(1))^{\frac{1}{n}}$, with $J_0(1)$ equals J_0 obtained by evaluating (7) for $EQE_{EL}(1)$. For the material systems investigated in this work we find values for n between 1 and 1.5.

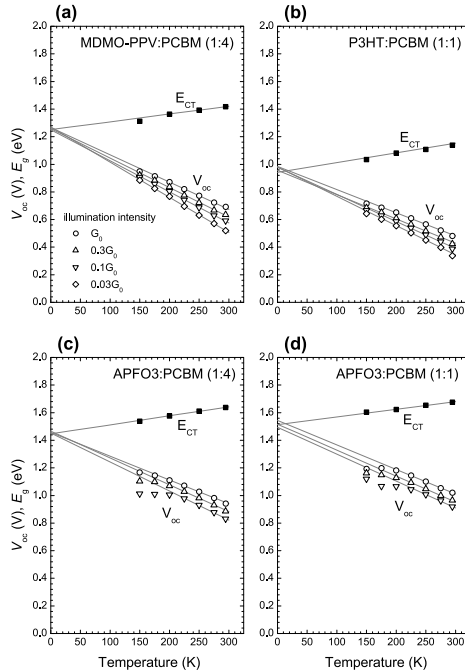


FIG. 4: V_{oc} and E_{CT} in function of temperature. E_{CT} is represented as the filled squares. V_{oc} was measured for different illumination intensities. The highest illumination intensity was G_0 , about 0.1 sun, represented by open circles. The other illumination intensities are $0.3G_0$ (open triangles up), $0.1G_0$ (open triangles down) and $0.03G_0$ (diamonds). Both extrapolation of V_{oc} and E_{CT}/q to 0 K results in the same value.

Using expression (9), the equation for V_{oc} becomes:

$$V_{oc} = \frac{nkT}{q} \ln \left(\frac{J_{sc}}{J_{0,n}} \right) \quad (10)$$

Relations of this type including an ideality factor n have been used before to describe the illumination intensity of V_{oc} of organic solar cells^{7,24,28,29}, though the origin of the n term is often hidden in obscurity. It originates from the fact that non-radiative recombination mechanisms are present. These mechanisms depend differently on the charge density or injected current as compared to the radiative recombination mechanism. This causes $E_{QE}E_{EL}$ to depend on the injected current. The exact non-radiative recombination mechanisms are not known at present but should be investigated further, as a reduction of these recombination pathways will cause an increase in $E_{QE}E_{EL}$ and V_{oc} .

VI. VOLTAGE LOSSES IN POLYMER:FULLERENE SOLAR CELLS AT AM1.5 CONDITIONS

We will now do a more detailed study of the energetic losses $q\Delta V$ between qV_{oc} and the gap E_{CT} under solar conditions. In analogy to¹⁰, this loss can be seen as consisting of 2 parts, $q\Delta V_{rad}$ and $q\Delta V_{non-rad}$. Equation (8), allows us to calculate these losses :

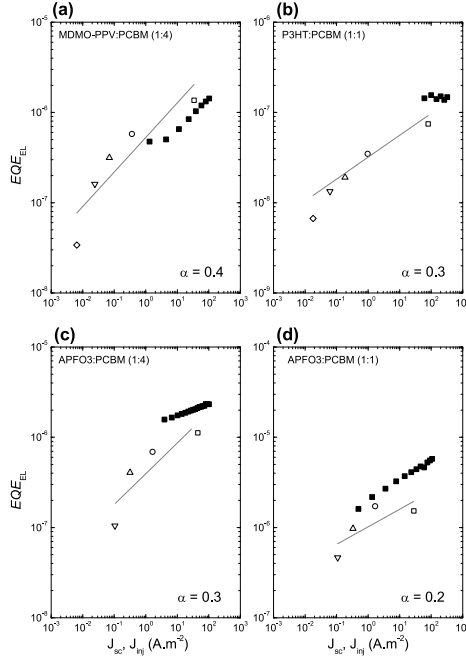


FIG. 5: The calculated and measured EQE_{EL} . The open symbols represent EQE_{EL} versus J_{sc} , calculated from V_{oc} measurements with the aid of formula (8). The filled squares are measurements of EQE_{EL} versus J_{inj} . The red lines represent a power law dependence of EQE_{EL} on J_{sc} with a power α .

$$q\Delta V_{rad} = -kT \ln \left(\frac{J_{sc} h^3 c^2}{f q 2\pi (E_{CT} - \lambda)} \right) \quad (11)$$

$$q\Delta V_{non-rad} = -kT \ln (EQE_{EL}) \quad (12)$$

When all recombination is radiative CT emission, $EQE_{EL} = 1$ and $\Delta V_{non-rad}$ vanishes. In this case ΔV equals ΔV_{rad} , a loss due solely to radiative emission. It is logarithmically dependent on properties of the CTC and incident light intensity ($\sim J_{sc}$). For a given donor/acceptor pair with fixed E_{CT} , λ and f , this term is constant, and represents a minimum loss between E_{CT} and qV_{oc} , for a perfect device in which the only recombination mechanism present is a radiative one. Because of the logarithmic dependence the variation of the parameters E_{CT} and λ will not affect this loss much. However the parameter f can be varied over several decades by varying the electronic coupling between polymer and fullerene. Choosing donor/acceptor pairs with a reduced interfacial coupling will thus result in a decreased f and ΔV_{rad} .

The part which takes into account the non-radiative recombination mechanisms, omni-present in real devices, is reflected in the term $\Delta V_{non-rad}$. This term becomes larger than zero, if EQE_{EL} is smaller than unity. As seen above, this part is also logarithmically dependent on J_{sc} , as $EQE_{EL} \sim J_{sc}^\alpha$ for the polymer:fullerene solar cells we have investigated. Similar formulas were derived for the V_{oc} of inorganic solar cells, but assumed to be valid for all solar cells operating in quasi-equilibrium conditions.³³ It is argued that while ΔV_{rad} is a thermodynamically unavoidable loss mechanism for a given material system, $\Delta V_{non-rad}$ can in principle be avoided, by reducing the non-radiative

TABLE II: radiative and non-radiative energetic losses at V_{oc} . The radiative loss were calculated from the FTPS spectra. The non-radiative losses are related to EQE_{EL} .

	ΔV (V)	ΔV_{rad} (V)	$\Delta V_{non-rad}$ (V)
MDMO-PPV:PCBM (1:4)	0.58	0.24	0.34
P3HT:PCBM (1:1)	0.53	0.11	0.42
APFO3:PCBM (1:4)	0.59	0.24	0.35
APFO3:PCBM (1:1)	0.59	0.25	0.34

recombination paths. We experimentally find EQE_{EL} at room temperature in the range 10^{-9} to 10^{-6} , when using Ca/Al and ITO/PEDOT:PSS contacts. Using non-ohmic contacts will decrease the value of EQE_{EL} even further. For Si and GaAs solar cells, EQE_{EL} values are in the range of 10^{-3} .³³ The question remains if these values can also be achieved for polymer:fullerene solar cells.

In table 2 the loss factors are shown for the 4 investigated devices with ITO/PEDOT:PSS bottom contacts and Ca/Al top contacts, under solar conditions. The overall offset ΔV is fairly constant, with a value between 0.5 V and 0.6 V. The P3HT:PCBM system has a lower value for f than the other (non-crystalline) polymer:PCBM systems. This results in a lower radiative loss ΔV_{rad} . However in this system, there is no net benefit of this lower ΔV_{rad} because $\Delta V_{non-rad}$ is higher as compared to the other material systems. The increased non-radiative recombination in the P3HT:PCBM device can be explained by the decreased f or electronic coupling and thus lower radiative decay rate in this system (equation 2). A lower radiative decay rate gives electrons and holes more time to decay non-radiatively. This results in a fairly constant ΔV for all four material systems. This explains the widely observed relation between V_{oc} and the difference between HOMO(D) and LUMO(A) for polymer:fullerene bulk heterojunction solar cells, for this difference correlates with E_{CT} .²¹

VII. CONCLUSION

In this work, CTC parameters are related to V_{oc} . It was shown that the free energy difference E_{CT} between excited CTC and ground state CTC is an appropriate definition of donor:acceptor blend gap. This parameter is independent of the measurement method. It can be measured as the symmetry point of CT absorption and emission or by fitting either the CT band in the absorption or EQE_{PV} spectrum, or in the PL or EL spectrum. Its extrapolation to 0 K coincides with the extrapolation of V_{oc} to 0 K and the activation energy of the dark current. This is in analogy with the bandgaps of several inorganic solar cells. For the material blends P3HT:PCBM, APFO3:PCBM and MDMO-PPV:PCBM E_{CT} is found to be slightly temperature dependent, with E_{CT} increasing with increasing temperature.

A formula for the open-circuit voltage V_{oc} in function of the CTC properties E_{CT} , λ and f as well as the temperature T , the short-circuit current J_{sc} and the electroluminescence external quantum efficiency EQE_{EL} is deduced and shown to be valid for 4 polymer:fullerene bulk heterojunction solar cells. We show further that EQE_{EL} is not constant but depends on the injected current, thus on the number of charge carriers present in the device. This phenomenon is the origin of the ideality factor n , often used in the fitting of dark IV curves of organic solar cells.

The energetic losses between E_{CT} and qV_{oc} at room temperature and AM1.5 illumination conditions are around 0.5-0.6 eV for the investigated blends. The origin of these losses are twofold. About ~ 0.25 eV of this loss is due to unavoidable radiative losses, related to properties of the CTC formed between polymer donor and fullerene acceptor. ~ 0.35 eV is due to non-radiative losses. As these last terms represents a major loss factor for the devices investigated in this work, identification and possibly removal of the non-radiative decay paths is crucial in the future development of donor/acceptor based organic solar cells.

Acknowledgments

We acknowledge the institute for the promotion of science and technology in Flanders (IWT-Vlaanderen), the Swedish Energy Agency for funding through the program Tandem and Mats R. Andersson at Chalmers University for supplying us APFO3. Dirk Vanderzande and Wibren D. Oosterbaan are thanked for valuable discussions.

APPENDIX A: DERIVATION OF EQUATION (7)

In equation (6)

$$J_0 = \frac{q}{EQE_{EL}} \int EQE_{PV}(E) \phi_{BB}^T dE \quad (A1)$$

We use expression (4) for EQE_{PV}

$$EQE_{PV} = \frac{f}{E} FC(E_{CT} - E) \quad (A2)$$

If $E \gg kT$, the black body spectrum at temperature T can be approximated by:

$$\phi_{BB}^T = \frac{2\pi}{h^3 c^2} E^2 \exp\left(-\frac{E}{kT}\right) \quad (A3)$$

We get for J_0 :

$$J_0 = \frac{q}{EQE_{EL}} \frac{2\pi}{h^3 c^2} f \int \frac{E}{\sqrt{4\pi\lambda kT}} \exp\left(\frac{-(E_{CT} - E + \lambda)^2}{4\lambda kT}\right) \exp\left(\frac{-E}{kT}\right) dE \quad (A4)$$

Collecting both exponentials in one exponential function gives:

$$J_0 = \frac{q}{EQE_{EL}} \frac{2\pi}{h^3 c^2} f \int \frac{E}{\sqrt{4\pi\lambda kT}} \exp\left(-\frac{(E_{CT} - E + \lambda)^2 + 4\lambda E}{4\lambda kT}\right) dE \quad (A5)$$

We will concentrate on the term within the exponential. Working out the quadrate gives:

$$J_0 = \frac{q}{EQE_{EL}} \frac{2\pi}{h^3 c^2} f \int \frac{E}{\sqrt{4\pi\lambda kT}} \exp\left(-\frac{(E_{CT} - E)^2 + 2\lambda(E_{CT} - E) + \lambda^2 + 4\lambda E}{4\lambda kT}\right) dE \quad (A6)$$

Rearrangement of the terms gives:

$$J_0 = \frac{q}{EQE_{EL}} \frac{2\pi}{h^3 c^2} f \int \frac{E}{\sqrt{4\pi\lambda kT}} \exp\left(-\frac{(E_{CT} - E)^2 - 2\lambda(E_{CT} - E) + \lambda^2 + 4\lambda E_{CT}}{4\lambda kT}\right) dE \quad (A7)$$

This can also be written as:

$$J_0 = \frac{q}{EQE_{EL}} \frac{2\pi}{h^3 c^2} f \exp\left(\frac{-E_{CT}}{kT}\right) \int \frac{E}{\sqrt{4\pi\lambda kT}} \exp\left(\frac{-(E_{CT} - E - \lambda)^2}{4\lambda kT}\right) dE \quad (A8)$$

The expression under the integral sign is a normalized Gaussian peaking at $E_{CT} - \lambda$, multiplied by the photon energy E . Integrating this function will give a value close to the peak of the gaussian, i.e. $E_{CT} - \lambda$. This gives the expression (7) for J_0 :

$$J_0 \approx \frac{q}{EQE_{EL}} f \frac{2\pi}{h^3 c^2} (E_{CT} - \lambda) \exp\left(-\frac{E_{CT}}{kT}\right) \quad (A9)$$

* Electronic address: koen.vandewal@uhasselt.be

¹ B. C. Thompson and J. M. J. Fréchet, *Angew. Chem. Int. Ed.* **47**, 58 (2008).

- ² G. Denmler, M. C. Scharber, and C. J. Brabec, *Adv. Mater.* **21**, 1323 (2009).
- ³ S. H. Park, A. Roy, S. Beaupré, S. Cho, N. Coates, J. S. Moon, D. Moses, M. Leclerc, K. Lee, and A. J. Heeger, *Nature Phot.* **3**, 297 (2009).
- ⁴ M. C. Scharber, D. Mühlbacher, M. Koppe, P. Denk, C. Waldauf, A. J. Heeger, and C. J. Brabec, *Adv. Mater.* **18**, 789 (2006).
- ⁵ A. Gadisa, M. Svensson, M. R. Andersson, and O. Inganäs, *Appl. Phys. Lett.* **84**, 1609 (2004).
- ⁶ V. D. Mihailetschi, P. W. M. Blom, J. C. Hummelen, and M. T. Rispen, *J. Appl. Phys.* **94**, 6849 (2003).
- ⁷ B. P. Rand, D. P. Burk, and S. R. Forrest, *Phys. Rev. B.* **75**, 115327 (2007).
- ⁸ K. Vandewal, K. Tvingstedt, A. Gadisa, O. Inganäs, and J. V. Manca, *Nature Mater.* **8**, 904 (2009).
- ⁹ W. Shockley and H. Queisser, *J. Appl. Phys.* **32**, 510 (1961).
- ¹⁰ U. Rau, *Phys. Rev. B* **76**, 085303 (2007).
- ¹¹ L. Goris, A. Poruba, L. Hod'áková, M. Vanecek, K. Haenen, M. Nesladek, P. Wagner, D. Vanderzande, L. D. Schepper, and J. V. Manca, *Appl. Phys. Lett.* **88**, 052113 (2006).
- ¹² J. J. Benson-Smith, L. Goris, K. Vandewal, K. Haenen, J. V. Manca, D. Vanderzande, D. D. C. Bradley, and J. Nelson, *Adv. Funct. Mater.* **17**, 451 (2007).
- ¹³ M. A. Loi, S. Toffanin, M. Muccini, M. Forster, U. Scherf, and M. Scharber, *Adv. Funct. Mater.* **17**, 2111 (2007).
- ¹⁴ M. Hallermann, S. Haneder, and E. D. Como, *Appl. Phys. Lett.* **93**, 053307 (2008).
- ¹⁵ T. Drori, C. X. Sheng, A. Ndobe, S. Singh, J. Holt, and Z. V. Vardeny, *Phys. Rev. Lett.* **101**, 037401 (2008).
- ¹⁶ K. Vandewal, A. Gadisa, W. D. Oosterbaan, S. Bertho, F. Banishoeb, I. V. Severin, L. Lutsen, T. J. Cleij, D. Vanderzande, and J. V. Manca, *Adv. Funct. Mater.* **18**, 2064 (2008).
- ¹⁷ D. Veldman, O. Ipek, S. C. J. Meskers, J. Sweelssen, M. M. Koetse, S. C. Veenstra, J. M. Kroon, S. S. van Bavel, J. Loos, and R. A. J. Janssen, *J. Am. Chem. Soc.* **130**, 7721 (2008).
- ¹⁸ Y. Zhou, K. Tvingstedt, F. Zhang, C. Du, W.-X. Ni, M. R. Andersson, and O. Inganäs, *Adv. Funct. Mater.* **19**, 3293 (2009).
- ¹⁹ K. Tvingstedt, K. Vandewal, A. Gadisa, F. Zhang, J. V. Manca, and O. Inganäs, *J. Am. Chem. Soc.* **131**, 11819 (2009).
- ²⁰ D. Veldman, S. C. J. Meskers, and R. A. J. Janssen, *Adv. Funct. Mater.* **19**, 1939 (2009).
- ²¹ P. Panda, D. Veldman, J. Sweelssen, J. J. A. M. Bastiaansen, B. M. W. Langeveld-Voss, and S. C. J. Meskers, *J. Phys. Chem. B* **111**, 5076 (2007).
- ²² M. D. Perez, C. Borek, S. R. Forrest, and M. E. Thompson, *J. Am. Chem. Soc.* **131**, 9281 (2009).
- ²³ W. J. Potscavage, A. Sharma, and B. Kippelen, *Acc. Chem. Res. Articles* **ASAP** (2009).
- ²⁴ V. Dyakonov, *Appl. Phys. A* **79**, 21 (2004).
- ²⁵ R. A. Marcus, *J. Phys. Chem.* **93**, 3078 (1989).
- ²⁶ I. R. Gould, D. Noukakis, L. Gomez-Jahn, R. H. Young, J. L. Goodman, and S. Farid, *Chem. Phys.* **176**, 439 (1993).
- ²⁷ L. Goris, K. Haenen, M. Nesladek, P. Wagner, D. Vanderzande, L. D. Schepper, J. D'Haen, L. Lutsen, and J. V. Manca, *J. Mat. Sci.* **40**, 1413 (2005).
- ²⁸ C. Waldauf, M. C. Scharber, P. Schilinsky, J. A. Hauch, and C. J. Brabec, *J. Appl. Phys.* **99**, 104503 (2006).
- ²⁹ W. J. Potscavage, S. Yoo, and B. Kippelen, *Appl. Phys. Lett.* **93**, 193308 (2008).
- ³⁰ K. Kanemoto, I. Akai, H. Hashimoto, T. Karasawa, N. Negishi, and Y. Aso, *phys. stat. sol. (c)* **6**, 193 (2009).
- ³¹ G. Wantz, L. Hirsch, N. Huby, L. Vignau, A. S. Barrère, and J. P. Parneix, *J. Appl. Phys.* **97**, 034505 (2005).
- ³² M. O. Osotov, V. V. Bruevich, and D. Y. Paraschuk, *J. Chem. Phys.* **131**, 094906 (2009).
- ³³ M. A. Green, *Prog. Photovolt: Res. Appl.* **11**, 333 (2003).

Paper E

The ultimate efficiency of organic donor/acceptor single junction solar cells

K. Vandewal, A. Gadisa, J. V. Manca, K. Tvingstedt, O. Inganäs, unpublished (2009)

The ultimate efficiency of organic donor/acceptor single junction solar cells

Koen Vandewal,* Abay Gadisa, and Jean V. Manca
 IMEC-IMOMEC, vzw and Institute for Materials Research,
 Hasselt University, Wetenschapspark 1, 3590 Diepenbeek (Belgium)

Kristofer Tvingstedt and Olle Inganäs
 Biomolecular and Organic Electronics, Center of Organic Electronics (COE),
 Department of Physics, Chemistry and Biology, Linköping University, 58183 Linköping (Sweden)
 (Dated: October 27, 2009)

In this work, upper limits are derived for the short-circuit current, open-circuit voltage (V_{oc}), fill factor and power conversion efficiency (η) for donor/acceptor based organic solar cells. In these devices, donor and acceptor material are weakly coupled, forming a weak ground-state charge transfer complex (CTC). The maximum value of V_{oc} in particular is strongly influenced by these donor/acceptor molecular interactions. The obtained maximum η value under standardized solar conditions is presented as a function of two parameters: The optical gap of the main absorber and a parameter related to properties of the donor/acceptor CTC. We compare the maximum obtainable photovoltaic parameters of the present state-of-the-art organic donor/acceptor solar cells with their inorganic counterparts and we indicate possible further improvement.

Solar cells based on organic materials attract considerable interest nowadays, because they have the potential to be a low cost source of renewable energy. For this type of solar cells, currently power conversion efficiencies (η) of about 5-6 % are reached.^{1,2} In order to evaluate the potential of this new technology, attempts have been made to derive upper limits of η . Current papers addressing this issue are based on empirical arguments in order to find reasonable values for the short-circuit current (J_{sc}), open-circuit voltage (V_{oc}) and fill factor (FF) in future technologies.³⁻⁵ This approach has provided useful guidelines in order to achieve high efficiency devices.

From a more fundamental scientific point of view, however, it is possible to derive absolute upper limits for the photovoltaic parameters, only based on thermodynamic considerations. For inorganic, single absorber materials, this was done by Shockley and Queisser in a seminal paper using the principle of detailed balance.⁶ Extensions of this theory link absorption and emission properties of the single junction solar cells to the current density - voltage (JV) curve in the dark and under solar illumination.^{7,8} A similar approach has been used previously to describe the JV curves under monochromatic illumination of a molecular photovoltaic device consisting of a two level system, taking into account electron transfer rates and interfacial recombination.⁹ Recently it was shown that experimentally obtained V_{oc} values of polymer:fullerene bulk heterojunction devices can be explained by such an approach,¹⁰ if it is taken into account that the donor polymer and acceptor fullerene interact in the ground state, forming a charge transfer complex (CTC).

In donor/acceptor combinations exhibiting good charge generation, the excited CTC or charge transfer (CT) state is the lowest energy excited state.^{5,11,12} In these blends, the CT state is mainly populated by the diffusion of photogenerated excitons to the interface. However, excitation of the CTCs by long wavelength photons, with energy lower than the optical gap of donor and acceptor material also results in the creation of CT excitons, as observed for polymer:fullerene blends by sensitive measurements of the absorption¹³ and photocurrent^{14,15} spectrum. Decay of the CT state can occur radiatively, as observed in photoluminescence^{16,17} and electroluminescence¹⁸ spectra. Such sub-gap CT optical transitions are not limited to the polymer:fullerene case but have also been detected to occur at interfaces between small molecules and the C_{60} fullerene¹⁹ and at the polymer/metal oxide²⁰ interfaces. We therefore assume that CTC formation, exhibiting subgap CT transitions, occurs at all donor/acceptor interfaces able to efficiently generate free charge carriers upon light absorption.

When the CT state is the lowest energy excited state, V_{oc} is determined by its properties.^{10,12,15,21} However the maximum obtainable J_{sc} is not determined by CT absorption, as it does not contribute significantly to sunlight absorption when the coupling between donor and acceptor is weak. The pure donor or acceptor phase remain the main light absorbers, of which the optical gap determines the maximum obtainable J_{sc} . In the future, organic photovoltaic devices with a strong donor/acceptor coupling may be fabricated. In that case the CT absorption will contribute significantly to light absorption, causing both the maximum V_{oc} and the maximum J_{sc} to be determined by E_{CT} . In this case the classical Shockley - Queisser limit with E_{CT} as optical gap can be used to calculate the maximum efficiency limits.

In this work however, we are interested in the case of weak coupling between donor and acceptor as it seems that it represents the majority of the present day high efficiency donor/acceptor solar cells. For deriving the upper limit of the photovoltaic parameters, the following assumptions are made:

- (i) Perfect absorption of photons with energy E larger than the bandgap E_g of the main absorbing component

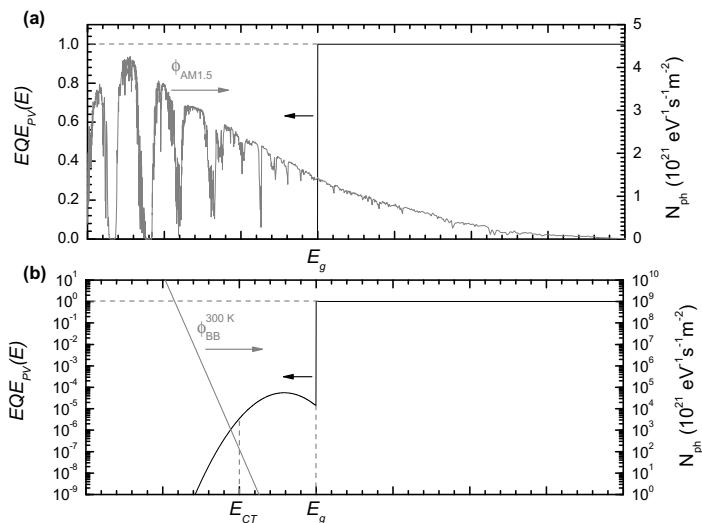


FIG. 1: The EQE_{PV} spectrum of an idealized organic donor/acceptor solar cell, shown on (a) a linear scale and (b) a logarithmic scale. To obtain $J_{sc,max}$, integrating of EQE_{PV} over the AM1.5 solar spectrum is performed. To obtain $J_{0,min}$, EQE_{PV} is integrated over the $\phi_{BB}^{300 \text{ K}}$ spectrum.

(donor or acceptor) with each photon creating exactly one electron-hole pair.

(ii) Perfect dissociation and collection of carriers, i.e perfect internal quantum efficiency. This requires complete absence of recombination of coulombically bound geminate charge pairs and mobility times lifetime products much larger than the device thickness.

(iii) Radiative, non-geminate, bimolecular recombination is the only allowed recombination mechanism. all non-radiative recombination mechanisms are absent. The radiative recombination sets an upper limit to the lifetime of the free charge carriers. If this radiative recombination is only a fraction of the total recombination, the efficiency is substantially reduced below the detailed balance limit.

Similar assumptions were recently made by Kirchartz et al.,²² in order to derive efficiency limits of organic bulk heterojunction solar cells. Their analysis however, includes only the case in which the energy of the CT state is very close to the optical gap of the main polymer absorber. In underlying work, we generalise this approach focussing in particular on the relevant case of weak donor/acceptor coupling and a quite large energy difference between the CT state and the optical gap of the main absorber. This analyses will result in a graph of the maximum efficiency as a function of two parameters: The optical gap of the main absorber and a parameter related to properties of the donor/acceptor CTC.

Figure 1 shows the photovoltaic external quantum efficiency EQE_{PV} spectrum of an ideal donor/acceptor based organic solar cell, fulfilling assumptions (i)-(iii). Assumption (i) and (ii) assume that EQE_{PV} for photon energies higher than E_g equals unity. A weak, sub- E_g band is always present, due to the formation of donor/acceptor CTCs. properties of the CT band can be measured by using highly sensitive techniques to measure the EQE_{PV} spectrum, such as Fourier-Transform Photocurrent Spectroscopy (FTPS).²³ The low energy part of the EQE_{PV} spectrum, for $E < E_g$, dominated by the CT band, can be described by²³⁻²⁵:

$$EQE_{PV} = \frac{f}{E\sqrt{4\pi\lambda kT}} \exp\left(\frac{(E_{CT} + \lambda - E)^2}{4\lambda kT}\right) \quad (1)$$

Hereby is E_{CT} the energy of the CT state, λ the reorganisation energy of the CT optical transition and f is proportional to the electronic coupling between donor and acceptor and the interfacial area present in the donor/acceptor device.²³

When donor and acceptor are weakly coupled, and f is low, the contribution of this CT band to the photocurrent, however, is negligible and thus is the maximum obtainable short-circuit current $J_{sc,max}$ for organic donor/acceptor solar cells a function of E_g only, and given by

$$J_{sc,max} = q \int_{E_g}^{+\infty} \phi_{AM1.5}(E) dE \quad (2)$$

For deriving an upper limit for V_{oc} , we must take into account the weak CT absorption, which determines the dark saturation current.¹⁰ The maximum open-circuit voltage $V_{oc,max}$ is obtained if the dark saturation current has its lowest value $J_{0,min}$.^{6,8}

$$V_{oc} = \frac{kT}{q} \ln \left(\frac{J_{sc}}{J_{0,min}} \right) \quad (3)$$

Hereby is $J_{0,min}$ given by:^{6,8}

$$J_{0,min} = q \int \phi_{BB}^T EQE_{PV}(E) dE \quad (4)$$

With ϕ_{BB}^T the black body spectrum at an absolute temperature T . ϕ_{BB}^T is shown in figure 1 and given by:

$$\phi_{BB}^T = \frac{2\pi E^2}{h^3 c^2} \frac{1}{\exp\left(\frac{E}{kT}\right) - 1} \quad (5)$$

Assuming an EQE_{PV} spectrum as in figure 1 with the CT band described by equation (1), an expression for $V_{oc,max}$ in function of the interfacial molecular parameters can be deduced²³. Using equation (3)-(5), we obtain a maximum obtainable open-circuit voltage $V_{oc,max}^{CT}$ for donor/acceptor solar cells:

$$V_{oc,max}^{CT} = \frac{E_{CT}}{q} + \frac{kT}{q} \ln \left(\frac{J_{sc,max}^{SQ} h^3 c^2}{2\pi q f (E_{CT} - \lambda)} \right) \quad (6)$$

In the original Shockley-Queisser paper, $J_{sc,max}$ as well as $V_{oc,max}$ are related only to the E_g of the main absorbing material. Using equation (3)-(5), for a material with a single bandgap E_g , the maximum obtainable open-circuit voltage in the Shockley-Queisser limit $V_{oc,max}^{SQ}$ equals^{6,26}:

$$V_{oc,max}^{SQ} = \frac{E_g}{q} + \frac{kT}{q} \ln \left(\frac{J_{sc,max}^{SQ} h^3 c^2}{2\pi q k T E_g^2} \right) \quad (7)$$

$V_{oc,max}^{CT}$ will always be lower than $V_{oc,max}^{SQ}$, with a difference Δ/q between them.

$$V_{oc,max}^{CT} = V_{oc,max}^{SQ} - \frac{\Delta}{q} \quad (8)$$

Δ can be calculated from (7) and (6).

$$\Delta = E_g - E_{CT} - kT \ln \left(\frac{k T E_g^2}{f (E_{CT} - \lambda)} \right) \quad (9)$$

Δ can be lowered by choosing a donor/acceptor combination for which E_{CT} is close to E_g and/or for which the donor/acceptor CT optical transition has a low oscillator strength, or low interfacial area, resulting in a low f . Note

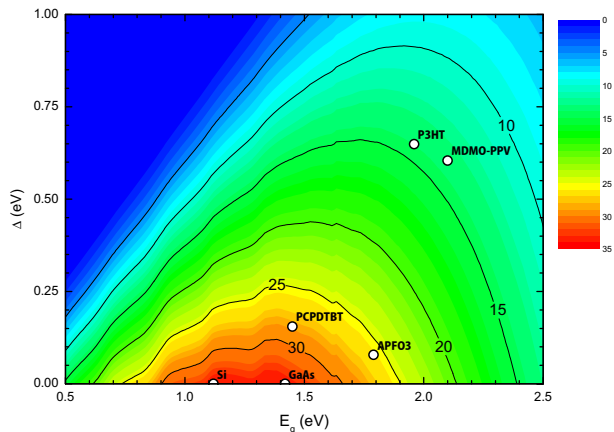


FIG. 2: η_{max} in function of E_g and Δ , calculated as indicated in the text. In the figure, some organic donor/acceptor as well as some inorganic solar cells are indicated.

that, because of the \ln function, f needs to be varied over at least one decade to see a substantial effect on Δ . For the same reason will changes in λ not affect Δ very much.

We are now able to calculate the maximum obtainable power conversion efficiency η_{max} for organic donor/acceptor solar cells in function of E_g and the CTC properties reflected in the parameter Δ . The calculation was performed for an AM1.5 incident spectrum with the device at a temperature of 300 K. It proceeds as follows: The value of E_g determines $J_{sc,max}$, which is calculated from equation (2). Once $J_{sc,max}$ is known, it can be used together with E_g and Δ to calculate $V_{oc,max}^{CT}$, using equation (7) and (8). If the only allowed recombination mechanism is the radiative recombination, it can be shown that the dark JV curve obeys the ideal diode equation.⁶ The JV curve under solar illumination of the idealized solar cell is than given by:

$$J(V) = J_{0,min} \left(\exp\left(\frac{qV}{kT}\right) - 1 \right) - J_{sc,max} \quad (10)$$

The knowledge of both $J_{sc,max}$ and $V_{oc,max}$ allows the calculation of $J_{0,min}$ via (3). Knowledge of the analytical expression of the JV curve allows the calculation of the fill factor FF , as presented in ref⁶ and eventually leads to the knowledge of the maximum efficiency η . This results in figure 2, giving η in function of E_g and Δ .

This graph allows us to evaluate the potential energy conversion efficiency for organic donor/acceptor solar cells and compare it to inorganic technologies, as the X-axis ($\Delta = 0$) in this figure represents the original Shockley-Queisser efficiency limit for inorganic solar cells. To indicate the evolution in the polymer:fullerene composite solar cell research, examples of well known material systems are shown in table I. The optical gap E_g of several polymer:fullerene composite devices, together with the interfacial properties E_{CT} and f , as determined by FTPS²³ and the resulting Δ are summarized in table I. The bandgap E_g of crystalline Si and GaAs solar cells are also given in I.

The maximum obtainable photovoltaic parameters of the devices in table I are summarized in table II, together with the obtained parameters of the best performing devices for each material system.

One of the first successful solution processable polymer:fullerene composite devices is the MDMO-PPV:PCBM material system.²⁷ In figure 1 it can be seen that this material system is limited by its high E_g and high Δ . The P3HT:PCBM material system²⁸ has only a slightly lower E_g but still suffers from a high Δ . However, in reality, higher efficiency is obtained for this system because higher FF and EQE_{PV} values of 70-80 % could be reached, due to the

TABLE I: material parameters for some organic and inorganic solar cells. E_{CT} and f are determined by FTPS.

	E_g (eV)	E_{CT} (eV)	f ((eV) ²)	Δ (eV)
MDMO-PPV:PCBM ^a	2.10	1.42	7E-3	0.60
P3HT:PCBM ^a	1.96	1.14	1E-4	0.65
APFO3:PCBM ^a	1.79	1.64	7E-3	0.08
PCPDTBT:PC ₇₀ BM ^b	1.45	1.25	1E-2	0.16
Si ^c	1.12	-	-	0
GaAs ^c	1.42	-	-	0

^aFTPS spectra are shown in²³. f was determined from these spectra after normalization of the EQE_{PV} above the bandgap.

^b f and E_{CT} were determined for PCPDTBT:PC₆₀BM¹⁰, and assumed to be the same for PCPDTBT:PC₇₀BM

^c E_g from²⁶

TABLE II: The currently obtained and maximum values of photovoltaic parameters for some organic and inorganic solar cells. The ratio between the obtained and maximum values is shown in brackets.

	η^{max} (%)	V_{oc}^{max} (V)	J_{sc}^{max} (A.m ⁻²)	FF^{max}	η (%)	V_{oc} (V)	J_{sc} (A.m ⁻²)	FF
MDMO-PPV:PCBM ^a	13.5	1.19	126	0.90	2.5	0.82 (0.69)	66 (0.52)	0.61 (0.68)
P3HT:PCBM ^b	14.0	1.01	156	0.89	5.1	0.63 (0.62)	119 (0.76)	0.68 (0.76)
APFO3:PCBM ^c	26.0	1.42	200	0.91	3.4	1.03 (0.73)	58 (0.29)	0.58 (0.64)
PCPDTBT:PC ₇₀ BM ^d	28.1	1.03	307	0.89	5.5	0.62 (0.60)	161 (0.52)	0.55 (0.62)
Si ^e	33.6	0.884	437	0.87	25.0	0.71 (0.80)	427 (0.98)	0.83 (0.95)
GaAs ^e	33.3	1.16	319	0.90	26.1	1.04 (0.88)	297 (0.93)	0.85 (0.94)

^aFrom²⁷. The illumination was an AM1.5 spectrum at 80 W.cm⁻². In the table the current is scaled linearly for 100 W.cm⁻²

^bFrom²⁸. The illumination was an AM1.5 spectrum at 80 W.cm⁻². In the table the current is scaled linearly for 100 W.cm⁻²

^cMultilayer device from²⁹. AM1.5 at 100 W.cm⁻²

^dFrom³⁰, AM1.5 at 100 W.cm⁻²

^e31

higher mobility and less geminate recombination as compared to the MDMO-PPV based system. A material with similar E_g as P3HT but with a much lower Δ is the APFO3:PCBM²⁹ material system. In this system there is only a difference of 0.15 eV between E_g and E_{CT} . With an f of 1E-2 this results in a low Δ of 0.08 eV. This causes η_{max} to increase strongly as compared to the previous systems. Most promising is the PCPDTBT:PC₇₀BM material system of which both E_g and Δ are low, resulting in an η_{max} of 28.1 %. Unfortunately the effectively obtained EQE_{PV} and FF in real devices are not so high as for the intensively investigated P3HT:PCBM system. For that material system about 76 % of the maximum J_{sc} , 76 % of the maximum FF and 62 % of the maximum V_{oc} has been reached. If these values can be reached for the PCPDTBT material system, 9-10 % of power conversion efficiency is within reach.

In table II the photovoltaic parameters as calculated by the SQ theory for the inorganic materials Si and GaAs are also shown. In the more than 50 years of research the performance of these crystalline solar cells is getting closer and closer to their predicted maximum. The FF and J_{sc} are above 90 % and the V_{oc} around 80% of their predicted maximum value.

Recently it has been shown that for some bulk heterojunction solar cells comprising new conjugated polymers blended with fullerenes, it is possible to have very efficient charge carrier generation with and absorbed photon to electron conversion efficiency of nearly 100 %. This resulted in power conversion efficiencies higher than 6%.¹ For these material systems EQE_{PV} values of 70-80% in the range of polymer absorption are obtained. Further increase of this efficiency is in principle possible through optimization of V_{oc} and FF , as they are still far from their maximum value, for the examples shown in this work. The presence of additional, non-radiative recombination paths will make $EQE_{EL} < 1$ in practical devices and will reduce V_{oc} , according to^{8,22,23}

$$V_{oc} = V_{oc, max}^{SQ} + \frac{kT}{q} \ln(EQE_{EL}) \quad (11)$$

For the best inorganic solar cells EQE_{EL} is in the order of 1E-3.²⁶ For polymer:fullerene devices, however the EQE_{EL} of CT emission is in the order of 1E-9 - 1E-6.^{10,23} There might be a fundamental reason, causing non-radiative recombination always to be present. For the inorganic devices, Auger recombination is suggested to be such a mechanism.³² For the organic donor/acceptor photovoltaic devices, identification and possible removal of the dominating non-radiative recombination pathways deserves high attention in the following years.

In conclusion we have determined the upper limit for the photovoltaic parameters of organic donor/acceptor solar cells in a general framework, taking into account weak donor/acceptor material interaction. While the maximum obtainable short-circuit current $J_{sc,max}$ is determined by the bandgap E_g of the main absorber, the maximum obtainable open-circuit voltage $V_{oc,max}$ also depends on the properties of ground-state CTC formed between donor and acceptor, summarized in a parameter Δ . Increasing the energy of the CT state E_{CT} or decreasing the total amount of CT absorption will increase the maximum obtainable $V_{oc,max}$. The latter can be achieved by decreasing the donor/acceptor coupling or by reducing the interfacial area where material interaction occurs. These conditions for a high $V_{oc,max}$ oppose those for a high J_{sc} . Therefore, the preparation of donor/acceptor interfaces fulfilling these properties, while maintaining a high free carrier generation rate, might be a challenge.

Acknowledgments

We acknowledge the institute for the promotion of science and technology in Flanders (IWT-Vlaanderen), the IWT-project polyspec, the FWO project nano-fibres and the Swedish Energy Agency for funding through the program Tandem.

* Electronic address: Koen.Vandewal@Uhasselt.be

- ¹ S. H. Park, A. Roy, S. Beaupré, S. Cho, N. Coates, J. S. Moon, D. Moses, M. Leclerc, K. Lee, and A. J. Heeger, *Nature Photonics* **3**, 297 (2009).
- ² J. Hou, H.-Y. Chen, S. Zhang, R. I. Chen, Y. Yang, Y. Wu, and G. Li, *J. Am. Chem. Soc.* **ASAP**, (2009).
- ³ M. C. Scharber, D. Mhlbacher, M. Koppe, P. Denk, C. Waldauf, A. J. Heeger, and C. J. Brabec, *Adv. Mater.* **18**, 789 (2006).
- ⁴ G. Dennler, M. C. Scharber, and C. J. Brabec, *Adv. Mater.* **21**, 1323 (2009).
- ⁵ D. Veldman, S. C. J. Meskers, and R. A. J. Janssen, *Adv. Funct. Mater.* **19**, 1939 (2009).
- ⁶ W. Shockley and H. Queisser, *J. Appl. Phys.* **32**, 510 (1961).
- ⁷ P. Würfel, *J. Phys. C: Solid State Phys.* **15**, 3967 (1982).
- ⁸ U. Rau, *Phys. Rev. B* **76**, 085303 (2007).
- ⁹ J. Nelson, J. Kirkpatrick, and P. Ravirajan, *Phys. Rev. B* **69**, 035337 (2004).
- ¹⁰ K. Vandewal, K. Tvingstedt, A. Gadisa, O. Inganas, and J. V. Manca, *Nature Mater.* **8**, 904 (2009).
- ¹¹ J. J. Benson-Smith, L. Goris, K. Vandewal, K. Haenen, J. V. Manca, D. Vanderzande, D. D. C. Bradley, and J. Nelson, *Adv. Funct. Mater.* **17**, 451 (2007).
- ¹² D. Veldman, O. Ipek, S. C. J. Meskers, J. Sweelssen, M. M. Koetse, S. C. Veenstra, J. M. Kroon, S. S. van Bavel, J. Loos, and R. A. J. Janssen, *J. Am. Chem. Soc.* **130**, 7721 (2008).
- ¹³ L. Goris, K. Haenen, M. Nesladek, P. Wagner, D. Vanderzande, L. D. Schepper, J. D'Haen, L. Lutsen, and J. V. Manca, *J. Mat. Sci.* **40**, 1413 (2005).
- ¹⁴ L. Goris, A. Poruba, L. Hod'áková, M. Vanecek, K. Haenen, M. Nesladek, P. Wagner, D. Vanderzande, L. D. Schepper, and J. V. Manca, *Appl. Phys. Lett.* **88**, 052113 (2006).
- ¹⁵ K. Vandewal, A. Gadisa, W. D. Oosterbaan, S. Bertho, F. Banishoeib, I. V. Severen, L. Lutsen, T. J. Cleij, D. Vanderzande, and J. V. Manca, *Adv. Funct. Mater.* **18**, 2064 (2008).
- ¹⁶ M. A. Loi, S. Toffanin, M. Muccini, M. Forster, U. Scherf, and M. Scharber, *Adv. Funct. Mater.* **17**, 2111 (2007).
- ¹⁷ M. Hallermann, S. Haneder, and E. D. Como, *Appl. Phys. Lett.* **93**, 053307 (2008).
- ¹⁸ K. Tvingstedt, K. V. J. V. Manca, and O. Inganas, *J. Am. Chem. Soc.* **131**, 11819 (2009).
- ¹⁹ G. Ruani, C. Fontanini, M. Murgia, and C. Taliani, *J. Chem. Phys.* **116**, 1713 (2002).
- ²⁰ I. Haelderms, K. Vandewal, W. D. Oosterbaan, A. Gadisa, J. D'Haen, M. K. V. Bael, J. V. Manca, and J. Mullens, *Appl. Phys. Lett.* **93**, 223302 (2008).
- ²¹ W. J. Potscavage, S. Yoo, and B. Kippelen, *Appl. Phys. Lett.* **93**, 193308 (2008).
- ²² T. Kirchartz, K. Taretto, and U. Rau, *J. Phys. Chem. C* **113**, 17958 (2009).
- ²³ K. Vandewal, K. Tvingstedt, A. Gadisa, O. Inganas, and J. V. Manca, *Phys. Rev. B* **submitted** (2009).
- ²⁴ R. A. Marcus, *J. Phys. Chem.* **93**, 3078 (1989).
- ²⁵ I. R. Gould, D. Noukakis, L. Gomez-Jahn, R. H. Young, J. L. Goodman, and S. Farid, *Chem. Phys.* **176**, 439 (1993).
- ²⁶ M. A. Green, *Prog. Photovolt: Res. Appl.* **11**, 333 (2003).
- ²⁷ S. E. Shaheen, C. J. Brabec, N. S. Sariciftci, F. Padinger, T. Fromherz, and J. C. Hummelen, *Appl. Phys. Lett.* **78**, 841 (2001).
- ²⁸ W. L. Ma, C. Y. Yang, X. Gong, K. Lee, and A. J. Heeger, *Adv. Funct. Mater.* **15**, 1617 (2005).
- ²⁹ C. M. B. Svanstrom, J. Rysz, A. Bernasik, A. Budkowski, F. Zhang, O. Inganas, M. R. Andersson, K. O. Magnusson, J. J. Benson-Smith, J. Nelson, et al., *Adv. Mater.* **21**, (2009).
- ³⁰ J. Peet, J. Y. Kim, N. E. Coates, W. L. Ma, D. Moses, A. J. Heeger, and G. C. Bazan, *Nat. Mater.* **6**, 497 (2007).
- ³¹ M. A. Green, K. Emery, Y. Hishikawa, and W. Warta, *Prog. Photovolt: Res. Appl.* **17**, 85 (2009).
- ³² M. A. Green, *IEEE transactions on electron devices* **31**, 671 (1984).

Paper F

Varying polymer crystallinity in nanofiber poly(3-alkylthiophene):PCBM solar cells: Influence on charge transfer state energy and open-circuit voltage

K. Vandewal, W. D. Oosterbaan, S. Bertho, V. Vrindts, A. Gadisa, L. Lutsen, D. Vanderzande J. V. Manca, *Appl. Phys. Lett.* **95**, 123303 (2009)

Varying polymer crystallinity in nanofiber poly(3-alkylthiophene): PCBM solar cells: Influence on charge-transfer state energy and open-circuit voltage

Koen Vandewal,^{a1} Wibren D. Oosterbaan, Sabine Bertho, Veerle Vrindts, Abay Gadisa, Laurence Lutsen, Dirk Vanderzande, and Jean V. Manca
Institute for Materials Research, Hasselt University, Wetenschapspark 1, 3590 Diepenbeek, Belgium and IMEC-IMOMECE, vzw Wetenschapspark 1, 3590 Diepenbeek, Belgium

(Received 23 July 2009; accepted 28 August 2009; published online xx xx xxxx)

The effect of poly(3-alkylthiophene) (P3AT) crystallinity in (nanofiber P3AT):PCBM photovoltaic devices on the energy of the charge-transfer state (E_{CT}) and on the open-circuit voltage (V_{oc}) is investigated for poly(3-butythiophene), poly(3-pentylthiophene) and poly(3-hexylthiophene). P3AT crystallinity, expressed as the crystalline nanofiber mass fraction f to the total P3AT mass in the spin-coating dispersion, is varied between ~ 0.1 and ~ 0.9 by temperature control. E_{CT} , as obtained by Fourier-transform photocurrent spectroscopy decreased with f as $E_{CT} = E_{CT}^0 - 0.2f$ eV. Alkyl side-chain length only influences E_{CT}^0 . V_{oc} relates to E_{CT} as $V_{oc} = E_{CT}/q - 0.6$ V. © 2009 American Institute of Physics. [doi:10.1063/1.3232242]

Their potential in low cost and flexible photovoltaics makes polymer:fullerene bulk heterojunction (BHJ) solar cells currently a topic of extensive research.¹ Promising power conversion efficiencies of 5% were achieved for material blends of regioregular poly(3-hexylthiophene) (P3HT) with [6,6]-phenyl-C₆₁ butyric acid methyl ester (PCBM).² In optimal devices, the presence of crystalline P3HT domains in the material blend is crucial. The crystallization of P3HT results in an increase in photon absorption, a decrease in polymer bandgap and a higher mobility, resulting in an increase in the short-circuit current and fill factor.^{3,4} The use of other regioregular poly(3-alkylthiophene)s (P3ATs), such as poly(3-butythiophene) (P3BT) and poly(3-pentylthiophene) (P3PT) for BHJ solar cells has been less studied. However, when blending these materials with PCBM, devices with efficiencies comparable to that of P3HT can be fabricated.⁵

The crystallization and resulting crystal quality of P3ATs in the blends is commonly enhanced by slow drying after solution deposition and/or by thermal post-treatment. An attractive alternative that avoids a thermal treatment step is casting of a dispersion of preformed highly crystalline P3AT nanofibers that contains well-dissolved PCBM.⁶ Efficiencies obtained for photovoltaic devices obtained in this way are in the 3%–4% range.^{6–8} The use of nanofiber dispersions, moreover, allows to adjust the mass fraction f of well-defined highly crystalline polymer to the total polymer content by means of temperature control.⁸ This in turn allows for a systematic study of the influence of this highly crystalline P3AT fraction on the photovoltaic parameters. This paper in particular will focus on the effect of f on the energy of the interfacial charge-transfer (CT) state (E_{CT}) and the open-circuit voltage (V_{oc}) of photovoltaic devices based on blends of PCBM with P3BT, P3PT, and P3HT.

The V_{oc} 's reported for P3AT:PCBM devices are usually in the range of 0.5–0.65 V.^{2,4–8} It has been shown that several factors affect V_{oc} . For example, a variation of more than 0.5 V was observed by varying the negative electrode work

function.^{9,10} The highest V_{oc} , however is reached using Ohmic contacts. In the latter case, V_{oc} relates to the effective bandgap of the material blend.^{11,12} Recently, it was argued^{13–15} that this effective bandgap relates to the excited state energy E_{CT} of the intermolecular CT complexes present in BHJ photovoltaic devices. We have shown¹⁵ that E_{CT} can be measured directly on BHJ devices as the onset of the weak CT absorption band, present in the external quantum efficiency (EQE) spectrum. Fourier-transform photocurrent spectroscopy (FTPS) made it possible to measure the EQE spectrum over several decades and resolve these weak CT transitions for several polymer:PCBM BHJ devices. We have found a linear correlation between E_{CT} , measured as such, and V_{oc} .¹³

In this paper we will describe the influence of P3AT crystallinity on E_{CT} and V_{oc} of blends comprising PCBM molecules dispersed in a P3AT matrix. P3BT, P3PT and P3HT were prepared by the Rieke method¹⁶ as described in Ref. 17. The polymers have similar molecular weights and regioregularities. We obtained M_n values [polydispersities] for P3BT, P3PT, and P3HT of 19.5 [2.29], 16.7 [1.93], and 23.7 kg mol⁻¹ [1.80], respectively, as measured with GPC in chlorobenzene versus polystyrene standards at 60 °C.¹⁷ The regioregularities of P3BT, P3PT, and P3HT are 96.5%, 94.5%, and 94.5%, respectively, as determined with ¹H-NMR spectroscopy.¹⁷ P3AT nanofibers were prepared by slow cooling of P3AT solutions in bad solvents.¹⁷ We used *o*-chlorotoluene for P3BT, and *p*-xylene for P3PT and P3HT. The high fiber fraction of 0.90 for P3HT was obtained in *cis/trans*-decalin. For the preparation of the photovoltaic devices, PCBM was dissolved in the fiber dispersions in a 1:1 wt ratio for all polymers by stirring at room temperature for 24 h. The fiber mass fraction f , defined by the weight of the nanofibers to the total polymer weight, was varied between 0.1 and 0.9 via temperature control of the fiber dispersion between 35 and 55 °C and was determined by UV-Vis spectroscopy in solution following the procedure described in Ref. 8. As PCBM inhibits P3AT crystallization during spin coating,^{4,18} and neither thermal annealing nor slow drying was applied, f of the solid-state spin-coated films was ap-

^{a1}Electronic mail: koen.vandewal@uhasselt.be.

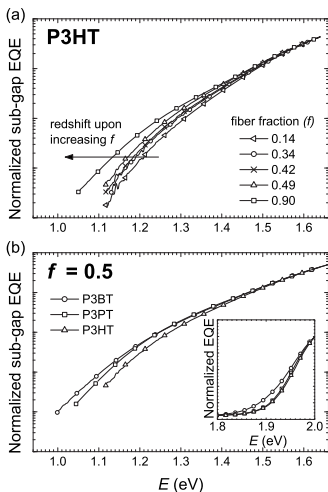


FIG. 1. (a) Normalized (at 1.64 eV) EQE spectra measured by FTPS in the subgap region of (nanofiber P3HT):PCBM photovoltaic devices with a defined P3HT nanofiber to total polymer fraction f . Upon increasing the fiber fraction, the CT absorption band redshifts. (b) Normalized EQE spectra measured by FTPS in the subgap region of photovoltaic devices based on P3BT, P3PT, and P3HT mixed with PCBM in a 1:1 ratio. The fiber fraction f for all three polythiophenes was ~ 0.50 . A decrease in side-chain length results in a slight redshift of the CT band.

proximated by f , as determined in dispersion. Device preparation was done using the standard procedure and is described elsewhere.⁸ As top negative electrode, Ca capped with Al was used. It has been shown that this top electrode is one of the best performing and stable top electrodes.¹⁰ The current-voltage curves in the dark and under solar illumination as well as the EQE spectra by FTPS were measured in N_2 atmosphere. The overall efficiency under solar conditions of the studied devices ranges between 0.5% and 3%. Detailed results about morphology and device parameters other than V_{oc} are described elsewhere.⁸

FTPS was used to spectrally resolve the low energy part of the EQE spectra of P3AT:PCBM photovoltaic devices. Using this technique, the CT absorption band is clearly visible in the range from ~ 1 to 1.7 eV. Upon increasing the fiber fraction from ~ 0.1 to ~ 0.9 , a redshift of the CT band is observed for all polymers. This is illustrated for P3HT in Fig. 1. The CT transition is accompanied by the promotion of an electron from the HOMO of P3AT to the LUMO of PCBM.¹⁹ Since the aggregation of P3HT into fibers increases the polymer's HOMO level (In the case of annealing P3HT:PCBM blends at 80 °C, a positive shift of the oxidation potential of P3HT of about 0.2 V has been measured²⁰), we attribute this redshift to the increase in the fraction of highly crystalline nanofibrillar P3AT. A small contribution due to an effect of the variation in temperature of the casting dispersion on the final size of the PCBM aggregates in the blend, and their LUMO, can however not be completely excluded.

Figure 1(b) shows spectra of P3BT, P3PT, and P3HT for a fixed fiber fraction of ~ 0.50 . It can be seen that, with decreasing P3AT alkyl side-chain length, the CT band slightly shifts to lower energies. As observed from the inset

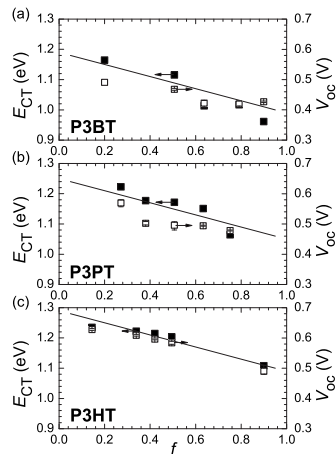


FIG. 2. The dependence of E_{CT} (■) and V_{oc} (□) on the mass fraction f of P3AT aggregated into nanofibers for P3AT:PCBM (1:1) photovoltaic devices with (a) P3BT, (b) P3PT, and (c) P3HT. The line has a slope of 0.2 eV (see text).

of Fig. 1(b), the onset of P3AT absorption around 1.9 eV also redshifts with decreasing side chain length. Therefore, we conclude that also the use of shorter side chains causes the P3AT HOMO level to shift slightly closer to the LUMO level of PCBM. Values for E_{CT} can be determined from the FTPS spectra by fitting the low energy part of the CT band with the following function, which can be used to extract CT properties from CT absorption bands:²¹

$$EQE(E) \propto \frac{1}{E} \exp \left[\frac{(E_{CT} + \lambda - E)^2}{4\lambda kT} \right].$$

Here, T is the temperature, k is the Boltzmann's constant, and λ is the reorganization energy related to the initial relaxation of the system after excitation of the CT complex. For the systems investigated in this work, we find λ in the range of 0.2–0.3 eV. Note that the above determination of E_{CT} is different than the one we used in previous work,¹³ where we used an empirical definition. However we believe that the definition of E_{CT} used in this work is more useful as it relates to Marcus theory.²² E_{CT} in this work is about 0.2 eV higher than it would be when using the definition in Ref. 13.

In previous work it was shown that the onset of the CT band relates to the V_{oc} of the photovoltaic device.^{13–15} Figure 2 shows E_{CT} and V_{oc} for the P3AT:PCBM blends with different fiber mass fractions. It confirms that V_{oc} follows the same trend as E_{CT} . For P3PT and P3HT in particular, a decrease in several tens of millivolts of E_{CT} , results in a decrease in the same magnitude of V_{oc} . For the three material systems, there is a difference between qV_{oc} and E_{CT} of about 0.6 eV. V_{oc} is mainly determined by E_{CT} but other factors, such as the electronic contacts can also have an influence. This correlation however, indicates that the widely observed voltage drop induced by thermal annealing²³ or slow drying²⁴ originates from the lowering of the energy of the CT state due to the increased crystallinity of the P3AT. Furthermore, for all three P3AT:PCBM blends, we find the empirical

relation $E_{CT} = E_{CT}^0 - 0.2f$ eV. For E_{CT}^0 a slight increase with increasing side-chain length is observed, from 1.19 to 1.25 to 1.29 eV for P3BT to P3PT to P3HT.

In conclusion, a detailed investigation of the energy of the intermolecular CT states (E_{CT}) of poly(3-alkylthiophene):PCBM photovoltaic devices was performed by FTPS. Upon variation of the fiber mass fraction f of poly(3-butylthiophene), poly(3-pentylthiophene) and poly(3-hexylthiophene) it was observed that in the range $0.1 < f < 0.9$, E_{CT} decreases linearly with increasing f , as $E_{CT} = E_{CT}^0 - 0.2f$ eV. Moreover, E_{CT} increases slightly with increasing side-chain length. For all investigated devices we observed that the open-circuit voltage (V_{oc}) follows the same trend as E_{CT} . As E_{CT} is defined by interfacial CT states, morphological changes affecting these interface states will have a direct influence on V_{oc} .

We acknowledge the institute for the promotion of science and technology in Flanders (IWT-Vlaanderen) for funding via the IWT-SBO project polyspec (060843) and the FWO project nanofibers (G039608N).

- ¹B. C. Thompson and J. M. J. Fréchet, *Angew. Chem., Int. Ed.* **47**, 58 (2008).
- ²W. Ma, C. Yang, X. Gong, K. Lee, and A. J. Heeger, *Adv. Funct. Mater.* **15**, 1617 (2005).
- ³M. Campoy-Quiles, T. Ferenczi, T. A. Gostinelli, P. G. Etchegoin, Y. Kim, T. D. Anthopoulos, P. N. Stavrinou, D. D. C. Bradley, and J. Nelson, *Nature Mater.* **7**, 158 (2008).
- ⁴P. Vanlaeke, A. Swinnen, I. Haelderms, G. Vanhoyland, T. Aernouts, D. Cheyens, C. Deibel, J. D'Haen, P. Heremans, J. Poortmans, and J. V. Manca, *Sol. Energy Mater. Sol. Cells* **90**, 2150 (2006).
- ⁵A. Gadisa, W. D. Oosterbaan, K. Vandewal, J.-C. Bolsée, S. Bertho, J. D'Haen, L. Lutsen, D. Vanderzande, and J. V. Manca, "Effect of alkyl side-chain length on photovoltaic properties of Poly(3-alkylthiophene)/PCBM bulk heterojunctions," *Adv. Funct. Mater.* (to be published).
- ⁶S. Berson, R. De Bettignies, S. Bailly, and S. Guillerez, *Adv. Funct. Mater.* **17**, 1377 (2007).
- ⁷H. Xin, F. S. Xin, and S. A. Jenekhe, *J. Am. Chem. Soc.* **130**, 5424 (2008).
- ⁸S. Bertho, W. D. Oosterbaan, V. Vrindts, J. D'Haen, T. J. Cleij, L. Lutsen, J. Manca, and D. Vanderzande, *Org. Electron.* **10**, 1248 (2009).
- ⁹V. D. Mihailetschi, P. W. M. Blom, J. C. Hummelen, and M. T. Rispen, *J. Appl. Phys.* **94**, 6849 (2003).
- ¹⁰O. Reese, M. S. White, G. Rumbles, D. S. Ginley, and S. E. Shaheen, *Appl. Phys. Lett.* **92**, 053307 (2008).
- ¹¹V. Dyakonov, *Appl. Phys. A: Mater. Sci. Process.* **79**, 21 (2004).
- ¹²L. J. A. Koster, V. D. Mihailetschi, R. Ramaker, and P. W. M. Blom, *Appl. Phys. Lett.* **86**, 123509 (2005).
- ¹³K. Vandewal, A. Gadisa, W. D. Oosterbaan, S. Bertho, F. Banishoeib, I. Van Severen, L. Laurence, T. J. Cleij, D. Vanderzande, and J. V. Manca, *Adv. Funct. Mater.* **18**, 2064 (2008).
- ¹⁴D. Veldman, O. Ipek, S. C. J. Meskers, J. Sweelssen, M. M. Koets, S. C. Veenstra, J. M. Kroon, S. S. van Bavel, J. Loos, and R. A. J. Janssen, *J. Am. Chem. Soc.* **130**, 7721 (2008).
- ¹⁵D. Veldman, S. C. J. Meskers, and R. A. J. Janssen, *Adv. Funct. Mater.* **19**, 1939 (2009).
- ¹⁶T.-A. Chen, X. Wu, and R. D. Rieke, *J. Am. Chem. Soc.* **117**, 233 (1995).
- ¹⁷W. D. Oosterbaan, V. Vrindts, S. Berson, S. Guillerez, O. Douhéret, B. Ruttens, J. D'Haen, P. Adriaensens, J. Manca, L. Lutsen, and D. Vanderzande, *J. Mater. Chem.* **19**, 5424 (2009).
- ¹⁸J. Jo, S.-S. Kim, S.-I. Na, B.-K. Yu, and D.-Y. Kim, *Adv. Funct. Mater.* **19**, 866 (2009).
- ¹⁹M. Pope and C. E. Swenberg, *Electronic Processes in Organic Crystal and Polymers* (Oxford University Press, Oxford, 1998).
- ²⁰T. J. Savenije, J. E. Kroeze, X. Yang, and J. Loos, *Thin Solid Films* **511**, 2 (2006).
- ²¹I. R. Gould, D. Noukakis, L. Gomez-Jahn, R. H. Young, J. L. Goodman, and S. Farid, *Chem. Phys.* **176**, 439 (1993).
- ²²R. A. Marcus, *J. Phys. Chem.* **93**, 3078 (1989).
- ²³Y. Kim, S. A. Choulis, J. Nelson, D. D. C. Bradley, S. Cook, and J. R. Durrant, *J. Mater. Sci.* **40**, 1371 (2005).
- ²⁴G. Li, H. Yang, V. Shrotriya, G. Yang, and Y. Yang, *Adv. Funct. Mater.* **17**, 1636 (2007).

